Project Acronym	CORMORAN (ANR 11-INFR-010)
Document Title	D2.2 - 1st Channel Measurement campaign and identification of relevant radio models and parameters
Contractual Date of Delivery	M12 (31/12/2012)
Actual Date of Delivery	01/03/2013
Editor	Oudomsack Pierre Pasquero (CEA)
Authors	Oudomsack Pierre Pasquero, Raffaele d'Errico (CEA), Meriem Mhedhbi, Bernard Uguen (UR1)
Participants	CEA, UR1
Related Task(s)	T2
Related Sub-Task(s)	T2.2
Security	Public
Nature	Technical Report
Version Number	1.2
Total Number of Pages	115

CONTACTS & CORRESPONDENCE

Oudomsack Pierre Pasquero (CEA)
- Address: CEA-Leti Minatec, 17 rue des Martyrs, Bât. 51D, p. D423, 38054 GRENOBLE, cedex 9, France
- Email: oudomsackpierre.pasquero@cea.fr
- Tel: (+33) (0)4 38 78 24 35

Raffaele D'Errico (CEA)
- Address: CEA-Leti Minatec, 17 rue des Martyrs, Bât. 51D, p. D423, 38054 GRENOBLE, cedex 9, France
- Email: raffaele.derrico@cea.fr
- Tel: (+33) (0)4 38 78 56 47

TABLE OF CONTENT

ABSTRACT

The aim of this document is to identify some relevant wireless body area network (WBAN) channel models exploitable for the design of WBAN systems in different communication scenarios. First of all, it presents a general overview of the existing WBAN channel models and an analysis of the WBAN measurement campaigns which had been performed at CEA-Leti. Then, it describes the WBAN channel measurement campaigns which will be carried out in the context of the CORMORAN project. Channel model tools which will be used for the process of these measurements are presented. Finally, human mobility models are described and a diagram presents the way to combine them to the channel models in order to obtain a realistic physical simulator.

In the state-of-the-art, a general overview of WBAN channel models for *on-body*, *off-body* and *body-to-body* communication scenarios is presented. It is completed by the analysis of previous WBAN channel measurements performed at CEA-Leti in narrow band and ultra-wide band. More precisely, these measurements allowed the characterization of space-time correlation properties between different intra-BAN radio links, i.e. for *on-body* communication scenarios. Furthermore, the influences of the body movement and orientation, and the antenna characteristics had been investigated for *off-body* and *body-to-body* communication scenarios.
Then, a description of the planned channel measurements campaigns is carried out. The interest of these measurement campaigns is twofold. First, the degradation of the estimation of the angles of arrival of the electromagnetic waves due to the presence of the body will be investigated. For this purpose, a modeling tool, namely *Space Alternating Generalized Expectation-maximization* (SAGE), is necessary. This algorithm developed and validated with indoor measurements at CEA-Leti is described in the document. Secondly, an analysis of a cooperative WBAN channel combining *off-body* and *body-to-body* radio links will be performed.

One of the final objectives of the Task 2 being the development of a physical simulator, the last chapter of this deliverable presents a body mobility model. Finally, methods for a possible general WBAN channel model implementation combining this body mobility model and the identified channel models are proposed.

1. INTRODUCTION

A good understanding of channel characteristics is of fundamental importance in order to design operative and reliable communication systems. Physical (PHY), Medium Access Control (MAC) and Upper Layers protocols are strictly connected to the knowledge of propagation mechanisms and channel models. A number of studies have been performed in that direction for Body-centric communications.

As far as Body Area Networks (BANs) scenarios are concerned, it is possible to point out three types of channels that have to be investigated separately. They are characterized by specific features and the nodes involved in the communication are located in different places related to the human body. The channel models classification can be organized according to the antennas location around the body:

- *On-Body channel:* in this case both end points of the communication link are placed on the human subject. The propagation takes place along or around the body by diffraction (creeping waves), by Line-of-Sight (LOS) path in specific scenarios such as a link between the waist and the wrist, and hybrid mechanisms (e.g. diffraction off of arms). The shadowing effect of the body could affect significantly the system performance.

- *In-Body channel:* the propagation takes place between an implanted device and another that is positioned in or on the body itself (we can distinguish between in-in and in-on body communication). Human tissues and organs are extremely lossy materials leading to sever attenuation.

- *Body-to-Body* or *Off-Body channel:* we refer to *body-to-body* channels when the communication takes place between at least two human subjects, wearing different BAN, free to move relatively to each other in the environment, whereas *off-body* channels occur when one of the end point of the communication link is represented by an external fixed device e.g. a gateway or a router. In these cases a free-space propagation component has also to be considered.

As described in the CORMORAN D1.1 deliverable, the CORMORAN project is focused on the development of WBAN systems for Large-Scale Individual Motion Capture (LSIMC) and the Coordinated Group Navigation (CGN). No implanted device is required for these kinds of applications. Consequently, only O*n-Body*, *Body-to-Body* and O*ff-Body* channels are investigated in this deliverable. *In-Body* communication scenarios are not studied.

2. ON-BODY CHANNEL

2.1. OVERVIEW

2.1.1 STATICS MODELS

First investigations on on-body propagation have been carried out in 2002-2003 [1], [2], although contributions concerning related questions (such as the strong influence of the body on antennas, beam shadowing by persons, etc.) have been published since the late 90s. In Europe, contributions have been provided by ETH Zurich [3], IMEC (NL), ULB (Brussels) and UCL (Louvain) [4], [5], [6], [7] the University of Birmingham and Queen Mary University of London [8] and Queen's University of Belfast [9], [10]. Worldwide, contributions have come from Japan, Korea, Singapore, Australia and the USA.

More recently, studies on the influences of the body shape and the surrounding environment on the static on-body channel characteristics have been carried out.
In [11] and [12], the authors classify the body as "thin", "normal" or "fat" to propose different channel models. From measurement campaigns, for several antenna locations on the body, they observed that the slimmer the body is, the lower the path loss is. They define the path loss as a linear function of the distance:

$$\mathrm{PL}(d) = a \cdot \log_{10} d + b + N \tag{1}$$

where d is the distance between Tx antenna and Rx antenna, a and b coefficients whose values are function of the body corpulence. Moreover, they observed that the slimmer the body shape is, the less dispersive in time the channel is. Thus, they define three Power Delay Profile models namely "sparse" for thin body, "medium" for normal body and "dense" for fat body. The lack in their study is the missing of criteria to classify body corpulence.

Likewise, recent analyses on the influences of the environment on on-body channel characteristics have been carried out. For instance, the effects of the room volume on the UWB on-body channel characteristics are studied in [13]. For this purpose, measurement campaigns have been carried out in five different room volumes. It has been concluded that the PDP could be divided in two domains. The first one, corresponding to delays lower than 4ns and characterized by the presence of a direct path and diffracted paths, is dependent of the propagation distance along the perimeter of the body. Therefore, the PDP in this first domain is modeled by a conventional power decay law. In the second domain, corresponding to delays higher than 4ns and characterized by multi-paths coming from the surrounding environment, the PDP is modeled by a modified Saleh-Valenzuela model considering the room volume.

In [15] and [16], analyses are made on the interest and the feasibility to separate the on-body cluster and the off-body clusters to simplify the on-body channel modeling process. Indeed, it is thus simpler to analyze the influence of the body posture, movement, corpulence, the antennas (on-body cluster) and the influence of the environment as the type and the size of the room (off-body clusters).

2.1.1 DYNAMICS MODELS

Despite the huge number of scientific contributions on BAN channel existing in literature, only few works address the issue of time-variant channel modeling, whereas most others focus on static or quasi-static scenarios. Obviously, the human body mobility should be taken into account in order to accurately describe the radio channel characteristics and design cooperative protocols for BANs applications. However, the characterization of these phenomena presents some technical difficulties in performing measurements. The path losses that have to be measured are generally very high (more than 70-80 dB), because of strong shadowing effect produced by the human body. This means that measurement test-beds with a reasonable signal dynamic must be employed. That is why frequency domain measurements are often performed by means of Vector Network Analyser (VNAs) to characterize BAN channel [17], [18], [19]. Quasi-static measurement campaigns employing VNA have been performed by Fort in the UWB by focusing on the arm movement. The authors found a log-normal distribution for the path loss fluctuations around the mean value at three different antenna locations on torso. No distinction between the slow and the fast fading components is considered, and the frequency dependence of the path loss is not included.

Narrowband quasi-static measurements at 2.45 GHz have been performed in anechoic chamber by highlighting the effect of body posture [17], [18] again a log-normal distribution variation of path gain around its means value has been proved, without any separation of the small and large fading component. A similar pseudo-dynamic measurement method has been applied in [20] to reproduce the human walking motion.

The measurement test-bed for on-body channel measurements at 868 MHz employed by Scanlon and Cotton presents some interesting features since different sensors on body are able to collect RSSI values, avoiding in that way cable parasitic effects [21]. The main drawback of this measurement setup is that no phase information is given, so that it is not possible to evaluate the channel dispersion characteristics. Nakagami and Rice distributions with high K-factor have been found to best fit fading distribution for respectively standing and moving scenarios. The same team also performed some measurements at 2.45 GHz with a transmitter on waist and the receiver on different positions on body [22], [23], [24]. In [22] the authors propose a Nakagami-m distribution to model the fading channel characteristics. In stationary scenario high m value of the Nakagami distribution suggests the existence of a predominant component.

Measurements by NICT have employed a channel sounder at 4.5 GHz [25]. The transmitting antenna was placed on the navel, while the receiving one was on different positions on body. The scenarios measured in anechoic chamber were: standing position, walking on the spot, and up-down movement. The authors propose three different distributions of the relative path gain. Normal or log-normal distribution seem the best suited distributions for static or little movement scenarios, while the Weibull distribution can be employed in larger human body movements.

An important work in on-body narrowband channel characterization has been carried out by NICTA in [36]. This work focuses on two frequencies relevant for the ISM band: 820 MHz and 2.36 GHz. The human subject was asked to perform three different actions: standing still, walking on the spot and running on the spot. The receiving antenna is placed on the right hip or chest, while the transmitting antennas were located on different body positions. The analysis carried out shows that a unique distribution is not suitable to describe all the scenarios for the three different body movements, moreover the authors pointed out the dependency of different fading characteristics on the carrier frequency and movement. Despite the fact that different statistical behaviors have been pointed out according to the scenario, the results presented in [36] have been integrated in the final IEEE 802.15.6 report [26] by merging all the scenarios together.

The same team has also performed some investigations on the stability and temporal correlation of the dynamic BAN channel, introducing a new parameter called channel variation factor, calculated as the ratio between the standard deviation and the square root of mean received power [26].

Recently real-time channel measurements have been exploited in order to define a channel model which keeps space-time correlation properties. In fact this kind of knowledge is mandatory to define the possibility for use of cooperative approaches in BANs [27], [28].

In [29], a specific scenario at 2.45 GHz is investigated to model the fading correlation between two antennas as a function of the distance *d*. With respect to the scenarios specification in IEEE 802.15.4a, sensors are distributed horizontally on the front abdomen at a given level of the torso. The measurements are conducted in a quasi-anechoic environment in the walking mode (torso is kept standing still without actual walking while the arms periodically move forward and backward). The fading distribution in BAN follows a lognormal distribution.

The measurement results show consistent relationships between correlation coefficient and the distance difference. An average linear approximation to model the fading correlation variation is proposed for the front abdomen body area:

$$\varrho = 1 - 0.043\, d[\mathrm{cm}] \qquad (2)$$

with a shared propagation distance of 12cm between the transmitting and the receiving antennas.

The measurement protocol presents the following parameters:

- Sampling rate: 1kHz,
- Observation time: 20s,
- Body movements. Natural arm swinging (around 1.2s/cycle),
- Perimeter of abdomen: 86cm,
- Torso's height: 183cm,
- Torso's weight: 80kg,
- Front body region: a span of 20cm from the centre to left/right side.

In [30], a front/back scenario is analyzed with the help of a human body model based on an ellipsoid representing the torso trunk. Two cylinders representing the arms are added with a swinging movement alternatively forward and backward in a periodical pattern. There are three propagation paths: propagation paths reflected by left/right arms and propagation path around body trunk. For the NLOS case, the reflected propagation paths are combined by the tangent free-space propagation path from the arm centre to the ellipse and the creeping waves from the tangent point to the destination.

It is observed that the fading correlation obtained at the back side of torso trunk has steep drops at given distances. This could be due to the body surface shape change at some position of the back side of torso trunk. The paper also demonstrates that even if there are only three MPCs for each channel, their different phase contribution to the channel can still affect the channel correlation under regular body movements.

One of the latest measurement campaign performed in order to investigate the characteristics of time-variant BAN channel at 2.45GHz has been carried out at CEA-Leti and the results are presented in [31]. The measurement campaign has been realized in both anechoic chamber and indoor environment involving different human subjects, who stood still just changing the arm position, walked in straight line and ran on the spot.

2.2. STANDARDIZED CHANNEL MODELS

This sub-section presents a state-of-the-art of the IEEE on-body channel models. Before entering into the details of each model that will be presented, it is necessary to underline that all these models are far from giving an exhaustive characterization of the propagation channel for BAN scenarios. Each of them lacks in taking into account more than one source of variability, such as population (human subjects), postures and movements, antenna and frequency variability, and only few studies consider the time varying characteristics of the channel.

It would be also very difficult to compare the results presented in these works because there is no standardized measurement protocol that could be used as a reference and often the data have been collected for too specific scenarios, losing in this way the desirable generality that a model should present.

2.2.1 IEEE 802.15.4A

IEEE 802.15.4a standard proposes UWB channel models [32] [33] for different applications including on-body communication. Although this model has been partially checked with a few measurements of “control”, it is worthwhile to point out that its initial version – and notably its structure – was extracted from electromagnetic simulations (with the anatomic model of the “Visual Human Project” over a reflecting ground) over a [2-6] GHz bandwidth. Moreover, the model is restricted to scenarios for which the antennas are located only on the torso, and the antennas behaviors are completely excluded from the model.
This model is consequently more or less restricted to the anechoic chamber environment with ground echoes, which may be considered as a representation of an outdoor environment.

The electromagnetic simulations emphasized the existence of creeping waves around the torso and the quasi non-penetration of the waves in the body for frequencies in the GHz range. Therefore, the distance between the transmitter and the receiver has been defined around the perimeter of the body instead of a straight-line through the body. Three scenarios – corresponding to the receiver position on the front, side and back of the body – are specified with different parameterizations as illustrated in Figure 1.

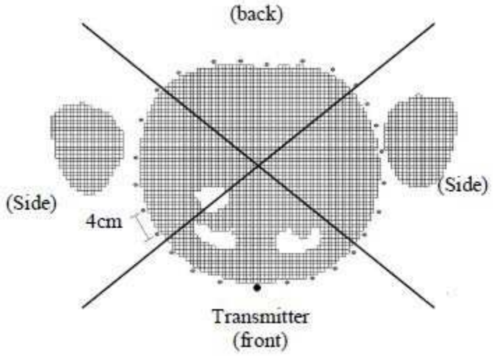

Figure 1: Scenarios of the receiver positions

The path loss is modeled as an exponential decay with the distance:

$$P_{dB} = \gamma(d - d_0) + P_{0dB} \tag{3}$$

where γ is in units of dB/meter, d the distance from the antenna, d_0 is the reference distance and P_0 is the power at the reference distance. The parameters values of this path loss model extracted from the simulator are given in the Table 1.

Parameter	Value
γ	107.8 dB/m
d_0	0.1 m
P_0	35.5 dB

Table 1: 802.15.4a path loss model

Although a slight increase of the path loss with the increasing of frequency has been measured, it is considered as negligible for the 2-6GHz frequency band in the standard. Thus, the path loss model is assumed independent of the frequency.

Contrary to conventional Rayleigh or Ricean models, amplitude distributions are found to be log normal and bin to bin correlated (mainly between adjacent ones) as showed in the Figure 2. This is due to the fact that the uncorrelated scattering assumption is violated. The Table 2 summarizes the simulated mean, the variance, and the correlation matrices of the log amplitudes.

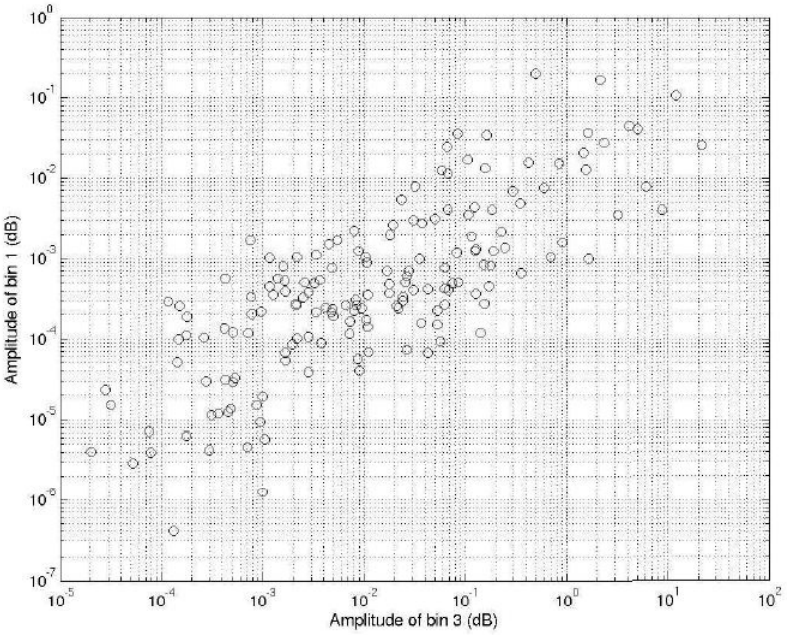

Figure 2: Correlation between bins 1 et 3 (side of body)

$$R_{side} = \begin{bmatrix} 1 & 0.9 & 0.78 & 0.77 & 0.73 & 0.64 & 0.62 & 0.53 & 0.53 & 0.45 \\ 0.9 & 1 & 0.88 & 0.83 & 0.77 & 0.74 & 0.72 & 0.64 & 0.64 & 0.59 \\ 0.78 & 0.88 & 1 & 0.84 & 0.76 & 0.77 & 0.76 & 0.7 & 0.69 & 0.66 \\ 0.77 & 0.83 & 0.84 & 1 & 0.86 & 0.81 & 0.81 & 0.74 & 0.75 & 0.73 \\ 0.73 & 0.77 & 0.76 & 0.86 & 1 & 0.85 & 0.83 & 0.74 & 0.72 & 0.69 \\ 0.64 & 0.74 & 0.77 & 0.81 & 0.85 & 1 & 0.92 & 0.81 & 0.75 & 0.72 \\ 0.62 & 0.72 & 0.76 & 0.81 & 0.83 & 0.92 & 1 & 0.86 & 0.81 & 0.77 \\ 0.53 & 0.64 & 0.70 & 0.74 & 0.74 & 0.81 & 0.86 & 1 & 0.92 & 0.86 \\ 0.53 & 0.64 & 0.69 & 0.75 & 0.72 & 0.75 & 0.81 & 0.92 & 1 & 0.91 \\ 0.45 & 0.59 & 0.66 & 0.73 & 0.69 & 0.72 & 0.77 & 0.86 & 0.91 & 1 \end{bmatrix}$$

$$R_{front} = \begin{bmatrix} 1 & 0.86 & 0.56 & 0.66 & 0.66 & 0.51 \\ 0.86 & 1 & 0.74 & 0.74 & 0.73 & 0.59 \\ 0.56 & 0.74 & 1 & 0.82 & 0.79 & 0.71 \\ 0.66 & 0.74 & 0.82 & 1 & 0.87 & 0.62 \\ 0.66 & 0.73 & 0.79 & 0.87 & 1 & 0.76 \\ 0.51 & 0.59 & 0.71 & 0.62 & 0.76 & 1 \end{bmatrix}$$

$$R_{back} \quad \begin{bmatrix} 1 & 0.88 & 0.84 & 0.78 & 0.55 & 0.59 & 0.54 & 0.48 & 0.62 & 0.72 \\ 0.88 & 1 & 0.91 & 0.76 & 0.70 & 0.74 & 0.63 & 0.57 & 0.71 & 0.81 \\ 0.84 & 0.91 & 1 & 0.81 & 0.68 & 0.80 & 0.72 & 0.63 & 0.74 & 0.81 \\ 0.78 & 0.76 & 0.81 & 1 & 0.69 & 0.69 & 0.79 & 0.68 & 0.69 & 0.70 \\ 0.55 & 0.70 & 0.68 & 0.69 & 1 & 0.83 & 0.76 & 0.84 & 0.82 & 0.82 \\ 0.59 & 0.74 & 0.80 & 0.69 & 0.83 & 1 & 0.85 & 0.84 & 0.83 & 0.81 \\ 0.54 & 0.63 & 0.72 & 0.79 & 0.76 & 0.85 & 1 & 0.86 & 0.77 & 0.71 \\ 0.48 & 0.57 & 0.63 & 0.68 & 0.84 & 0.84 & 0.86 & 1 & 0.85 & 0.77 \\ 0.62 & 0.71 & 0.74 & 0.69 & 0.82 & 0.83 & 0.77 & 0.85 & 1 & 0.91 \\ 0.72 & 0.81 & 0.81 & 0.70 & 0.82 & 0.81 & 0.71 & 0.77 & 0.91 & 1 \end{bmatrix}$$

	Front		Side		Back	
Bin	μ_{dB}	σ_{dB}	μ_{dB}	σ_{dB}	μ_{dB}	σ_{dB}
1	5.7	4.7	9.6	6.3	9.2	6.3
2	12.1	4.2	12.9	5.7	12.0	6.5
3	17.0	5.2	16.8	5.2	14.6	6.3
4	20.7	5.1	19.6	5.0	15.1	5.7
5	23.2	5.1	21.4	4.8	18.2	5.4
6	25.6	4.5	24.1	4.8	20.9	5.7
7	28.4	4.6	26.7	5.0	22.7	5.5
8	31.4	4.6	28.9	5.0	23.9	5.2
9	34.5	4.8	30.9	5.2	24.0	5.1
10	37.1	4.7	32.4	5.6	24.9	5.4

Table 2: Amplitude distribution of each bin

The number of clusters is fixed (only 2 are considered, one for the "on-on" and another for the ground reflection), as long as the inter-cluster and inter-path arrival time. As in the initial cluster, the multi-paths components (MPC) reflecting off the ground is modeled by correlated lognormal variables. The resulting amplitude distributions for the three first bins are summarized in the Table 3. The mean path loss is given relative to the reference path loss near the antenna, $P_0 = 35.5$dB.

$$R_{floorf} = \begin{bmatrix} 1 & 0.91 & 0.76 \\ 0.91 & 1 & 0.84 \\ 0.76 & 0.84 & 1 \end{bmatrix} \qquad R_{floors} = \begin{bmatrix} 1 & 0.93 & 0.79 \\ 0.93 & 1 & 0.85 \\ 0.79 & 0.85 & 1 \end{bmatrix} \qquad R_{floorb} = \begin{bmatrix} 1 & 0.96 & 0.89 \\ 0.96 & 1 & 0.9 \\ 0.89 & 0.9 & 1 \end{bmatrix}$$

	Front		Side		Back	
Bin	μ_{dB}	σ_{dB}	μ_{dB}	σ_{dB}	μ_{dB}	σ_{dB}
1	24.4	4.3	28.8	5.2	29.3	4.9
2	28.7	4.4	32.2	5.0	33.0	4.7
3	29.3	4.3	37.4	5.4	40.0	5.5

Table 3: Amplitude distributions of ground reflection off a perfect electrical conductor

Improvements to take into account the multi-path components (MPCs) originating from the surrounding environment have been proposed in [5], [6] and recalled in [33]. Components creeping around the body are generated according to the previous correlated log-normal model, whereas the MPCs coming from the environment are added using a SV model modified as follows:

- The original exponential decay model of the Power Delay Profile (PDP) is replaced by a dual slope exponential decay model, with slopes $\Gamma 1$ (dB/ns), then $\Gamma 2$ (dB/ns) after an empirically derived breakpoint of T1 = 40 ns. Variation around this trend is log-normally distributed with a standard deviation σ. Intra-cluster exponential decay (γ) model is unchanged.
- The cluster arrival time statistics of the measurements (office environment) are more closely fitted by a Weibull distribution (with shape parameter α and scale parameter β) than by the Poisson process of the "generic" (SV-based) model.
- The small-scale fading statistics, extracted from the received energy in each bin, turned out to be either Nakagami-m or log-normal with almost the same confidence levels.
- In addition, a large-scale statistics of the energy reflected back from the surrounding environment – corresponding to the exploration of various locations in a room – is found to follow a lognormal distribution; the first empirical moments (lognormal mean $\mu_{off,dB}$ and standard deviation $\sigma_{off,dB}$) are obtained as ML estimates of the distribution of the integrated energy received after the arrival time of the diffracted MPCs (creeping waves around the body) and normalized to the transmitted energy. Note that, comparing these figures with the path loss of the IEEE 802.15.4a BAN model, it appears that, for the scenarios where the antennas are placed on the same side of the body, the contribution of the surrounding environment is almost insignificant (ground reflection excluded), whereas it can be the reverse when antennas are placed on both sides. Due to the shadowing effect of the body, $\mu_{off,dB}$ varies typically from about -70 dB for the "front scenario" (antennas on the same side) to about -80 dB for the "back" one.

2.2.2 IEEE 802.15.6

In November 2007, the IEEE 802.15 Task Group 6, also known as IEEE 802.15.6, was formed in order to standardize BANs, which were not covered by any existing communication standard yet.

The IEEE 802.15.6 standard [26] appeared in February 2012 defines the PHY and MAC layers optimized for short-range transmissions in, on or around the human body. The purpose is to support a low complexity, low cost, ultra-low power and highly reliable wireless communication for use in close proximity to, or inside, a human body (but not limited to humans) to serve a variety of applications both medical/healthcare and non-medical.

The broad range of possible application fields in which BANs could be involved into, leads to an equally wide variety of system requirements that have to be met. The definition of a unique PHY layer has turned to be not a feasible solution. Hence, the IEEE 802.15.6 standardization group has proposed three different alternatives: narrowband centred at different frequencies, UWB and Human Body Communication (HBC). Figure 3 graphically summarizes the spectrum allocation chart of all available frequencies for BAN applications, with the specification of the related country or region where they could be used.

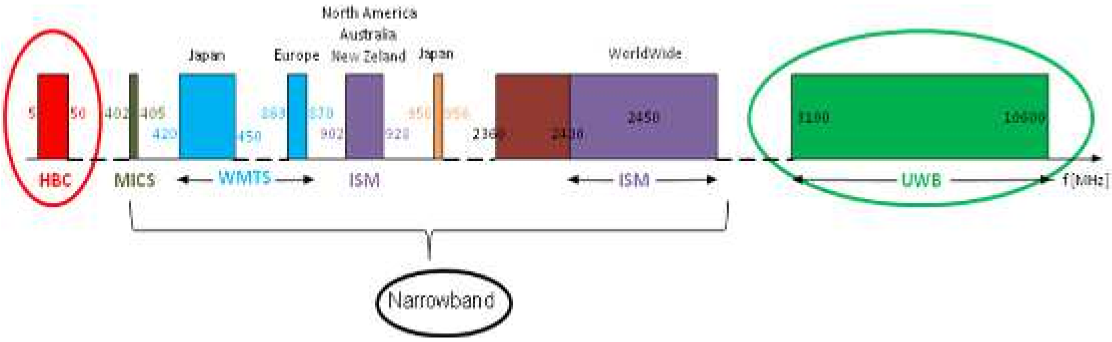

Figure 3: WBAN frequency bands allocated in different countries.

The channel models presented by the "Channel Modeling Subgroup of IEEE802.15.6" generally characterize the path loss in different BAN scenarios, also taking into account possible shadowing effects due to the human body or obstacles near it and postures of the subject [26].

As shown in Table 4, the standardization group has identified a list of scenarios in which BAN IEEE 802.15.6 compliant devices will operate, along with their description and the frequency band of interest:

Scenario	Description	Frequency Band	Channel Model
S1	Implant to Implant	402-405 MHz	CM1
S2	Implant to Body Surface	402-405 MHz	CM2
S3	Implant to External	402-405 MHz	CM2
S4	Body Surface to Body Surface (LOS)	13.5, 50, 400, 600, 900 MHz 2.4, 3.1-10.6 GHZ	CM3
S5	Body Surface to Body Surface (NLOS)	13.5, 50, 400, 600, 900 MHz 2.4, 3.1-10.6 GHZ	CM3
S6	Body Surface to External (LOS)	900 MHz 2.4, 3.1-10.6 GHZ	CM4
S7	Body Surface to External (NLOS)	900 MHz 2.4, 3.1-10.6 GHZ	CM4

Table 4: List of scenarios and their description

The scenarios are determined based on the location of the nodes; according to their physical emplacement, three different types of nodes have been identified:

- *Implant node*: placed inside the human body, immediately below the skin or further deeper inside the body tissue.
- *Body Surface node*: placed on the surface of the human skin or at most 2cm away.

- *External node*: not in contact with human skin (between a few centimeters and up to 5 meters away from the body).

In Table 4, the scenarios are grouped into classes that can be represented by the same Channel Model (CM).
It is important to remark that the channel model for scenarios involving implanted devices is fundamentally different from the one characterizing body surface communications, for that reason the CMs could be divided into two subgroups: CM1 and CM2 for channel model involving at least one implant device, and CM3 along with CM4 for the Body Surface to Body Surface or to external nodes communications. A graphical representation of the scenarios and the relative channel model is presented in Figure 4.

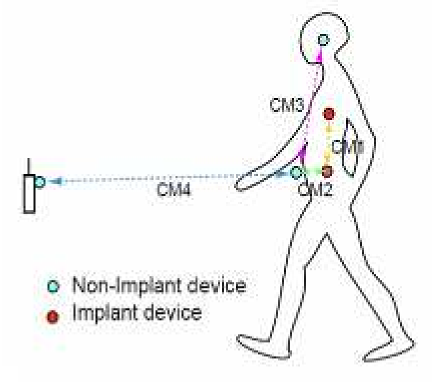

Figure 4: IEEE Channel models

As mentioned previously, the main applications identified in the CORMORAN D1.1 deliverable are the Large-Scale Individual Motion Capture (LSIMC) and the Coordinated Group Navigation (CGN). Thus, in this sub-section, we analyse only the CM3 channel model for the scenarios S4 and S5 corresponding to on-body channel models for line of sight (LOS) and non-line of sight (NLOS) contexts respectively.

• *CM3 at 2.4GHz*

One of the main parameters in channel modeling is the mean path loss and the shadowing and fading characteristics. The conventional approach for modeling the Path Loss (PL), precisely as a function of the distance PL(*d*), is still widely used, although it is questionable.
Different kinds of model are proposed in the literature and all of them are for example retained in the IEEE 802.15.6 proposal.

Power law model

$$PL(d_{[\mathrm{mm}]})_{[\mathrm{dB}]} = a \cdot \log(d_{[\mathrm{mm}]}) + b + N \tag{4}$$

where *a* and *b* are parameters of the model and *N* is a normally distributed variable, centred and with standard deviation σ_N (see Table 5). It is used for both Narrowband and UWB channels.

Note that variants, in particular dual-slope models, are also proposed in the literature.

This path loss model, namely CM3A in the IEEE 802.15.6 standard, is based on measurements that cover the frequency interval of 2.4-2.5GHz. Details of the measurement set up, derivation and data analysis can be found in [34].

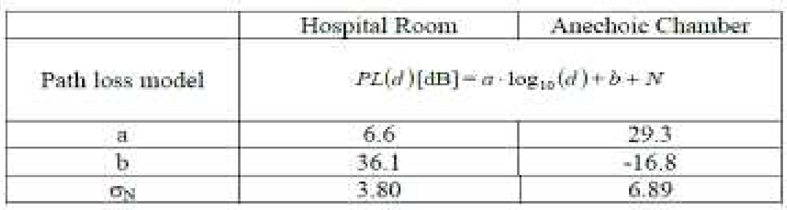

	Hospital Room	Anechoic Chamber
Path loss model	$PL(d)[\text{dB}] = a \cdot \log_{10}(d) + b + N$	
a	6.6	29.3
b	36.1	-16.8
σ_N	3.80	6.89

Table 5: CM3 A model parameters

- *a* and *b*: Coefficients of linear fitting
- *d*: Tx-Rx distance in mm.
- *N*: Normally distributed variable with standard deviation σ_N

Saturation model

This kind of model is "hybrid" in the sense that it merges a local propagation model (on-body to on-body, or "on-on") and the influence of the environment (typically Multi-Paths Components – MPCs – reflecting off of the walls) resulting in an exponential part for "short distances" (on-on mechanism) and a "plateau" for larger distances, accounting for a "saturation" behaviour of the PL in indoor premises whose MPCs reflecting off the room become dominant (saturation due to "environmental MPCs"). It has been proposed for Narrowband channels at 915 MHz and 2.4 GHz.

The corresponding formula (which is really ambiguous as written for example in the table of §8.2.5 B of [26]) should be read:

$$PL(d_{[\text{cm}]})_{[\text{dB}]} = -10 \cdot \log(10^{P_0/10} e^{-(M_0 d_{[\text{cm}]})/4.343} + 10^{P_1/10}) + \sigma_P n_P \qquad \textbf{(5)}$$

where P_0, P_1, and M_0 are parameters of the model, n_P is a unit variance centred normal random variable and σ_P is the PL standard deviation (relative to mean).

This model, namely CM3B, is based on measurements at 2.45GHz. Details of the measurement set up, derivation and data analysis can be found in [35]. The path loss follows an exponential decay around the perimeter of the body. It flattens out for large distances due to the contribution of MPCs from indoor environment. Table 6 presents the model and the corresponding parameters.

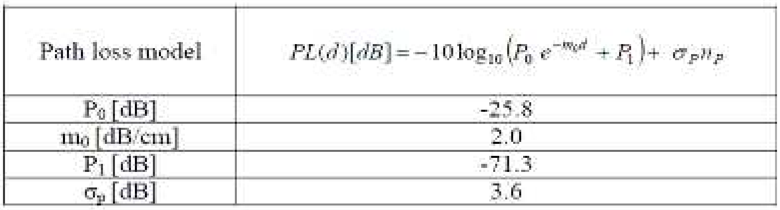

Path loss model	$PL(d)[dB] = -10\log_{10}\left(P_0\, e^{-m_0 d} + P_1\right) + \sigma_P n_P$
P_0 [dB]	-25.8
m_0 [dB/cm]	2.0
P_1 [dB]	-71.3
σ_p [dB]	3.6

Table 6: CM3 B model parameters

- P_0: The average loss close to the antenna
- M_0: The average decay rate in dB/cm for the surface wave travelling around the perimeter of the body
- P_1: The average attenuation of components in an indoor environment radiated away from the body and reflected back towards the receiving antenna
- σ_P: The log-normal variance in dB around the mean, representing the variations measured at different body and room locations. This parameter will depend on variations in the body curvature, tissue properties and antenna radiation properties at different body locations.
- n_P: Zero mean and unit variance Gaussian random variable

The small scale fading is represented by a Ricean distribution with *K* factor that decreases as the path loss increases. The delay spread is normally distributed. Table 7 and Table 8 summarize the model and the corresponding parameters.

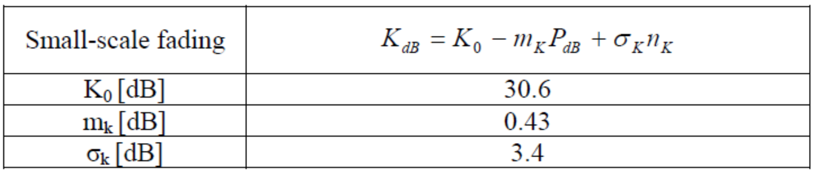

Small-scale fading	$K_{dB} = K_0 - m_K P_{dB} + \sigma_K n_K$
K_0 [dB]	30.6
m_k [dB]	0.43
σ_k [dB]	3.4

Table 7: Small scale fading in CM3 B model

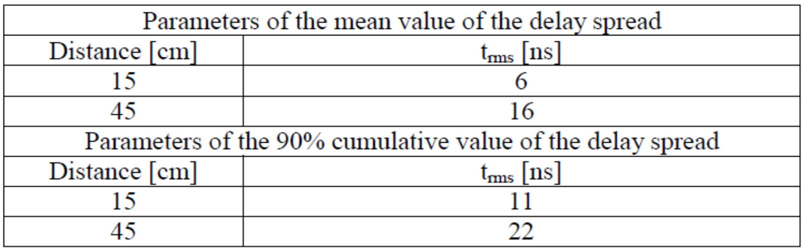

Parameters of the mean value of the delay spread	
Distance [cm]	t_{rms} [ns]
15	6
45	16
Parameters of the 90% cumulative value of the delay spread	
Distance [cm]	t_{rms} [ns]
15	11
45	22

Table 8: Delay spread fading in CM3 B model

Scenario-based models

In this more recent approach, application-dependent radio link "scenarios" are retained, e.g. belt to chest for ECGs (Electrocardiograms), and PLs are derived from measurements averaging various sources of variability (human subject, and/or "local positioning", posture, unwanted movements, antennas, etc.). It has been proposed for both Narrowband and UWB channels.

The following path loss measurements have been performed at frequency of 2.36GHz for everyday activities such as walking around the office, working in the office, driving, at home, etc… and sleeping on a bed and in a bedroom. Details of the measurement set up, derivation and data analysis can be found in [36] [37]. Table 9 summarizes the results.

As observed, the dominant factor affecting fading in the channel appears to be the movement of the test subject. This is to be expected, as movement causes the separation and orientation of the antennas to change.

Path loss	$PL[dB] = P_{tx} - P_{rx} + G_{amplifiers} - L_{cable}$								
	Receiver at right hip						Receiver at chest		
Action	Chest	Right Wrist	Left Wrist	Right Ankle	Left Ankle	Back	Back	Right Wrist	Right Ankle
Standing	65.3	44.5	74.7	60.9	70.7	75.3	73	70.5	66.3
Walking	59.1	47.3	59.8	53.9	58.5	67.4	72	64.9	62.4
Running	55.9	36.3	52.5	55	59	68.5	71.7	57.4	63.3

Table 9: CM3 C model parameter

- P_{tx}: Transmitted power
- P_{rx}: The RMS received power
- $G_{amplifiers}$: Amplifier gain
- L_{cable}: Cable loss

The first-order statistics fits to everyday and sleeping on-body channel gain data, where the data has been normalized to mean of each link data set. The gamma distribution is the best fitting distribution type for this data, apart from overall sets, non-normalized, which is lognormal.

The shadowing term, i.e. the stochastic term added to the PL model (expressed in dB) and accounting for its variance, is generally assessed as a centred normal variable with standard deviation σ_N, resulting in the "classical" log-normal behaviour.

A small parametric analysis of the antenna-body spacing δ effect on the PL is provided in [34]. As expected, the PL exponent n essentially does not depend on δ whereas the PL_0 does:

$$\begin{aligned} \partial n / \partial \delta &\approx 0 \\ \partial PL_0 / \partial \delta &< 0 \end{aligned} \qquad \textbf{(6)}$$

This is due to the fact that *n* depends only on the physical phenomena along the propagation path (creeping waves, absorption, diffraction, etc.) whereas PL_0 is "source dependent" (antenna type and coupling to the body). This trend is confirmed by several works.

- *CM3 for UWB*

CM3A

Measurement campaigns in the 3.1-10.6 GHz frequency band have been carried out for UWB on-body channel modeling [34]. The table below summarizes the model and corresponding parameters.

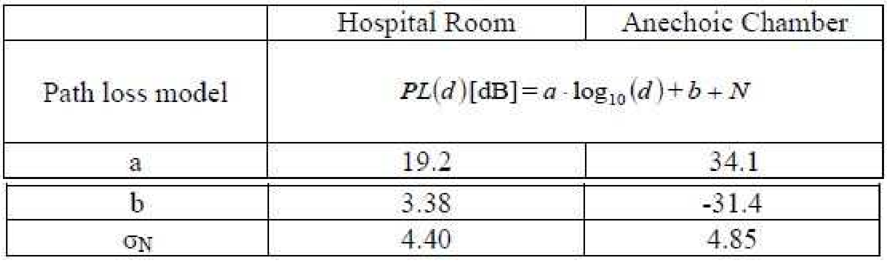

	Hospital Room	Anechoic Chamber
Path loss model	$PL(d)[\mathrm{dB}] = a \cdot \log_{10}(d) + b + N$	
a	19.2	34.1
b	3.38	-31.4
σ_N	4.40	4.85

Table 10: CM3A model for UWB

- *a* and *b*: coefficients of linear fitting
- *d*: Tx-Rx distance in mm
- *N*: normally distributed variable with zero mean and standard deviation $\boldsymbol{\sigma}_N$

A power delay profile (PDP) model – proposed by NICT – is also given in [34]. It corresponds to a classical single cluster tapped delay line/Poisson process model, with:

$$h(\tau) = \sum_{\ell=0}^{L-1} a_\ell \exp(j\varphi_\ell)\delta(\tau - \tau_\ell) \tag{7}$$

where, a_l, τ_l, ϕ_l, are respectively the amplitude, arrival time and phase for *l*-th path. The phase ϕ_l is modeled as a uniformly distributed random variable (r.v.) (over [0, 2π[).

The path amplitude a_l is modeled by an exponential decay Γ with a Ricean factor γ_0, which reads:

$$(a_\ell)_{dB} = \begin{cases} 0 & \ell = 0 \\ \gamma_0 + 10\log(\exp(-\tau_\ell / \Gamma) + S & \ell > 0 \end{cases} \tag{8}$$

where *S* is a stochastic term modeled by a log-normal distribution with zero-mean and standard deviation of σ_S. The path arrival time τ_l is modeled by a Poisson distribution, which is given by:

$$p(\tau_\ell | \tau_{\ell-1}) = \lambda \exp[-\lambda(\tau_\ell - \tau_{\ell-1})] \tag{9}$$

where λ is the path arrival rate. The number of the arrival paths L is modeled by a Poisson distribution, which reads:

$$P(L)=\frac{\bar{L}^{L}\exp(\bar{L})}{L!} \tag{10}$$

where $\bar{L}$ is the average of L. The parameters values extracted by model fitting from measurements are listed below: γ_0=-4.6 dB, Γ = 59.7 ns, σ_S = 5.02 dB, λ = 1.85 ns^{-1} and $\bar{L}$ = 38.1 for the hospital room environment.

CM3B

Another path loss model is proposed in the standard, based on another measurement campaign described in [35]. The table below summarizes the corresponding parameters.

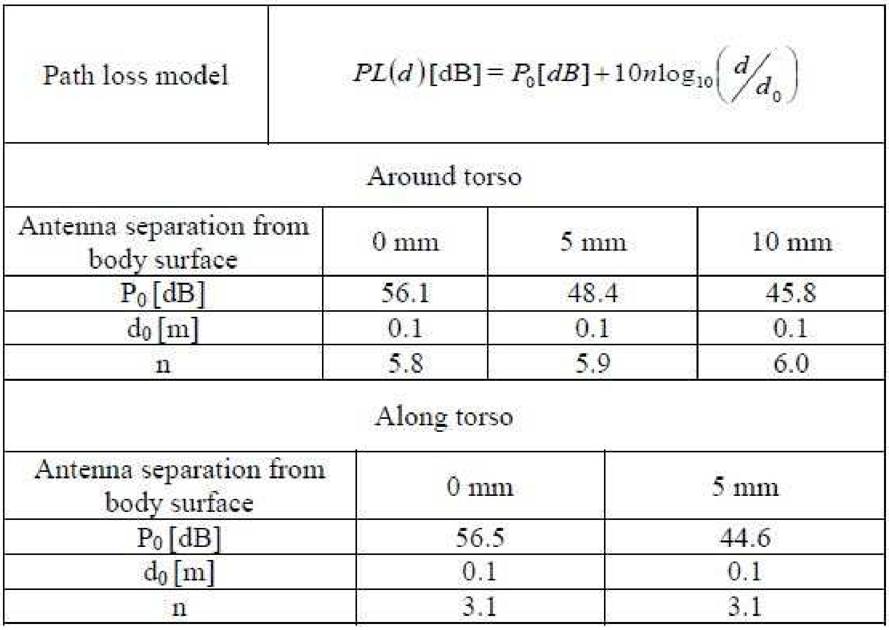

Path loss model	$PL(d)[\text{dB}]=P_0[dB]+10n\log_{10}\left(d/d_0\right)$		
Around torso			
Antenna separation from body surface	0 mm	5 mm	10 mm
P_0 [dB]	56.1	48.4	45.8
d_0 [m]	0.1	0.1	0.1
n	5.8	5.9	6.0
Along torso			
Antenna separation from body surface	0 mm	5 mm	
P_0 [dB]	56.5	44.6	
d_0 [m]	0.1	0.1	
n	3.1	3.1	

Table 11: CM3B model for UWB

- n: path loss exponent
- P_0: path loss at the reference distance
- d_0: reference distance

2.3. CEA ON-BODY CHANNEL INVESTIGATIONS

Previous measurement campaigns have been carried out at CEA-Leti to investigate the time-variant on-body channel [31]. The measurements have been carried out in narrow band (at 2.45GHz) and in ultra wide band (3-5 GHz). Different communication scenarios have been considered: different human subjects, body movements, antenna locations on the body, kind of antennas, environments.

A common assumption is to define the radio channel as a composite of the linear wave interactions, which occur between a transmitting and a receiving antenna, and can be represented by means of a time-varying linear filter characterized by its impulse response $h(t;\tau)$, also known as input-delay spread function according to the classical Bello's definition A snapshot of $h(t;\tau)$ at observation time t_n can be expressed as:

$$h(t_n;\tau) = \sum_{k=1}^{K(t_n)} a_k(t_n) e^{j\theta_k(t_n)} \delta(\tau - \tau_k(t_n)) \tag{11}$$

where $a_k(t_n)$, $\theta_k(t_n)$ and $\tau_k(t_n)$ represent respectively the amplitude, phase and delay of the *k*-th path, while $K(t_n)$ is the total number of multi path components.

Imposing a limited rectangular bandwidth B, the discrete delays are combined into L delays bins.

When the delay separation between of a number of paths ($\tau_i(t_n) - \tau_j(t_n)$ for $i, j = 1,2,..., N(t_n)$) is less than the bin separation $T = 1/B$, they cannot be resolved as distinct. As a consequence the resolved path is:

$$A_l(t_n) = \sum_{k=1}^{N(t_n)} a_k(t_n) e^{j\theta_k(t_n)} \tag{12}$$

The channel impulse response can be written as:

$$h(t_n;\tau) = \sum_{l=1}^{L(t_n)} A_l(t_n) \sin c[B(\tau - \tau_l(t_n))] \tag{13}$$

where $\tau_l(t_n)$ are the discrete time bin.

The time variant transfer function can be expressed as:

$$H(t;f) = \int_{-\infty}^{+\infty} h(t;\tau) e^{-j2\pi f\tau} d\tau \tag{14}$$

By integrating over the frequency we obtain the time dependent power transfer function averaged over the band of interest:

$$P(t) = \frac{1}{B} \int_B |H(t;f)|^2 df \tag{15}$$

where B is the bandwidth of interest. This quantity is often approximated by the RSSI signal at the receiver.

2.3.1 CHANNEL GAIN MODEL

For a given channel transfer function the total power, or *channel gain*, is given by:

$$G_0 = \frac{1}{T_{obs}B}\int_{T_{obs}}\int_{B}\left|H(t;f)\right|^2 df\,dt \qquad \textbf{(16)}$$

where T_{obs} is the averaging observation period. The channel gain is a key parameter, which determines the signal-to-noise ratio, averaged over small-scale and large-scale fading, which can be achieved by the wireless system. The averaging operation over the bandwidth supposes that all the dielectric constant of materials and all propagation phenomena related with, do not depend on the frequency. This assumption corresponds in a certain way to a WSS assumption in Bello's definitions. In classical indoor and outdoor channels, the G_0 is often expressed as a function of antenna separation. A number of studies in the literature investigated the channel gain, or equivalently the mean path loss, as a function of the antenna separation, by defining a path loss coefficient.

Here we use a "scenario-based" approach as explained above. We computed the channel gain by means of (16) for each scenario and we found a significant variation between different human subjects. These results can be easily explained by the fact that even if the antenna position is carefully reproduced on each human subject, the differences on body shape and dielectric proprieties yield to different path losses.

From measurement results we found that the most appropriate way to describe G_0 is a log-normal distribution. As a consequence the channel gain in dB can be represented by a Gaussian random variable (r.v.):

$$G_0\big|_{dB} \sim N\left(\mu_{0S}, \sigma_{0S}\right) \qquad \textbf{(17)}$$

where the mean value and standard deviation depend on the scenario S, as described above. The statistical analysis is here performed on the mean channel gain of the different subjects, so that normal distribution accounts for the dissimilarities between human bodies. Some local micro-variations of the antenna emplacement, due to dissimilar body shapes, produce also differences in mean channel gain, and their effect is taken into account by (17). In Table 12 and Table 13, we list the results for the investigated scenarios.

TX on hip RX on		Anechoic chamber				Indoor			
		ISM 2.45 GHz		UWB [3–5] GHz		ISM 2.45 GHz		UWB [3–5] GHz	
		μ_{0s} (dB)	σ_{0s}(dB)	μ_{0s} (dB)	σ_{0s} (dB)	μ_{0s} (dB)	σ_{0s} (dB)	μ_{0s} (dB)	σ_{0s} (dB)
Still	Chest	−60.8792	4.1500	−56.0735	4.3555	−54.6518	4.8124	−52.6205	4.3557
	Thigh	−64.3146	1.5457	−67.9143	3.1032	−60.7145	2.6247	−63.3036	2.3128
	R wrist	−63.2105	2.6178	−62.6940	2.7450	−57.8699	5.1064	−59.9577	3.2800
	R foot	−67.1255	5.1838	−72.4117	1.8445	−60.4444	2.2669	−62.9308	1.6910
Walking	Chest	−53.3737	7.8693	−51.1525	2.1419	−51.7554	7.2704	−51.1099	5.1969
	Thigh	−61.9708	6.4907	−64.5859	4.8125	−59.4894	3.0444	−62.3148	1.5189
	R wrist	−62.1787	5.9615	−61.6258	5.3892	−59.5920	4.2025	−61.7206	2.6024
	R foot	−68.6067	7.4110	−70.5375	4.9560	−58.3369	2.5985	−61.6193	1.4452
Running	Chest	−52.7866	3.3482	−52.4244	4.8385	−47.9470	7.5404	−49.1412	5.2697
	Thigh	−59.1210	4.4368	−62.6505	4.8607	−57.8446	3.5210	−60.7294	2.6594
	R wrist	−65.8698	4.3149	−63.8395	2.2846	−61.7829	3.8987	−60.1702	3.3161
	R foot	−71.2233	8.4303	−72.3628	7.4711	−60.4773	1.9647	−64.4700	1.1307

Table 12: Channel gain: transmitter on hip

TX on left ear RX on		Anechoic chamber				Indoor			
		ISM 2.45 GHz		UWB [3–5] GHz		ISM 2.45 GHz		UWB [3–5] GHz	
		μ_{0s} (dB)	σ_{0s} (dB)	μ_{0s} (dB)	σ_{0s} (dB)	μ_{0s} (dB)	σ_{0s} (dB)	μ_{0s} (dB)	σ_{0s} (dB)
Still	R Ear	−63.2533	6.3566	−63.4038	1.9335	−60.2220	3.1504	−59.9519	2.3074
	Hip	−60.1378	8.9410	−66.0411	2.4280	−60.2879	6.0754	−62.6346	3.9294
	R wrist	−72.9014	2.6375	−75.4553	1.4040	−64.4708	3.2828	−67.2240	0.9855
	R foot	−75.3591	4.5385	−77.8079	2.2942	−62.7263	2.1910	−65.0598	1.1077
Walking	R ear	−61.0003	2.7018	−62.1485	1.8514	−60.0321	3.0879	−60.6388	3.6631
	Hip	−57.9352	7.1715	−63.6140	2.2443	−58.7770	4.9483	−61.8767	2.2518
	R wrist	−71.8550	2.9189	−73.3252	2.8333	−63.0413	1.9839	−65.7443	1.5340
	R foot	−72.9939	4.6507	−74.9548	2.3615	−61.0049	1.3100	−63.0086	1.0698
Running	R ear	−61.3644	3.6490	−62.7325	3.3694	−60.7473	5.3087	−59.0271	3.6600
	Hip	−63.8337	7.5450	−68.4237	2.6864	−60.7622	5.7060	−62.7400	1.6554
	R wrist	−71.9968	2.2282	−69.1763	2.9781	−63.5684	2.2375	−62.7320	2.4954
	R foot	−77.7146	3.4217	−78.3609	2.0264	−62.7026	1.1543	−66.0428	0.8888

Table 13: Channel gain: transmitter on left ear

As shown in Table 12 and Table 13, the dispersion on channel gain can be considerable especially in anechoic chamber (large σ_{0S}), where the propagation occurs mainly by creeping waves on-body, line-of-sight and by a small reflection on the ground.

Moreover the path loss is stronger in the anechoic chamber, while in indoor the propagation occurs by multiple bounces (e.g. reflections, diffractions...) in the environment, which results into an additional energy contribution. This phenomenon is particularly clear when the receiving antenna is significantly masked by the human body. For instance in the Hip-Foot and Ear-Foot links, we measured a channel gain up to 10dB and 15dB stronger in the indoor environment. We can remark a more important dispersion in the Hip-Chest and Ear-Hip links, showing a significant variability of the human body. When the antennas are placed on torso, the propagation is mainly due to creeping waves and no "on-air" propagation occurs. Thus, in these kinds of scenarios the body shape and composition plays a more important role, which yields to a large σ_{0S}. Generally, by integrating over a larger bandwidth in (8), we obtain a smaller r_{0s} , with except for same cases in anechoic chamber and TX on Hip. As a consequence the results in lower UWB band are less dispersed than in the ISM (2.45 GHz) bandwidth, which was somewhat expected.

2.3.2 SHADOWING AND FADING MODEL

It is well-known that one can distinguish a slow fading component $S(t_n)$ and a fast one $F(t_n)$ in the time-dependent power transfer function:

$$P(t_n) = G_0 \cdot S(t_n) \cdot F(t_n) \quad \textbf{(18)}$$

We extracted from our measurements the slow fading component by applying a low pass filter, practically realized by averaging the time-dependent power transfer function on a sliding temporal window of length *W*=10:

$$S(t_n) \approx \frac{1}{W} \sum_{n-W/2}^{n+W/2} \frac{P(t_n)}{G_0} \quad \textbf{(19)}$$

The slow component is basically due to the shadowing by human body. As shown in Figure 5, the shadowing strictly depends on the movement condition. When the human subject does not move, the slow component is quite moderated since the shadowing condition basically remains identical. The shadowing also depends on the way of moving of each human subject. Figure 6 shows for instance that the amplitude of the slow component is larger in subject B than D, since one oscillates his arms more the other one, when walking.

The statistical analysis on the slow component has been carried out on the time dependent samples $S(t_n)\big|_{dB}$ of the whole population of the human subjects. It has been found that the shadowing in dB follows a normal distribution:

$$S(t_n)\big|_{dB} \sim N(0, \sigma_{sS}) \quad \textbf{(20)}$$

where the standard deviation σ_{sS} accounts for the slow variations of the power transfer function given by shadowing from human body, in a specific scenario.

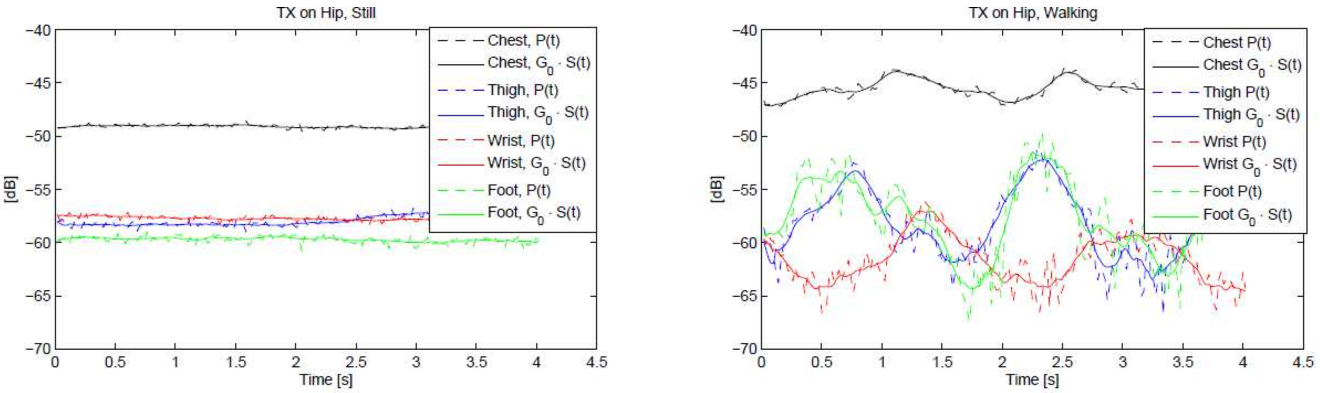

Figure 5: Time-variant power transfer function and slow fading in indoor: TX on Hip, 2.45 GHz band, still (left) and walking subject (right)

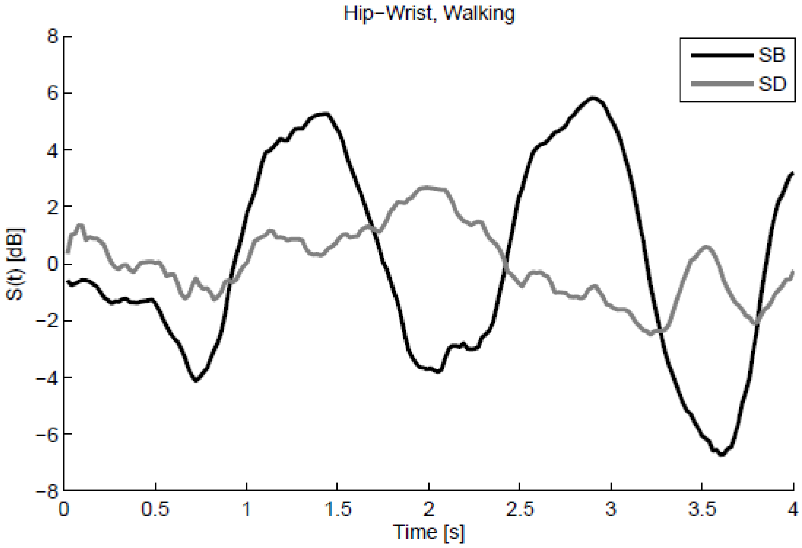

Figure 6: Shadowing for human subject B and D: Walking Hip-to-Wrist link

In Table 14 and Table 15, we list the values of σ_{sS} when TX is on hip and the left ear respectively. As expected, we have a larger standard deviation in moving scenarios. It is interesting to notice that the largest variations around the mean value have been found in the walking case. The standard deviation of the running subject is smaller than the walking one, since people tend to keep arms close to the body, limiting their oscillating movement. Similarly, the legs' movement is faster than in the walking scenario but, since the subject keeps standing on the same spot, the feet do not move backwards and forwards in a circular arc with respect to the body axis. As a consequence, the shadowing condition is less time-varying than in the walking scenario, which results into a smaller σ_{sS}. Moreover, the slow fading effect is smaller in indoor since the propagation occurs also by reflections on the surrounding environment, which somewhat mitigate the shadowing caused by the human body. The two random variables describing the channel gain and shadowing are obtained by statistical analysis on human body variability and human body movement, so that it is reasonable to consider that they are uncorrelated. As a consequence, the channel gain (in dB) presents a slow variation around the mean value μ_{0S}, which is described by a total variance $\sigma_{0S}{}^{2} + \sigma_{sS}{}^{2}$.

		TX on Hip			
		Chest	Thigh	R Wrist	R Foot
Anechoic	Still	0.6329	0.4269	1.0185	0.4564
	Walking	2.2892	5.4279	4.4565	5.2028
	Running	2.3997	2.5117	3.6504	2.8322
Indoor	Still	0.638	0.2578	0.2706	0.2593
	Walking	1.6049	3.486	2.7915	2.734
	Running	2.0977	2.0965	2.5062	1.8854

Table 14: Shadowing parameters TX on Hip

		TX on Left Ear			
		R ear	Hip	R Wrist	R Foot
Anechoic	Still	0.7205	1.1237	1.781	0.8133
	Walking	0.7293	2.1193	3.5141	4.4149
	Running	0.5409	2.9261	3.1742	1.7009
Indoor	Still	0.5768	1.5246	0.8373	0.7621
	Walking	0.9393	2.2444	1.8723	2.1241
	Running	0.7259	2.282	1.9811	1.3007

Table 15: Shadowing parameters TX on Ear

The shadowing effect discussed above, represents a large scale variation of the power transfer function which is mainly due to the masking effect by human body. Nevertheless, a fast fading component is also present, as depicted in Figure 5. Obviously, by integrating over a large bandwidth in (22) the fast fading is sensibly reduced. As a consequence, here we focus on the power transfer function at single frequency at 2.45 GHz. The bandwidth is implicitly the one employed in measurements, i.e. 10 MHz. The slow fading is extracted by applying a sliding temporal window.

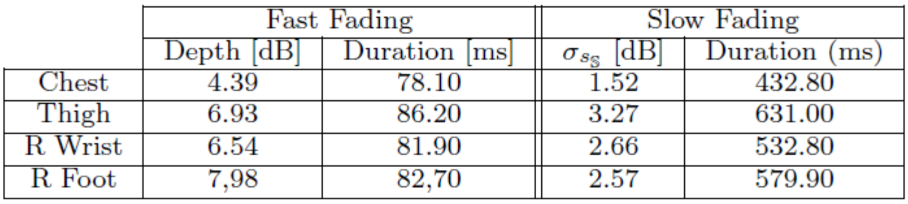

	Fast Fading		Slow Fading	
	Depth [dB]	Duration [ms]	σ_{s_S} [dB]	Duration (ms)
Chest	4.39	78.10	1.52	432.80
Thigh	6.93	86.20	3.27	631.00
R Wrist	6.54	81.90	2.66	532.80
R Foot	7,98	82,70	2.57	579.90

Table 16: Fading characteristics at 2.45 GHz (B =10 MHz): TX on Hip, Indoor, walking scenarios.

In Table 16, we report the slow and fast fading characteristics when the human subject walks in an indoor environment. The fading duration is computed as the average time below the mean value. Measurement results show that the fade duration can affect directly the single symbol transmission, while the shadowing can affect the packet one (Table 17).

Measurement results show that fast fading follows a Rice distribution:

$$pdf_\chi = \frac{\chi}{\sigma_\chi^2} \exp\left(\frac{-\chi^2 + \nu_\chi^2}{2\sigma_\chi^2} \right) I_0\left(\frac{\chi \nu_\chi}{\sigma_\chi^2} \right) \qquad \textbf{(21)}$$

where $I_0(\bullet)$ represents the modified Bessel function of the first kind with order zero, and ν_χ and σ_χ are the parameters of the distribution. Figure 7 shows the good agreement of data and the Rice model, in the walking and running scenarios.

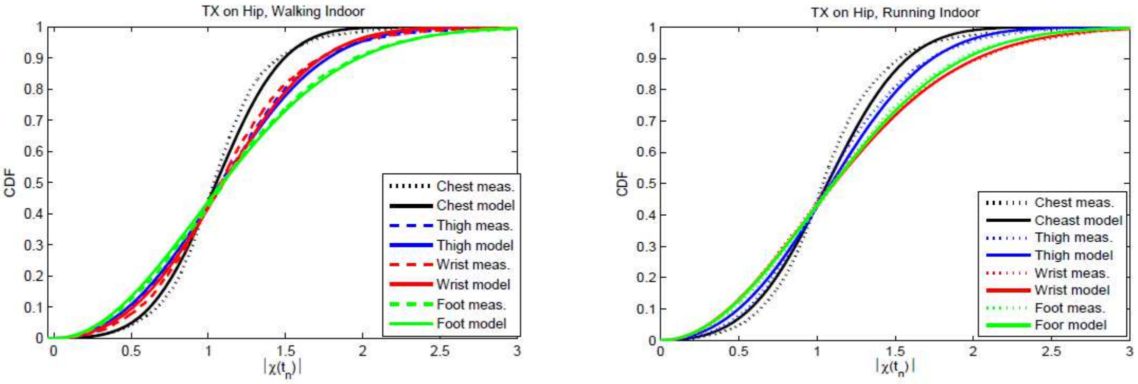

Figure 7: Fast fading distribution in indoor: TX on Hip, walking (left) and running (right).

In Table 17, we list the parameters of the Rice distribution of $|\chi(t_n)|$ obtained by Akaike method from measurement results. Results show a high k-factor ($K = \nu_\chi^2 / 2\sigma_x^{é}$) when the human subject does not move, which means that there is a main path with a strong energy contribution. As a consequence, the channel experiments a little fast fading, which is mainly due to involuntary breathing movements. In walking scenarios, the K-factor is low, which results in a more important fast fading. For instance in the Hip-Foot link, the nodes are often masked by the body and propagation occurs by reflections on surrounding environments. As a consequence, K-factor is close to 0 and we can approximate the fading statistic with a Rayleigh distribution.

	Still			Walking			Running		
	ν_χ	σ_χ	K	ν_χ	σ_χ	K	ν_χ	σ_χ	K
Chest	0,998	0,220	10,266	0,991	0,351	3,983	0,981	0,413	2,821
Thigh	0,999	0,210	11,328	0,923	0,566	1,331	0,944	0,533	1,568
R Wrist	0,998	0,114	38,424	0,962	0,519	1,720	0,001	0,943	0,000
R Foot	1,000	0,109	42,030	0,582	0,825	0,249	0,740	0,754	0,482

Table 17: Fading statistics at 2.45 GHz (B =10 MHz): TX on Hip, Indoor.

When moving from anechoic chamber to indoor scenario, the multi-paths coming from surrounding scatterers superpose to the purely on-body propagation (i.e.

diffraction on the body and transmission in line of sight). Since each multi-path component yields an energy contribution the mean channel gain increases, as shown in the previous section. On the other hand, increasing the number of multi-path gives out an enhancement of fast fading. This effect is directly transposed on the statistic of $|\chi(tn)|$. In Figure 8, we compare the K factor of the fast fading distribution in indoor and anechoic chamber. We can notice that the K factor in indoor is quite lower than in anechoic chamber, which describes a more important contribution of the non-line of sight components and consequently a larger fading.

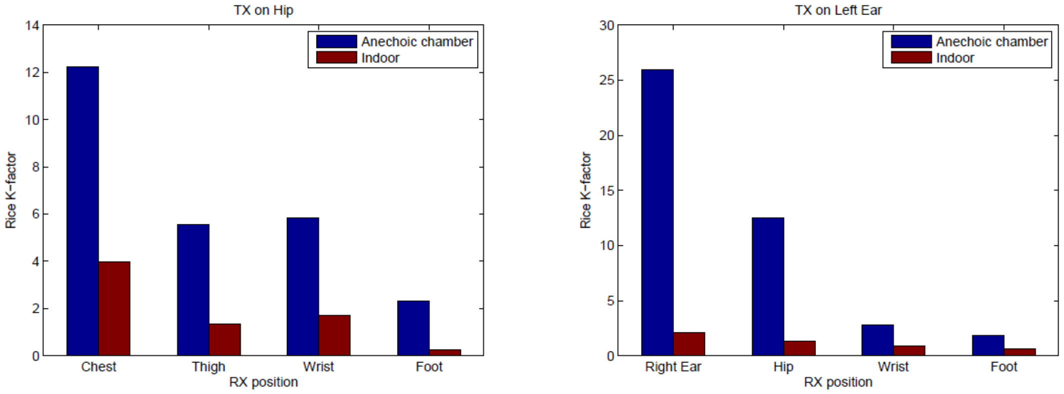

Figure 8: K factor in Walking scenarios: TX on hip (left) and on the left ear (right)

2.3.3 DELAY DISPERSION

In the previous sub-section, it has been shown that movement conditions produce slow variations of the power transfer function. The consequential effect on the Power Delay Profile (PDP) is a variation of the delay dispersion characteristics [38].

- *Delay dispersion characteristics*

The most common way to mathematically represent the channel is a time-varying linear filter characterized by its impulse response:

$$h(t_n;\tau) = \mathrm{G}_0 \cdot S(t_n) \cdot \sum_{k=1}^{K(t_n)} \alpha_k(t_n) e^{j\theta_k(t_n)} \delta(\tau - \tau_k(t_n)) \tag{22}$$

where $\alpha_k(t_n)$, $\theta_k(t_n)$, $\tau_k(t_n)$ denote respectively the amplitude, phase and arrival time of the *k*-th path. A common metric characterizing the delay dispersion is the delay spread:

$$\tau_{rms}(t_n) = \sqrt{\frac{\sum_{k=1}^{K(t_n)} |\alpha_k(t_n)|^2 \left(\tau_k(t_n) - \tau_m(t_n)\right)^2}{\sum_{k=1}^{K(t_n)} |\alpha_k(t_n)|^2}} \tag{23}$$

where $\boldsymbol{\tau}_m(t_n)$ is the mean delay. Here, we focus on the analysis and modeling of our measured results in the 3-5 GHz band. The path extraction has been performed up to achievement of the 90% of the CIR's energy, by considering a bin width of 1 ns of each multi-path component (MPC).

In Figure 9 we show the temporal evolution of the delay spread, together with the slow fading component, of the Hip-to-Wrist radio link, when the human subject is walking in an indoor environment. Each time sample corresponds to 20 ms. The arm oscillation causes a variation of delay spread from 194 ps to 23 ns according to the shadowing conditions. When the antennas are in Line-of-Sight (LOS) the energy is concentrated in a small number of paths, which yields to a less dispersive channel, i.e. lower delay spread, while in NLOS the power decreases and delay spread increases.

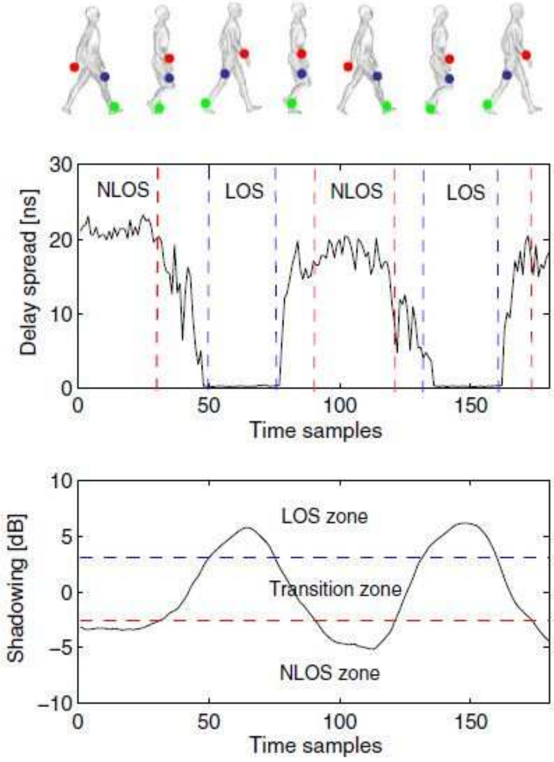

Figure 9: Hip-to-Wrist link in walking scenario : delay spread (up), shadowing (down)

This effect is clearly shown for the same scenario in Figure 10, in which the cumulated energy is depicted as a function of number of MPCs and the observation time. When the antennas are in LOS a very small number of MPCs is needed to achieve the 90% of the CIR's energy. Obviously the variation of the delay spread strongly depends on the type of movement and the antenna emplacement.

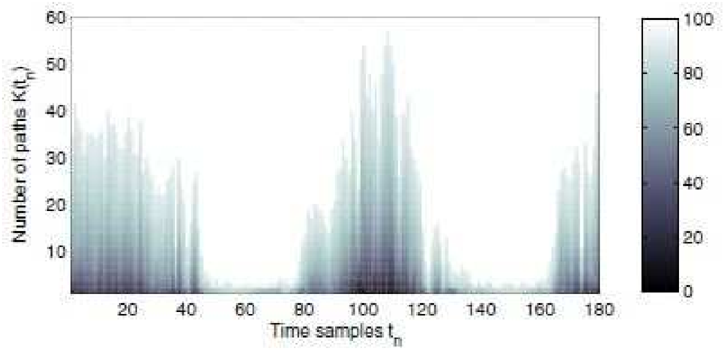

Figure 10: Percentage of cumulated energy as a function of the number of multi-path components

For instance, in the same walking scenario, the antenna on the chest experiments only a little slow fading, since the masking effect by the body is quite stable. As a consequence also the delay spread is quite stable during the walking cycle, as depicted in Figure 11. Generally we can identify three different operating zones according to antennas reciprocal position during the movement: LOS, NLOS and a Transition one. Nevertheless this distinction has more sense in scenarios where the channel experience high shadowing, such as the links with receiving antennas on the limbs.

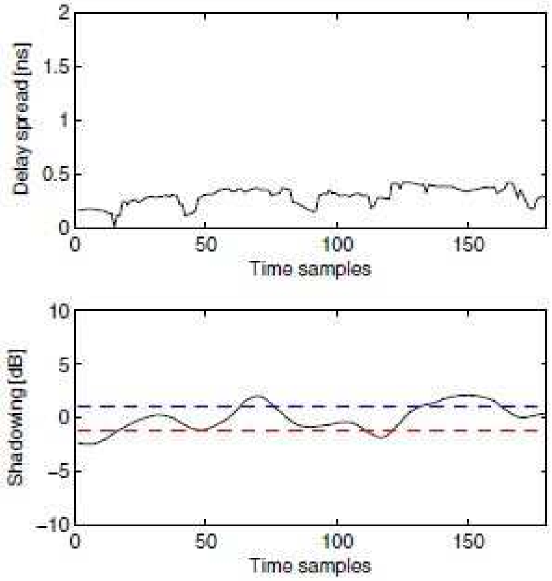

Figure 11: Hip-to-Chest link in walking scenario: delay spread (up), shadowing (down)

In Table 18 we report the measured delay spread in the indoor scenarios, when Tx is on the hip. When the human subjects do not move (i.e. "Still" scenario) the results on delay spread are quite similar in LOS and NLOS since there is no slow fading given by the movement. Similarly when the receiving antenna is on the chest, the shadowing is rather flat, so that the delay dispersion characteristics of the channel are unchanged even in moving conditions.

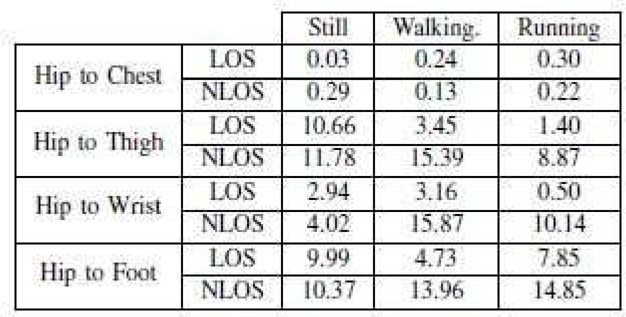

		Still	Walking	Running
Hip to Chest	LOS	0.03	0.24	0.30
	NLOS	0.29	0.13	0.22
Hip to Thigh	LOS	10.66	3.45	1.40
	NLOS	11.78	15.39	8.87
Hip to Wrist	LOS	2.94	3.16	0.50
	NLOS	4.02	15.87	10.14
Hip to Foot	LOS	9.99	4.73	7.85
	NLOS	10.37	13.96	14.85

Table 18: Delay spread in nanoseconds

- *Delay profile modeling*

The analysis carried out in the previous section shows that a unique PDP model is not suited to reproduce the characteristics of the on-body dynamic channel. Therefore we identify here different PDP models according to the scenario and the shadowing condition. As classically done in wide-band channel modeling [39], the path amplitude can be modeled by an exponential decay (t_n) and a Rician factor $\gamma_0(t_n)$:

$$\mathbb{E}[\alpha_k(t_n)|_{dB}] \propto \gamma_0(t_n) + 10\log_{10}\left\{\exp\left[-\frac{\tau_k(t_n)}{\Gamma(t_n)}\right]\right\} \tag{24}$$

Tab. II lists some of PDP characteristics, obtained by averaging the measured results over seven different human subjects. The average exponential decay Γ and number of paths K increase progressively when changing from a LOS to NLOS condition because of body movement. These results are somewhat dependent on the MPC extraction: for instance the number of MPCs K doubles when the cumulated energy threshold goes from 90% to 99%. In Fig. 5 we show the LOS and NLOS CIRs (normalized with respect to the first path) of the Hip-to-Wrist link for one human subject walking and the exponential decay extracted.

		LOS	Trans.	NLOS
Hip to Chest	Γ [ns]	25.9	-	-
	$\widetilde{\gamma_0}$ [dB]	3.37	-	-
	K	26	-	-
	Λ^{-1} [ns]	2.13	-	-
	σ_α	4.02	-	-
Hip to Thigh	Γ [ns]	24.9	46.7	58.9
	$\widetilde{\gamma_0}$ [dB]	2.1	1.6	1.6
	K	7	19	30
	Λ^{-1} [ns]	3.13	2.46	2.35
	σ_α	4.62	4.58	4.32
Hip to Wrist	Γ [ns]	22.3	45.5	63
	$\widetilde{\gamma_0}$ [dB]	2.3	2.7	2.5
	K	5	13	27
	Λ^{-1} [ns]	3.27	2.69	2.39
	σ_α	4.55	4.28	4.31
Hip to Foot	Γ [ns]	29	40.5	55
	$\widetilde{\gamma_0}$ [dB]	3.3	2.2	1.4
	K	10	23	32
	Λ^{-1} [ns]	2.98	2.37	2.21
	σ_α	4.57	4.61	4.65

Table 19: PDP decay: walking subject, Indoor scenario

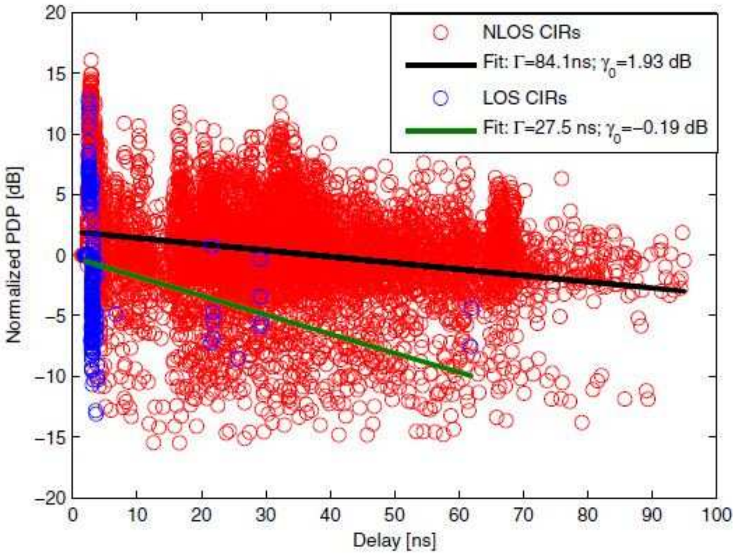

Figure 12: Example of CIRs and exponential decay

By defining the first MPC arriving at $\tau_0(t_n) = 0$, the inter-ray arrival delay can be modeled by a Poisson distribution:

$$p(\tau_{k,n}|\tau_{k-1,n}) = \Lambda \cdot \exp\left[-\Lambda\left(\tau_{k,n} - \tau_{k-1,n}\right)\right] \tag{25}$$

where we denote $\tau_{k,n} = \tau_k(t_n)$ for simplicity. The results reported in Tab. II show that the inter-arrival delays in the different zones are only slightly different. This is due to the fact that this characteristic is basically related to the surrounding environments, since a part of MPCs comes from scatterers out of the body.

According to the arrival time, each component of the normalized PDP has a mean value given by (24). The variation around this mean value can be described by a normal distribution:

$$\alpha_k(t_n)|_{dB} \sim \mathcal{N}(\mathbb{E}[\alpha_k(t_n)|_{dB}], \sigma_\alpha) \qquad (26)$$

Actually in most of scenarios, a Nakagami distribution should fit as well as the normal distribution. The results show a $\sigma_{\uparrow}$ which has almost the same value in the three different zones. For instance, in Figure 13 we depict the normalized amplitude of the MPCs in LOS ans NLOS in the Hip-to-Wrist channel, when the human subject is moving. Basically, to properly model the PDP the main parameters are the decay factor $\widetilde{\Gamma}$ and the mean number of paths $\widetilde{K}$.

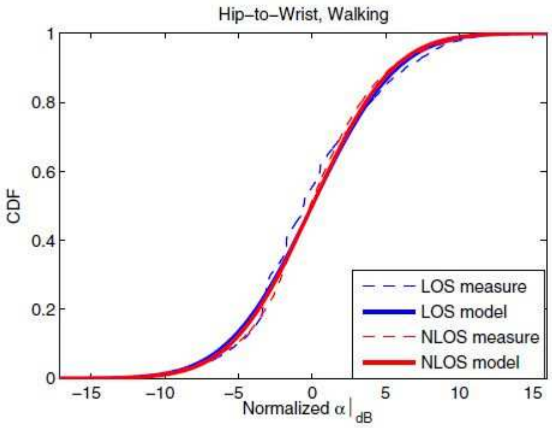

Figure 13: Normalized MPC amplitude in Hip-to-Wrist channel

2.3.4 SPACE-TIME SLOW FADING CORRELATION

In cooperative networks, if the quality of communication is too low on a radio link, one can hop to a second link which presents a higher SNR with respect to the first one. This idea can also be used in BANs when different sensors are placed on-body. Obviously, one has to estimate the correlation between two different links, which undergo to different shadowing effects. To this aim, for a given scenario S, the correlation coefficient has been computed as follows:

$$\rho_{i,j} = \frac{E\left[\left(S_{TX,i} - E\left[S_{TX,i}\right]\right)\left(S_{TX,j} - E\left[S_{TX,j}\right]\right)\right]}{\sqrt{E\left[S_{TX,i}^2 - E^2\left[S_{TX,i}\right]\right]E\left[S_{TX,j}^2 - E^2\left[S_{TX,j}\right]\right]}} \qquad (27)$$

where $S_{TX,i}$ represents the slow fading component in dB in the radio link associated to the TX transmitting antenna position and *i*-th receiving antenna position. The statistical mean operator E has been applied on the samples $S(t_n)\big|_{dB}$, relative to the considered link, of the whole population of human subjects. So that the correlation coefficient defined above is obtained by a statistical analysis on the time-variant slow fading.

In Figure 14 we present the correlation coefficients at 2.45 GHz in indoor environments when transmitting antenna is on the Hip. Measurement results in anechoic chamber are not reported for sake of briefness, but they show that the correlation is only slightly higher than in indoor. This can be explained by the fact that only propagation around the body and reflection on the ground are present in anechoic chamber, but body movement is mainly responsible of slow fading. Shadowing correlation is relatively high when the human body does not move. Nevertheless the small value of σ_{sS} reduces the correlation significance in Still scenarios.

The scenarios which present high shadowing (generally when one antenna is on a limb) present the highest correlation. For instance in walking scenarios the Hip-Wrist, Hip-high and Hip-Foot are strongly correlated. It is very interesting to see that correlation is inverted for Wrist/Thigh and Wrist/Foot. This is due to the fact that the receiving antennas are all on right limbs while the transmitting antenna is on the left side. During a walk, humans tend to alternate the movement of legs and arms. As a consequence, shadowing on right wrist is the opposite of shadowing on right thigh and right foot, while shadowing on foot and thigh follow the same temporal behavior (as depicted in Figure 14).

This macro effect is verified in both anechoic and indoor environments. Finally in running scenarios the shadowing on limbs are more correlated than shadowing on chest, but generally less correlated than in walking scenarios. This is due to the fact that the human subjects have less control on the synchronism of movements, which results into a higher asynchronism of shadowing thus a lower correlation.

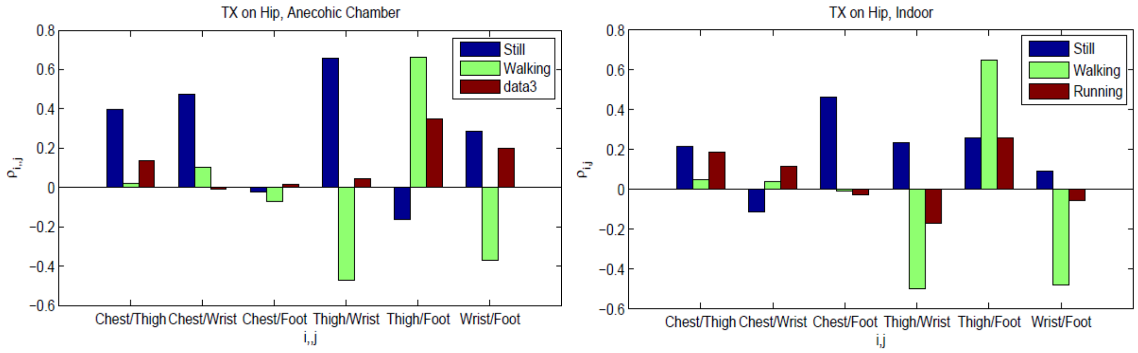

Figure 14: Correlation coefficients: TX on Hip

In order to describe the temporal evolution of shadowing, here we use an Auto-Regressive (AR) model:

$$\sum_{p=0}^{P} a_p \widehat{S}(n-p) = \mathcal{E}(n) \tag{28}$$

where $\widehat{S}(n)$ represents the estimation of shadowing, in dBs, which is given by a linear combination of the past *P* outputs plus a zero-mean white noise input $\epsilon(n)$. The weights a_p on the *P* past outputs minimize the mean-square prediction error of the autoregression $var(\epsilon)^2$. Here the Yule-Walker method has been used to extract the AR model of the shadowing of the Hip to Limbs channel in Walking scenarios (Table 20). So to generate *N* simultaneous shadowings, one uses the filter coefficients for the desired on-body channels. Each system is then driven by *N* correlated zero-mean Gaussian white noise, which variance $var(\epsilon)$ has been obtained by AR modeling. These *N* correlated noises are obtained by Cholesky factorization of the shadowing correlation matrix. An example of results of AR model is reported in Figure 15: Example of measured correlated shadowing (up) and its AR model (down): the output of the filter respects the same statistical properties of the two correlated shadowings.

Once the simultaneous correlated, slow fading components have been generated, one can use the appropriate PDP model according to the shadowing zone. Nevertheless the choice of the PDP model should be ambiguous, especially for what concerns the parameter $\widetilde{K}$. The number of MPCs follows a certain regularity according the shadowing conditions, as depicted in Fig. 3. In Figure 16Figure 16: MPCs vs. Shadowing in the Hip to Wrist channel the number of MPCs as a function of the shadowing value is depicted for the Hip-to-Wrist channel. An exponential dependence of $K(t_n)$ versus $S(t_n)|_{dB}$ has been found for most of scenarios:

$$K(t_n) = \exp(m \cdot S(t_n)|_{dB} + m_0) \tag{29}$$

Thus once the correlated shadowing on each node is generated, the mean number $\widetilde{K}$ can be obtained from (8) by using the parameters reported in Table 21. Then, the PDP can be obtained from the parameters reported in Tab. II with except of $\widetilde{K}$.

Channel	a_0	a_1	a_2	a_3	a_4	a_5	a_6	a_7	a_8	a_9	a_10	$var(\mathcal{E})$
Thigh	1.0000	-1.2675	0.1123	0.0723	0.0362	0.0038	0.0459	0.0089	0.0326	0.0086	-0.0234	0.1157
Wrist	1.0000	-1.2272	0.0520	0.0522	0.0266	0.0198	0.0523	0.0257	0.0152	0.0075	-0.0000	0.0439
Foot	1.0000	-1.2828	0.1198	0.0780	0.0453	0.0120	0.0265	0.0251	0.0247	0.0300	-0.0380	0.0821

Table 20: Coefficient of the AR model in walking scenarios, TX on hip

Channel	$\rho_{i,j}$			m	m_0
Hip to Thigh	1,00	-0,51	0,65	-0.2431	2.601
Hip to Wrist	-0,51	1,00	-0,48	-0.2491	2.1588
Hip to Foot	0,65	-0,48	1,00 1	-0.2266	2.8305

Table 21: Shadowing correlation and exponential decay of $K(t_n)$ vs. $S(t_n)|_{dB}$, in walking scenario, TX on Hip

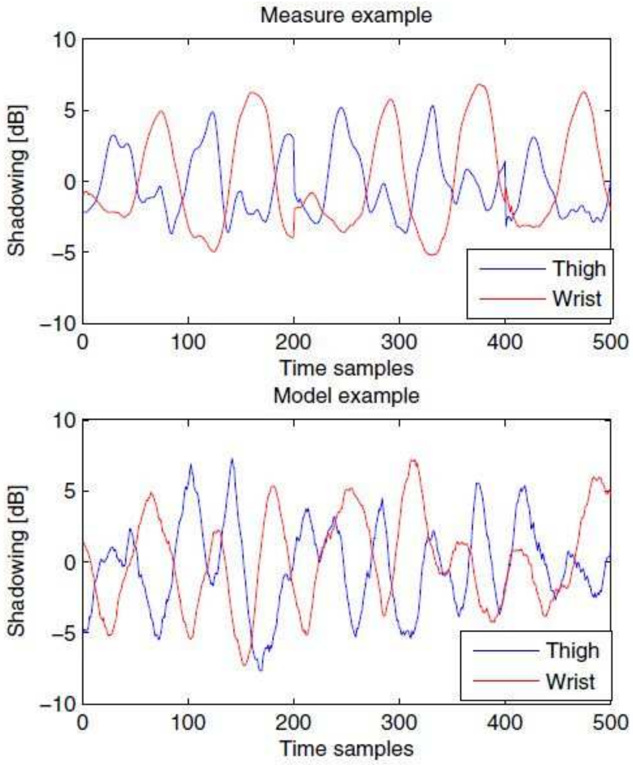

Figure 15: Example of measured correlated shadowing (up) and its AR model (down)

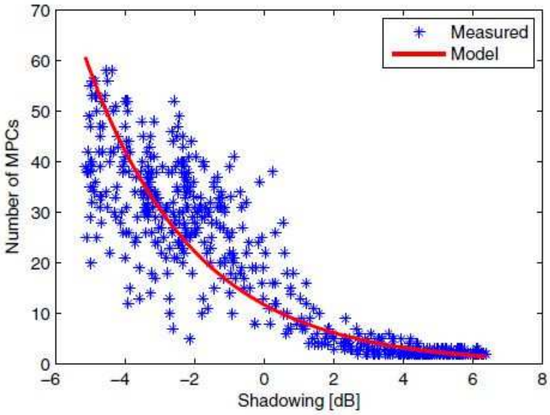

Figure 16: MPCs vs. Shadowing in the Hip to Wrist channel

2.3.5 DOPPLER SPECTRUM MODELING

In classical time-variant channel models, the mobility is often taken into account by a movement of the receiving antenna at speed v with respect to the transmitting one.

By considering that a small movement, corresponding to a time separation Δt, the amplitude and phase of the k-th MPC can be considered constant, while the phase variation is $\left(2\pi/\lambda\right)\cdot v\cdot\Delta t\cdot\cos\phi_k$. In the case of isotropic scattering, the received signals come from all directions with equal probabilities. The isotropic scattering model, also known as the Clarke's model, corresponds to the uniform distribution for the angle of arrival $\phi_k\in[-\pi,\pi[$. This assumption and hypothesis of uncorrelated scatters (US) yields to the classical Jake's bath-tube like Doppler spectrum[40]. Previous works on indoor channel with fixed antennas and moving scenarios have highlighted Doppler behaviour different from the Jakes/Clarke model [41][42] . In these scenarios, the time variance of the channel is given by the people movement in the environment where the fixed antennas are placed. The Doppler spectrum in this case is centred around a mean value at 0 Hz and can be modeled by a Laplacian distribution [43].

In BANs, the antennas are placed on-body and the human subject is set free to move. The scatters are given by the surrounding environment and the human body itself. In practical situations, the antennas reciprocal positions do not vary significantly, while the scatters position, with respect to the TX-RX link, can change with the human movement. Thus, the on-body channel can be assumed, in a first approximation, as a fixed TX-RX situation with moving scatters, producing the time variance of the channel. This assumption is quite correct when both transmitting and receiving antennas are placed on the torso or on the same limb, or more generally, when there is a slight movement of the receiver antenna with respect to transmitter (e.g. Hip-Foot link, and arm swinging). In these cases, the Doppler function is centred at $\nu =$ 0Hz.

In anechoic chamber no scatters are present with except the body itself. In Figure 17, we show the normalized Doppler Spectra at 2.4 GHz, when the human subject walks in anechoic chamber. When one antenna is on the torso and the other on a moving limb, the distance between TX and RX can change slightly. However, the velocity of the receiving antenna with respect to the transmitting one is very low, and the time-variance is mainly given by the varying position of the scatters. As a consequence the Doppler function is still centred at ν = 0, but it presents a smoother behaviour, as shown in Figure 17.

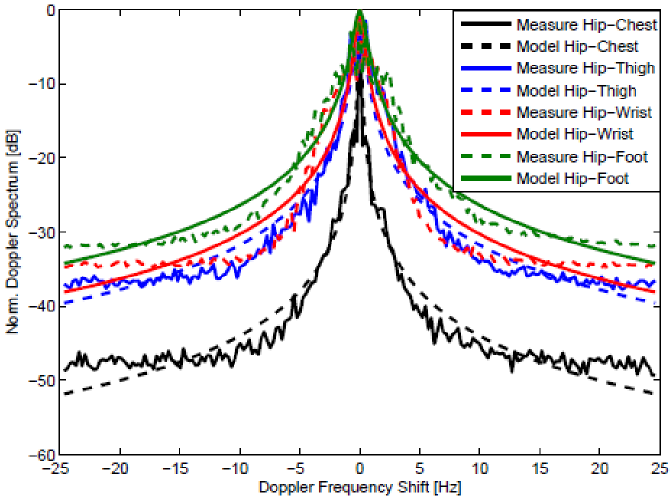

Figure 17: Normalized Doppler Spectra: human walking in anechoic chamber

The difference between the levels of the floor when the receiving node is on the chest, with respect to the nodes on the limbs, can be explained by the increased degree of mobility in the latter case. Given this behaviour of the Doppler spectra it is useful to identify the bandwidths with respect to a threshold, e.g. -20 dB below the peak value at 0 Hz, instead of the maximum Doppler Shift. In Table 22 we list the results obtained from our measurements in anechoic chamber.

A rigorous mathematical formulation of Doppler spectrum from moving scatterers has been recently given in [44]. By assuming uniform scattering pattern and independence of scatterers, the Doppler spectrum can be decomposed by Bessel and Legendre functions. Instead of Laplacian distribution a simplified expression of the normalized Doppler spectrum can be the following:

$$D_{ON-BODY}(\nu) = \frac{1}{\gamma + \nu^2} \qquad \textbf{(30)}$$

In Figure 17 we show the good approximation of this model with the measurement results, by using the values of listed in Table 22. A small value of γ represents a modest degree of mobility, as in the Hip-Chest, Ear-Ear and Ear-Hip links.

Radio link	BW_{-20dB}[Hz]	γ
Hip-Chest	1.5	0.004
Hip-Thigh	6.4	0.067
Hip-Wrist	7.3	0.094
Hip-Foot	10	0.231
L. Ear-R. Ear	0.3	0.013
L. Ear-Hip	1.3	0.007
L. Ear-Wrist	8	0.574
L. Ear-Foot	12.6	0.862

Table 22: Doppler Bandwidth at -20 dB and model parmeter of on-body Doppler

Some important differences can be noticed when moving from the anechoic scenario to a realistic one. In Figure 18 we show the normalized average power of effective scattering distribution, for the Hip to Wrist channel in walking scenarios. When the human subject is in anechoic chamber, since no off-body scatterers are present, most of energy is concentrated around 3ns, which is close to time-of-flight between the node locations. The effective scattering distribution presents a high peak at the frequency Doppler ν = 0. When human subjects are in indoor environment, we can clearly identify some off-body scatterers, far away from the on-body ones. It is interesting to notice that the presence of these scatterers yields to no-symmetric scattering distribution. This is mainly due to the fact that the antennas are placed on the front side of the body. As a consequence the scatterers in a half space behind the body are strongly masked by the shadowing of the body itself.

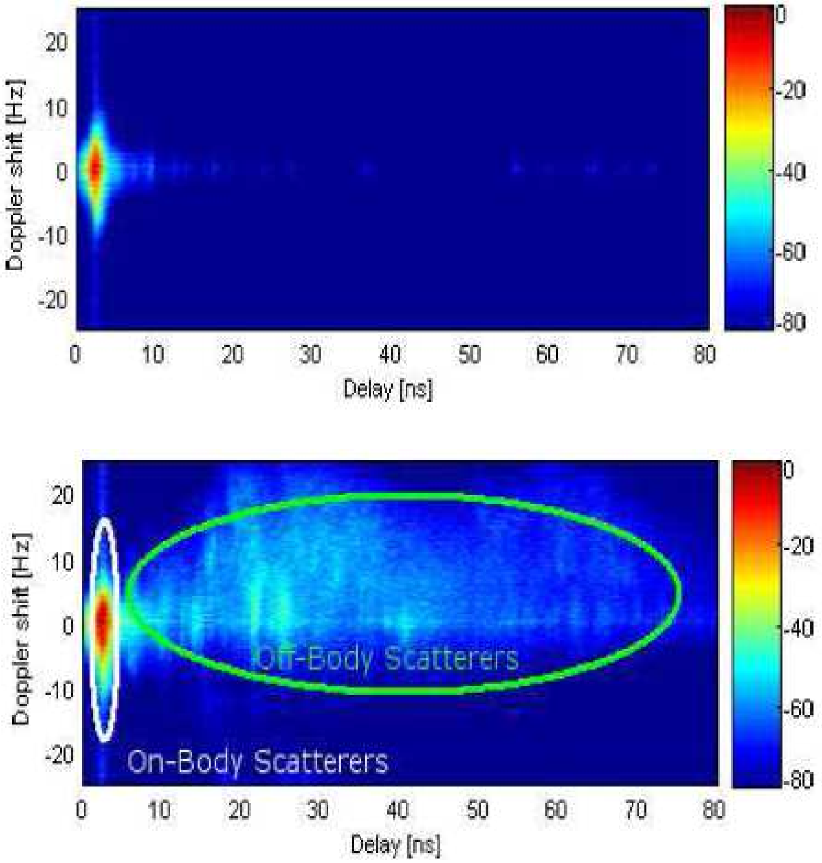

Figure 18: Average power of effective scattering distribution in dB: Hip-Wrist link walking in anechoic chamber (up) and in office environment (down)

As depicted in Figure 19, the effect on the Doppler spectrum is a component at around 10 Hz when the Tx is on the Hip. This frequency is related to mobility of the human subject, who walks at about v = 0.7m/s. Since both transmitting and receiving antennas are moving at the same time, the equivalent Doppler shift is twice the maximum shift at the frequency of interest. When the transmitter is on the Left Ear, the shadowing effect from the body is different and the angular distribution of the off-body scatterers is not concentrated in half space like in the previous scenarios. As a consequence a Doppler component at positive frequencies is not present, and the main effect of on-body scatterers is to enlarge the -20 dB Doppler band around 0 Hz.

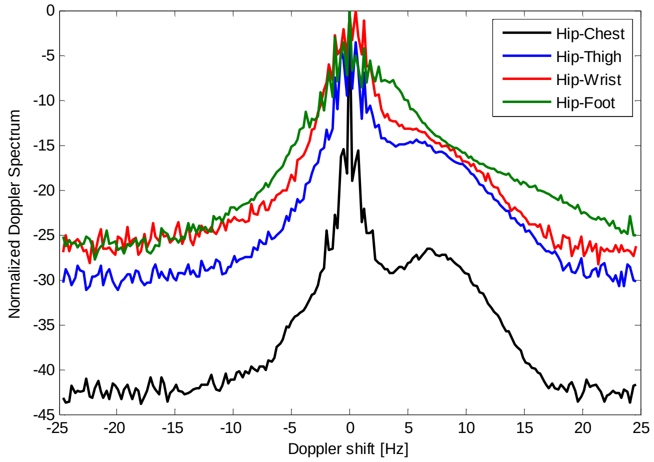

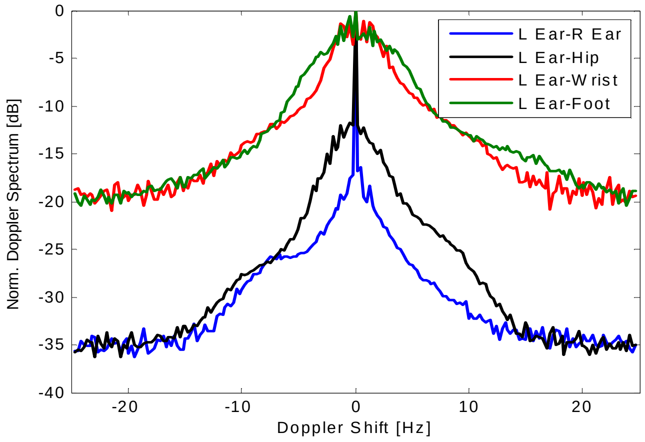

Figure 19: Normalized Doppler Spectra by human walking in anechoic chamber: TX on Hip (up), TX on Left Ear (down)

When a well-identified Doppler component is present, like in the on Hip scenario, it is possible to separate the off-body scatterer Doppler contribution from the purely on-body one. In these cases, one can express the total Doppler Spectrum as the combination of two independents factors:

$$D_{TOT}(\nu) = D_{ON-BODY}(\nu) \cdot D_{OFF-BODY}(\nu) \tag{31}$$

where $D_{ON-BODY}$ is the component related to the on-Body scatterers, as in (28), and $D_{OFF-BODY}(\nu)$ to the off-body ones. Obviously the factorization of these two components is a strong approximation, but it yields to a simple model. In the scenarios with TX on the Hip, it was found that the off-boy presents a Gaussian shape in dB:

$$D_{OFF-BODY}(\nu)\Big|_{dB} = D_0 \cdot \exp\left[\frac{(\nu - \nu_m)^2}{2\sigma_\nu{}^2}\right] \tag{32}$$

In Figure 20 we show the good agreement between measurements and the model expressed in (29). Table 23 lists the parameters of Doppler Spectrum for some scenarios in indoor on-body channels. It is interesting to notice that the off-body component presents in all scenarios a mean value around 10 Hz, showing some reproducibility of the effect of the off-body scatterers.

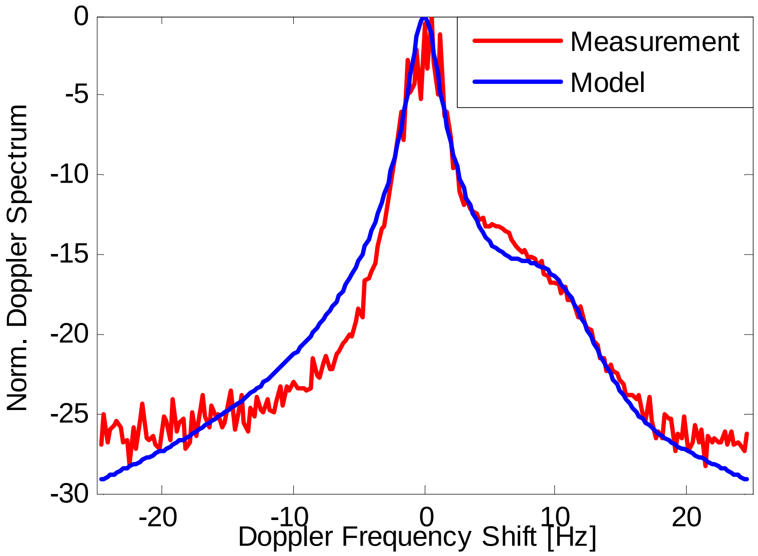

Figure 20: Normalized Doppler Spectra: human walking in Indoor, Hip- Wrist Channel

Radio link	γ	D_0	ν_m [Hz]	σ_ν [Hz]
Hip-Chest	0.0017	8.178	9	2
Hip-Thigh	0.358	4.920	10	3
Hip-Wrist	0.74	4.924	10	3
Hip-Foot	1.091	2.952	12	5

Table 23: Doppler parameters in indoor

The knowledge of Doppler Spectrum allows the quantification of how much broadening is imposed on the spectrum of signal, according to the rate of change in the channel state. In multi-path scenarios, the Doppler shift of each path can be different from that of another path, which results into a Doppler spreading. The Doppler spread can be used to evaluate the time-variance of the channel and estimate the coherence time at 0.5 correlation threshold and shown in Figure 21, [45].

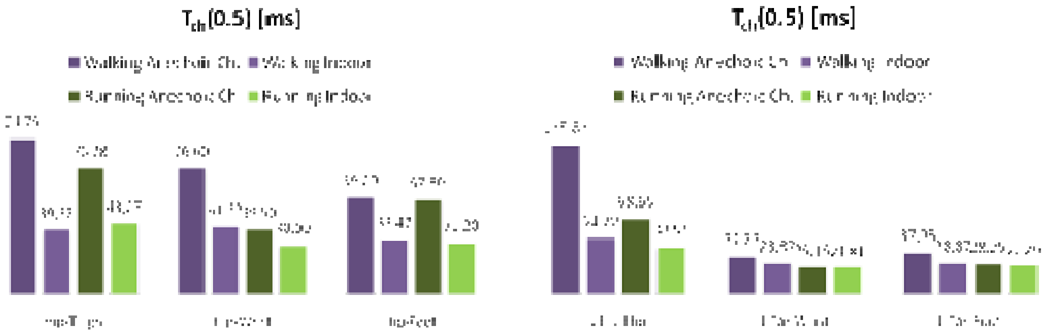

Figure 21: Coherence time: TX on Hip (left), on Ear (right)

2.3.6 ANTENNA POLARIZATION INFLUENCES

In order to study the influences of the polarization, another measurement campaign has been carried out at CEA [46]. The measurement scenarios are similar to those presented in the previous sub-sections. Two different sets of antennas have been used: Top Loaded (TL) Monopole antennas presenting a normal polarization with respect to the body surface, and Planar Loaded (PL) Monopole antennas presenting a tangential polarization. More precisely, for each set of measurements, the same kind of antenna (TL or PL monopole) has been used for the transmitter and the receivers.

The numerical results presented in **Table 24**, **Table 25** and **Table 26** are useful in order to make some comparative considerations between the two different sets of antennas, and the influence of the environments where the measurements have taken place.

		Tx Heart Top Loaded Monopole				**Tx Heart Planar Monopole**			
		Quasi-anechoic chamber		*Indoor Office*		*Quasi-anechoic chamber*		*Indoor Office*	
	Rxs	μ_{OS} *[dB]*	σ_{OS} *[dB]*	μ_{OS} *[dB]*	σ_{OS} *[dB]*	μ_{OS} *[dB]*	σ_{OS} *[dB]*	μ_{OS} *[dB]*	σ_{OS} *[dB]*
Walking	Right Thigh	-38,45	1,06	-38,65	1,15	-66,77	3,35	-62,72	2,41
	Rigth Hand	-47,07	2,16	-49,47	1,2	-63,87	6	-60,15	5,79
	Left Hand	-43,86	2,46	-42,97	3,19	-60,42	4,35	-58,35	1,5
	Left Ear	-48,62	3,62	-46,82	4,57	-61,06	5,18	-60,48	3,5

Sitting/ Standing	Right Thigh	-39,45	1,59	-41,04	1,44	-63,96	5,36	-58,02	3,61
	Rigth Hand	-46,54	2,46	-47,73	4,6	-58,41	2	-56,06	4,89
	Left Hand	-43,52	2,35	-43,02	2,76	-54,62	3,07	-56,21	3,53
	Left ear	-48,34	2,43	-43,47	1,98	-63,07	2,72	-59,13	4,47
Standing Still	Right Thigh	-38,75	0,92	/	/	-68,34	4,92	/	/
	Rigth Hand	-46,58	1,69	/	/	-66,25	6,17	/	/
	Left Hand	-42,12	1,87	/	/	-62,43	2,36	/	/
	Left Ear	-45,01	1,36	/	/	-60,96	2,27	/	/

Table 24: Channel Gain values for scenarios where Tx is placed on Heart

		Tx Left Hip - Top Loaded Monopole				Tx Left Hip - Planar Monopole			
		Quasi-anechoic chamber		*Indoor Office*		*Quasi-anechoic chamber*		*Indoor Office*	
	Rxs	μ_{OS} [dB]	σ_{OS} [dB]	μ_{OS} [dB]	σ_{OS} [dB]	μ_{OS} [dB]	σ_{OS} [dB]	μ_{OS} [dB]	σ_{OS} [dB]
Walking	Right Thigh	-38,78	2,06	-38,4	1,17	-63,85	2,4	-60,77	4,89
	Rigth Hand	-52,09	4,58	-53,09	2,89	-67,54	7,5	-61,69	6,9
	Left Hand	-40,32	3,17	-40,74	4,32	-50,38	1,08	-49,62	2,95
	Left Ear	-47,24	2,02	-48,3	2,69	-68,45	5,4	-64,26	3,3
Standing Still	Right Thigh	-42,78	2,26	/	/	-61,17	1,06	/	/
	Rigth Hand	-48,35	4,8	/	/	-68,97	1,29	/	/
	Left Hand	-34,52	1,37	/	/	-47,59	2,4	/	/
	Left Ear	-46,77	1,46	/	/	-69,77	3,63	/	/

Table 25: Channel Gain values for scenarios where Tx is placed on Left Hip

		Tx Right Ear - Top Loaded Monopole				Tx Right Ear - Planar Monopole			
		Quasi-anechoic chamber		*Indoor Office*		*Quasi-anechoic chamber*		*Indoor Office*	
	Rxs	μ_{OS} [dB]	σ_{OS} [dB]	μ_{OS} [dB]	σ_{OS} [dB]	μ_{OS} [dB]	σ_{OS} [dB]	μ_{OS} [dB]	σ_{OS} [dB]
Walking	Right Thigh	-55,13	3,29	-57,57	1,84	-72,53	5,96	-67,01	2,77
	Rigth Hand	-53,82	3,92	-53,31	3,19	-64,61	4,49	-59,18	2,27
	Left Hand	-66,59	4,98	-57,57	0,91	-74,89	2,63	-65,67	4,63

	Left Ear	-35,81	0,82	-37,01	2	-58,54	6,05	-54,67	4,73
Sitting/ Standing	Right Thigh	-56,77	2,99	-57,78	2,56	-72,27	3,58	-65,93	4,41
	Rigth Hand	-54,2	2,97	-55,18	1,95	-61,83	5,41	-61,22	2,5
	Left Hand	-61,52	3,62	-58	1,52	-73,82	3,26	-64,79	3,63
	Left ear	-36,33	1,56	-36,43	2,08	-57,41	8,28	-55,44	6,33
Standing Still	Right Thigh	-53,82	1,99	/	/	-76,22	3,05	/	/
	Rigth Hand	-49,92	2,47	/	/	-67,77	2,47	/	/
	Left Hand	-66,87	3,43	/	/	-78,83	2,05	/	/
	Left Ear	-33,69	0,81	/	/	-68,02	4,12	/	/

Table 26: Channel Gain values for scenarios where Tx is placed on Right Ear

First of all, it is possible to remark how the path loss is generally stronger when PL Monopole have been used, comparing to the case with TL Monopole, as shown in Figure 22. As expected, the antenna with normal polarization with respect to the body surface (TL Monopole) is more suited for On-Body applications, supporting the creeping-waves propagation over the body. This leads to higher values in terms of channel gain up to 22-25dB with respect to the ones found for tangentially polarized antennas (PL Monopole). This effect is particularly evident for those channels with a strong on-body propagation component and where no "on-air" propagation occurs, such as Heart-Thigh, Hip-Thigh and Ear-Ear links.

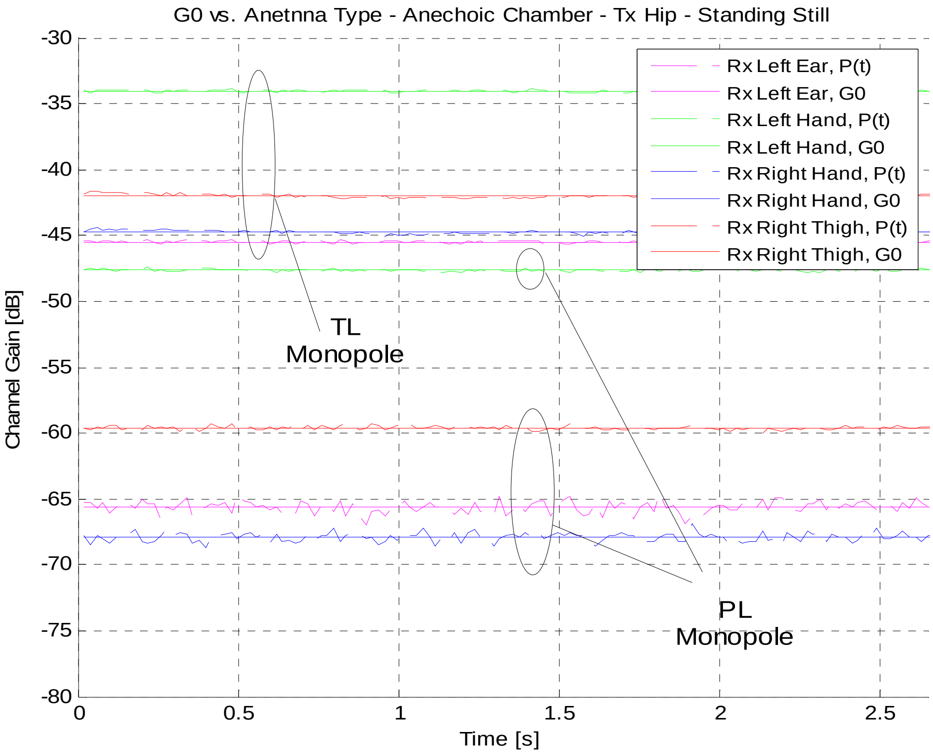

Figure 22: G_0 comparison for different antenna sets

For PL Monopoles, it could also be pointed out that the dispersion on the channel gain is relevant especially in quasi-anechoic environment, where the σ_{0S} values are larger than those found for the indoor scenario. Same considerations could not be drawn for the TL Monopole case, where the standard deviations are generally smaller than in the former case and the difference between indoor and anechoic environment is not so stressed. This is due to the fact that the presence of a ground plane makes the antenna less influenced but the human body.

The different behaviour of the two sets of antennas in respect with the environment considered could be explained assuming that in anechoic chamber the propagation occurs mainly by creeping waves on-body and small reflection on the ground, and these phenomena affects more the performances of tangentially polarized antennas, like the PL Monopole, than those of antennas with normal polarization.

For the PL antennas, it could also be noticed that the mean path loss is stronger in the anechoic chamber than in indoor, because in the latter environment the multi-paths contribution due to reflections and diffractions from the environment is very significant, leading to an additional energy contribution. This trend is more evident when one of the nodes composing the link is considerably masked by the human body. For instance, channel gain stronger up to 10 dB in indoor than anechoic chamber have been measured for the Right Ear-Left Hand channel, where the whole body shadows the communication.

For the same reasons explained above, this is not at all valid for the TL Monopoles, where all the scenarios present almost the same values for the channel gain. A graphical example is given in Figure 23.

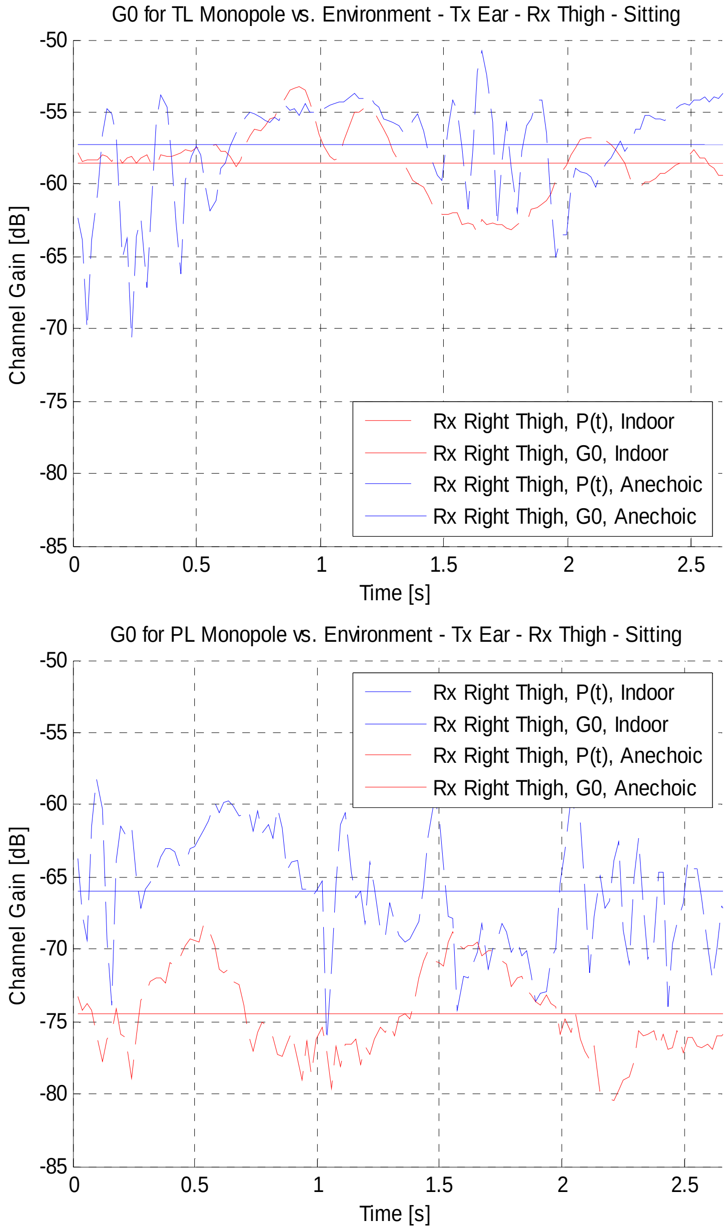

Figure 23: G_0 values in different environment for PL Monopole (up) and TL Monopole (down)

3. OFF-BODY AND BODY-TO-BODY CHANNEL MODELS

Even if a lot of efforts have been put on the study of propagation dynamics and channel characteristics for on-body communications, *body-to-body* (or *inter-body*) as well as *off-body* channels have been little investigated. Hereafter, a general overview on the proposed channel models for these scenarios is given.

3.1. OVERVIEW

- *Body-to-body communications*

Some research teams realized different measurement campaigns in order to collect data to characterize the *inter-body* channel. In particular, S.L. Cotton and W.G. Scanlon from the Queen University of Belfast performed the statistical description of the dynamic body to body communications at 2.45GHz. They considered a scenario representative of indoor sweep and search operations for fire and rescue personnel where four subjects move in a building, one of them held the transmitter device while the other three played the role of the receivers . The authors demonstrate (see Figure 24) that the k-μ distribution is able to provide a good fit to the distribution of small-scale fading for all the considered links, in comparison to other statistics such as Nakagami, Lognormal, Rice and Weibull.

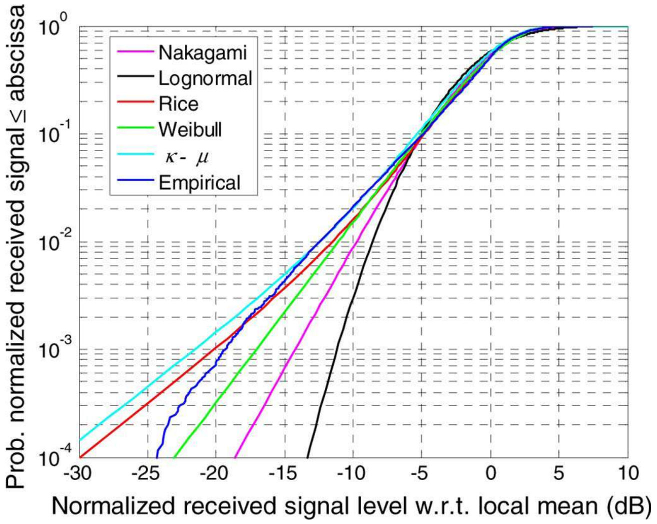

Figure 24: Fading distribution in body-to-body channel

Considering also the low cross correlation and comparable mean signal levels characterizing the received signals, the idea of employing spatial diversity to improve channel performance could be an interesting option.

Similar conclusions on diversity are presented in [49] and [50] even if measurements have been carried out wideband at the carrier frequency of 5.5GHz in an indoor environment. Considering the classical distance-dependent path loss model, the authors propose an inter-BAN channel model where the shadowing is best described by a Log-normal distribution and the path loss exponent results to be always smaller than 2.

Another statistical description of the inter-BAN channel is given in [51] and [52]. The authors investigated propagation characteristics in the frequency band centred at 2.45 GHz and 5.8 GHz through an extensive measurement campaign involving two subjects (one with the transmit antenna and the other equipped with the receiving devices) in an office environment. The users were positioned at different distances between each other, performing various random activities with random body orientations. Variations of the channel path gain was found to follow a gamma distribution with mean and variance values following a power law in respect to the distance between the two BANs, the rate of decrease resulted to be almost independent of the considered frequency, while more related on the device on-body position.

Moreover, the short-term fading turned to be described by a Rican distribution with K-parameter depending more on the on-body position of the antenna than on the distance, while the long-term fading followed either a gamma distribution (when the distance between the subjects remains constant) or a lognormal one (if the distance also changes randomly). For this distribution, the mean and the variance decrease with the distance following a power law with a rate of decrease almost independent from the frequency band but strictly related to the antenna position.

Investigations on the UWB have been performed by the Institute for Infocomm Research of Singapore [53]. Collecting data in an anechoic chamber environment for two subjects standing at various distances with different body orientations, the authors found that the path loss, calculated through the classical distance-dependent formula, was strongly related to the devices on-body emplacement as well as to the relative position of the human bodies.

Hanlen et al. performed some measurements focusing on coexistence problems when multiple BANs are co-located [54][55]. Since none of the networks has the right to stop the transmission of the others, they obviously mutually interfere, and this could lead to a severe degradation of the performances of the reference network. Collecting the RSSI values of all the investigated links (reference and interferer), the authors found that the interference signal power is dominated by factors which are not related to the distance but regard mostly subject movements, both local (e.g. arm swinging) and global (i.e. walking or running). Moreover, results show that Signal-to-Interference Ratio (SIR) could be low or even negative, since the interferers were often more powerful than the reference link because of the great shadowing effect of the human body that could lead to power absorption up to 60dB.

Authors also wandered if the reference and the interferer links were sufficiently independent, such that it would be possible to measure them separately and later combine them. The computation of correlation coefficients has revealed that the two signals are generally uncorrelated and also statistically independent when considered over large periods of time (order 100’s of seconds). Differently considering short intervals, the two channels may show correlation, in particular when the subject movement is not the main source of channel dynamic and hence it varies slowly. The answer to the initial question remains still open, since the correlation between interferers and reference signal is strongly related to the subject instantaneous activity.

Ray-Tracing methods have also been used recently in [56]for *off-body* and *body-to-body* communications. The 2D scenario considered in this work does not take into account the environment around the bodies and the latter are modeled as closed cylindrical surfaces with constitutive parameters chosen based on the "Muscle" model. This approach could represent a powerful building block in the perspective of modeling inter-BAN communications (i.e. at least the part which does not involve an interaction with the environment).

Differently from that, in [57] and [58] Cotton and Scanlon present a novel approach to simulate dynamic soldier-to-soldier signal propagation using jointly an animation-based technology, in order to take into account real body movements (Poser7 software tool), a computer generated environmental model (AutoCAD software package from Autodesk), and a commercial ray-launching engine to perform channel prediction. The reference scenario, in this case, was that of millimetre-wave (60GHz) soldier-to-soldier communication for counter-insurgency cordon and sweep operations. Authors simulated the field of action and the realistic movement of a team of four soldiers to extract important channel metrics such as root mean square, angle of arrival and delay spread.

In [59] the same team of researchers realised a simulated study of the co-channel inter-BAN interference at 2.45GHz and 60GHz. Using an accurate CAD model of an indoor location together with a human body model obtained through the use of Poser7 animation software and a full 3D ray-launching simulator tool, the authors found that on-body communications at 2.45GHz were heavily susceptible to interference caused by undesired signal reception from other nearby BANs, while operating at the 60GHz frequency generally provides mitigation of co-channel interference, allowing a greater number of networks to co-exist.

- *Off-body communications*

One of the first attempts in giving a complete insight on the *off-body* channel characteristics has been done by Ziri-Castro et al. in [60]. The authors presented a comparison between measured data and simulations of a narrowband 5.2GHz radio channel for two indoor scenarios (a corridor and an office). The measurements involved one fixed transmitter and one receiver placed on the hip of a subject walking towards (LOS conditions) and away (Non-LOS conditions) from the transmitting antenna, whereas the simulations were performed using a three-dimensional image-based propagation prediction technique. The use of a simulation tool seemed to be appropriate for LOS case but revealed some inaccuracies in NLOS situations. Statistical analysis on small-scale fading proved a good fitting with Rayleigh (signal level below the mean) or Lognormal (signal level above the mean) distribution for the corridor environment, whereas in the office case the Lognormal statistic turned to be the best one.

The research group at the Queen's University of Belfast performed a set of experiments in order to extract a channel model for off-body communications at the frequency of 868MHz [61][62][63] and [64]. Measurements have been done considering several receiving antennas placed on the subject's body, different environments (i.e. anechoic chamber, open office and hallway), LOS and NLOS conditions and a walking movement.

Data analysis pointed out how both antenna positioning and human body movement play an extremely important role in indoor propagation characteristics for wearable systems. Moreover, it has been verified that Nakagami-m distribution provides the optimum fit for the majority of the off-body propagation channel investigated in both anechoic and indoor multipath environments. This distribution turned out to be suitable for the considered scenarios as, differently from other distribution like Rice or Rayleigh, it does not assume scattered components of equal amplitude. Level Crossing Rate (LCR) and Average Fade Duration (AFD) were also provided, which are well described by Nakagami second order statistics.

In [64] the cross correlation level between fading experienced at different body locations was also evaluated, the low values found suggest the idea that a spatial diversity combining scheme could improve significantly the system performances.

A similar experiment is presented in [65], the authors perform a measurement campaign collecting real time channel responses at the carrier frequencies of 820MHz and 2.36 GHz for a subject equipped with two antennas and standing still in front of a fixed RX antenna, just changing body orientation and the relative distance or performing a walk towards the receiving device.

Different statistics have been compared in order to find the one that best describes the received signal amplitude; overall, the Lognormal distribution provides the most reliable fit for both the considered bands (see Figure 25).

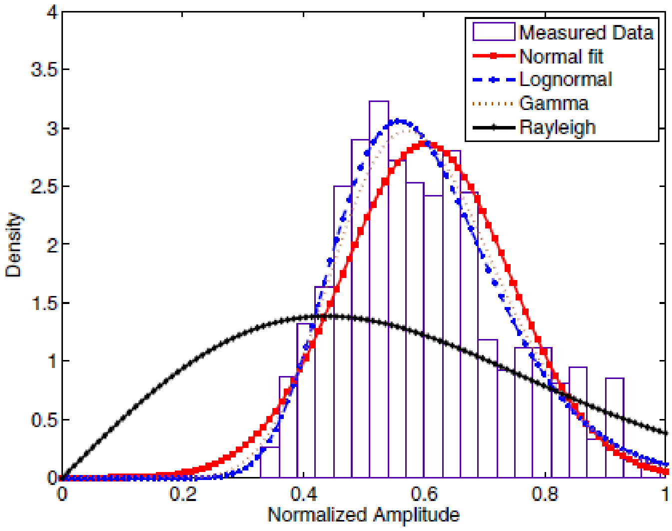

Figure 25: Fading distribution of off-body channel

In order to evaluate the channel stability, the authors introduced a new parameter called channel variation factor and calculated as the ratio between the standard deviation and the root mean square power of a channel response sequence. Off-body BAN channel turned out to be quite stable, more at 802MHz than at 2.36GHz, with a coherence time reasonably of the order of tens of milliseconds; on-body device position also played a significant role in the channel temporal stability.

Considering the great advantages that the use of UWB could bring to the system performances in terms of reduction of multipath fading, possibility of reaching high data rates and decrease of the operative power, some researches have also been performed focusing on the characterization of the channel at these frequencies.
Goulianos et al. from the University of Surrey [66][67][68], proposed to model the off-body communication channel with a multi-slope Path Loss equation obtained from the study of propagation mechanisms around the body (creeping waves) combined with the traditional distance-dependent Path Loss formula.
Based on the measured data, statistical channel parameters have been extracted with respect to both the radial coordinate ϱ, denoting the distance between the transmitter and the body centre, and the body orientation angle Θ_A, which is formed by the lines connecting the body centre to the transmitter and to the on-body antenna respectively.
Mathematically the model could be expressed as:

$$L(\rho,\theta_A)=\begin{cases} L_0(\rho)-n_\theta(\theta_A)(\theta_A-\theta_0), & 0\le\theta_A\le\theta_{AL}(\rho) \\ L(\theta_{AL})-n_\theta(\theta_A)[\theta_A-\theta_{AL}(\rho)] & \theta_{AL}(\rho)\le\theta_A\le\theta_{AS}(\rho) \\ L(\theta_{AS})-n_\theta(\theta_A)[\theta_A-\theta_{AS}(\rho)] & \theta_{AS}(\rho)\le\theta_A\le\pi \end{cases} \tag{33}$$

where $L_0(\varrho)$ is expressed by:

$$L_0(\rho)=L_0(\rho_0)+10n_\rho\log_{10}\left(\frac{\rho}{\rho_0}\right) \tag{34}$$

and Θ_{AL} and Θ_{AS} are the breaking point angles, that are defined as the angle after which the decay coefficient $n_\Theta(\Theta_A)$ changes its arithmetic value. These angles indicate respectively the passage from the lit zone and from the shadow region of the transmitter. Power delay profile analysis and modeling were also performed.

Focusing on a real hospital environment in [69] the authors present a measurement campaign for stationary and mobile UWB off-body channels. Measurements were made using RF-over-fibre technology to eliminate unwanted electromagnetic effects associated to the use of co-axial cables. The results show that Received Signal Strength (RSS) values depend on whether transmitting and receiving antennas are in relative line of sight or non line-of-sight conditions. For mobile tests, both LOS and

NLOS cases tend to have log-normally distributed fading with the latter having significantly lower mean signal strength. In stationary conditions, signal strength results also dependent on user orientation, with difference between standing and sitting in the same location.

3.2. STANDARDIZED CHANNEL MODELS

• *CM4 for 2.5GHz*

In the IEEE 802.15.6 standard, CM4 channel model address the body surface to external scenarios. The following path loss measurements have been performed at frequency of 2.36GHz for sleeping position on a bed and in a bedroom. Details of the measurement set up, derivation and data analysis can be found in [70]. Table 27 summarizes the results.

The transmitter is placed on the chest and the receiver is away from the body with various distances as outlined.

	LOS				NLOS			
Distance (m)	1	2	3	4	1	2	3	4
Standing	53.81	53.12	56.04	64.72	61.81	68.64	60.12	63.10
Walking	44.46	51.59	52.14	60.81	59.48	70.30	63.98	62.56

Table 27: CM4 channel model for 2.4GHz

The first-order statistics fit with off-body sleeping channel data, where the data has been normalized to mean of each link data set. The gamma distribution is the best fitting distribution type for this data, apart from overall sets, non-normalized, which is lognormal.

The second-order statistics fit with off-body sleeping channel data. Lognormal is the best fitting distribution type for channel outage distribution (linear magnitude values) for this data.

• *CM4 for UWB*

Measurements for the UWB frequency band of 3.1 – 10.6 GHz have also been carried out [71] to propose an UWB channel model in 802.15.6 standard for off-body communications. The measurements were done in an office environment. The transmitting antenna was fixed near to wall, while the receiving antenna (placed on the body) positions were changed in office area. The effect of ground is considered in the measurements. The further detail on set-up, derivation and data analysis can be found in [71]. Table 28 summarizes the results for different body orientation with respect to the transmitter.

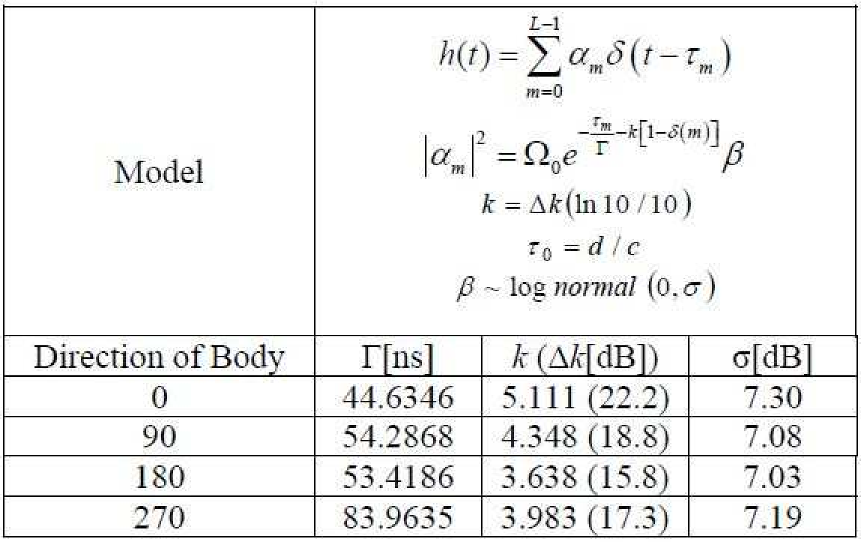

Model	$h(t)=\sum_{m=0}^{L-1}\alpha_m\delta(t-\tau_m)$ $\lvert\alpha_m\rvert^2=\Omega_0 e^{-\frac{\tau_m}{\Gamma}-k[1-\delta(m)]}\beta$ $k=\Delta k(\ln 10/10)$ $\tau_0=d/c$ $\beta\sim \log normal\ (0,\sigma)$		
Direction of Body	Γ[ns]	k (Δk[dB])	σ[dB]
0	44.6346	5.111 (22.2)	7.30
90	54.2868	4.348 (18.8)	7.08
180	53.4186	3.638 (15.8)	7.03
270	83.9635	3.983 (17.3)	7.19

Table 28: CM4 channel model for UWB

- $h(t)$: complex impulse response
- L : number of arrival paths, modeled as Poisson random variable with mean equal to 400
- a_m : amplitude of each path
- τ_m : timing of path arrivals, modeled as Poisson random process with arrival rate λ=1/(0.50125 ns)
- k : effecti of K-factor (NLOS)
- Ω_0 : path loss (can be assumed as free space)
- d : Tx-Rx distance
- c : light velocity

3.3. CEA OFF-BODY CHANNEL INVESTIGATIONS

Previous measurement campaigns have been carried out at CEA for the investigation of narrow band channels at 2.45GHz for off-body communications [46]. Thus, we present in this section a space-time varying channel model, where one end of the communication is stationary and placed outside the human body, while the other one is located on it in a specific position and moves according to the wearer movements.

The main idea that stands behind the analysis performed is to model the channel gain ($G_{|dB}$) extracting a main component dependent on the distance ($G_{0|dB}$) and/or on the angle between the body and the external gateway, plus a random variable ($F_{|dB}$) that accounts for the movement of the subject and the environment considered, defining in that way a sort of fading contribution.
The model could be represented through the following equation:

$$G(d)_{|dB} = G_{0|dB} + F_{|dB} = G(d_0)_{|dB} + 10n\log_{10}(d/d_0) + F_{|dB} \qquad \textbf{(35)}$$

where d_0 is the reference distance equal to 1 m.

3.3.1 DISTANCE-DEPENDENT MODEL: LOS AND NLOS CONDITIONS

In order to extract the distance dependent component of the channel gain ($G_{0|dB}$) some distance-discrete measurements have been performed.

The LOS condition represents the scenarios where the subject stands in front of the external gateway acting as the transmitter, and the angle α set between the body and the Tx antenna is considered equal to 0°.

On the contrary, in NLOS condition the subject stands with his backside facing the external transmitter, so that the body completely shadows the transmission, and α is set to 180°.

The characterization of $G_{0|dB}$ is achieved extracting from the data acquired the values of $G(d_0)_{|dB}$ and n, this last one considered as the path loss exponent. Figure 26 shows a graphical example of the analysis performed.

The vertical sets of crosses represent the data acquired during the measurements at each distance (from 1 to 4 meters far from the Tx with a resolution of 0.25 m), while the continuous line is the log-distance fit that allows the evaluation of $G(d_0)$ and n for each link.

Just looking at the graphs, it is possible to drawn some general considerations: in the LOS case the dispersion of the acquired samples at a fixed distance is very limited, meaning that there is a main direct path that leads the propagation. On the opposite, NLOS scenarios are characterized by a significant dispersion of the data, up to 10-12 dB in indoor, due to the fact that the propagation occurs mainly by reflections or diffractions on the body (if in anechoic chamber) and/or on the surrounding environment (if in indoor).

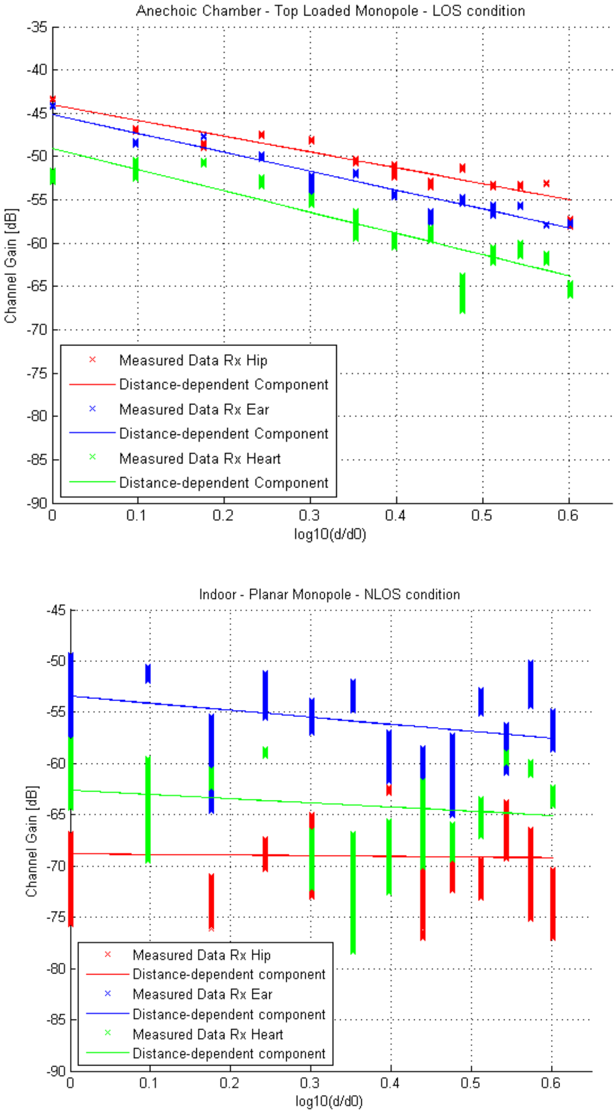

Figure 26: $G_{0|dB}$ *trends* for TL Monopole LOS conditions (up) and PL Monopole NLOS conditions (down)

Table 29 and Table 30 give an overview on the results obtained respectively for the Planar Monopole and the Top Loaded Monopole cases and for all possible scenarios.

Planar Monopole								
	Quasi-Anechoic Chamber				Indoor			
	LOS		NLOS		LOS		NLOS	
	n	*G(d₀)*	*n*	*G(d₀)*	*n*	*G(d₀)*	*n*	*G(d₀)*
Rx Right Ear	-2,2	-63,48	-2,2	-51,69	-1,47	-50,24	-0,69	-53,43
Rx Heart	-1,99	-41,75	-1,8	-72,46	-2	-38,92	-0,4	-62,62
Rx Left Hip	-1,61	-50,11	-0,9	-69,09	-2	-51,94	-0,1	-68,78

Table 29: G0 characterisation: $G(d_0)$ and n values for Planar Monopole antennas

Top Loaded Monopole								
	Quasi-Anechoic Chamber				Indoor			
	LOS		NLOS		LOS		NLOS	
	n	$G(d_0)$	*n*	$G(d_0)$	*n*	$G(d_0)$	*n*	$G(d_0)$
Rx Right Ear	-2,18	-45,14	-2,07	-45,82	-1,62	-45,7	-2,96	-46,03
Rx Heart	-2,44	-49,11	0	-71,42	-1,37	-54,71	0	-66,33
Rx Left Hip	-1,83	-43,99	-0,24	-66,48	-1,99	-47,67	-0,59	-61,33

Table 30: G0 characterisation: $G(d_0)$ and n values for Top Loaded Monopole antennas

The values presented in the tables could suggest some general considerations: the LOS case in anechoic premises presents a value of the path loss exponent *n* around -2, depending on the specific position of the receiver. This is in line to what has been expected, considering that for this scenario the propagation is mainly due to a Line of Sight component in the free space whose *n* value is commonly assumed to be equal to -2. The slight differences found could be referred to the body effect, the antenna used and the on-body position.

In indoor it is necessary to take into account the influence of the specific environment, and this could explain the higher variability of path loss exponent around the free space reference value.

In NLOS conditions, *n* generally assumes smaller values than in the LOS case; this is reasonable considering that when the body completely shadows the transmitting antenna from the receivers, the communication occurs mainly by multi-paths and there is no more main dominant LOS path. Naturally, this trend is more evident in indoor condition where the influence of the environment leads to a more significant multipath component. In this case, *n* presents values around 0, meaning that the randomness of different contributions to the propagation globally remove the distance dependence.

As far as the $G(d_0)$ value is concerned, when the user passes from LOS to NLOS condition the path loss could increase significantly, with a difference up to 31 dB in anechoic chamber. In indoor premises this phenomenon is still present even if slightly less intense with a channel gain decrease up to 23 dB.

In general, Top Loaded antennas present lower values for the channel gain (up to 8dB less in anechoic and 7dB in indoor), but the trend is not confirmed by the link with the Rx on Heart. This phenomenon supports the idea that the specific node location and the antenna type play an important part in the definition of the channel characteristics. In particular, when the TL monopole is on the heart or on the hip, the LOS path is in radiation pattern null, which gives higher losses.

When the antenna is on the Ear the TL monopole presents a non-null radiation pattern in both LOS and NLOS case. This evidently affects the propagation in a different way, and explain why $G(d_0)$ has very close values in both LOS and NLOS.

In order to complete the characterization of the Off-Body channel, the fading component *F(t)* has to be extracted and then statistically described.
Firstly, the distance dependent component previously described has been verified through the comparison with the data acquired in dynamic walking conditions (LOS and NLOS) both in anechoic and in indoor. Figure 27 shows the good agreement between the dynamic acquisitions and the fit for $G_{0|dB}$ extracted from the distance discrete measurements.

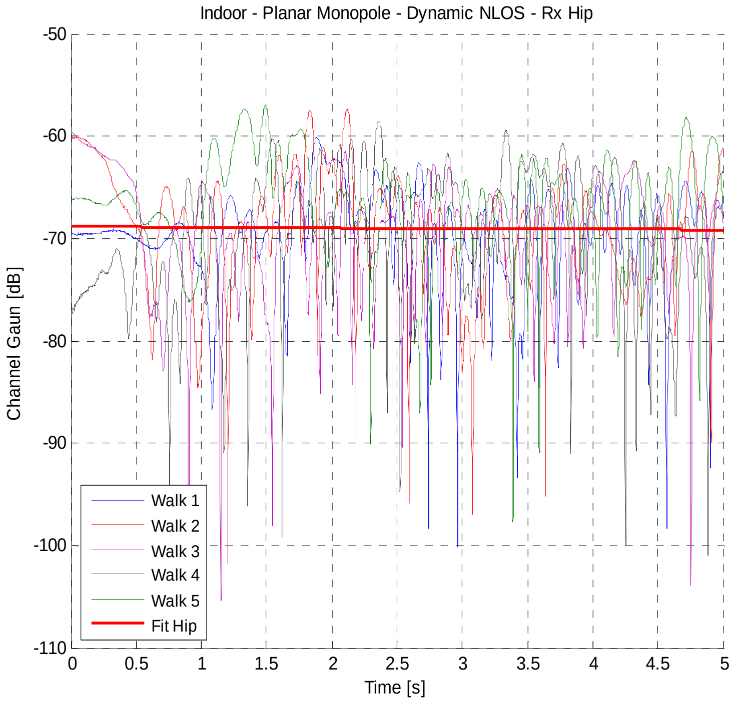

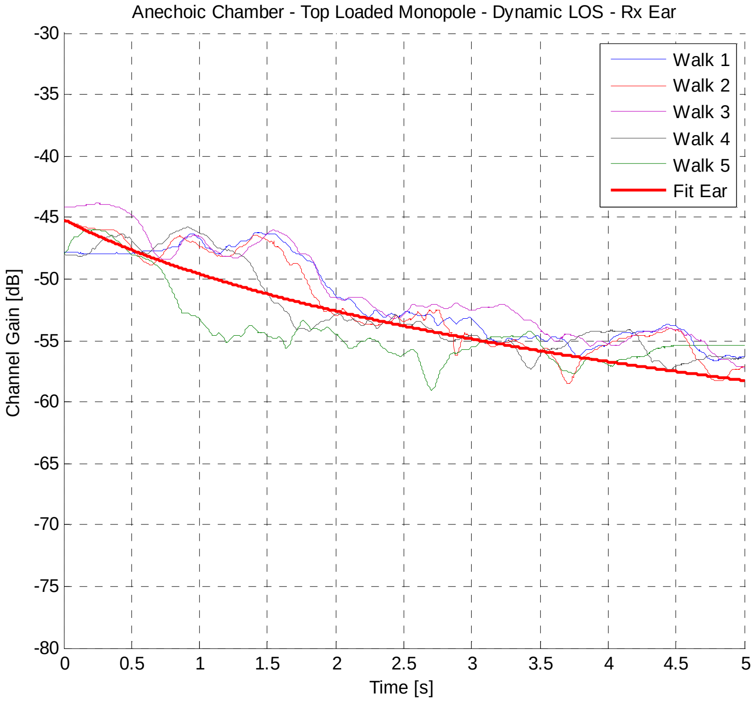

Figure 27: Comparison between the fit to distance-dependent component and dynamic acquisitions

Then, the fading component has been computed subtracting the $G_{0|dB}$ component from the continuous measurements; considering that *F(t)* could be expressed as $F(t) = |\chi(t)|^2$.

Measurements results show that $|\chi|$ follows a Nakagami distribution, which is defined through a shape and a spread parameters, respectively μ and w. A graphical example of the data fit to the proposed distribution is shown in Figure 28 for two different scenarios.

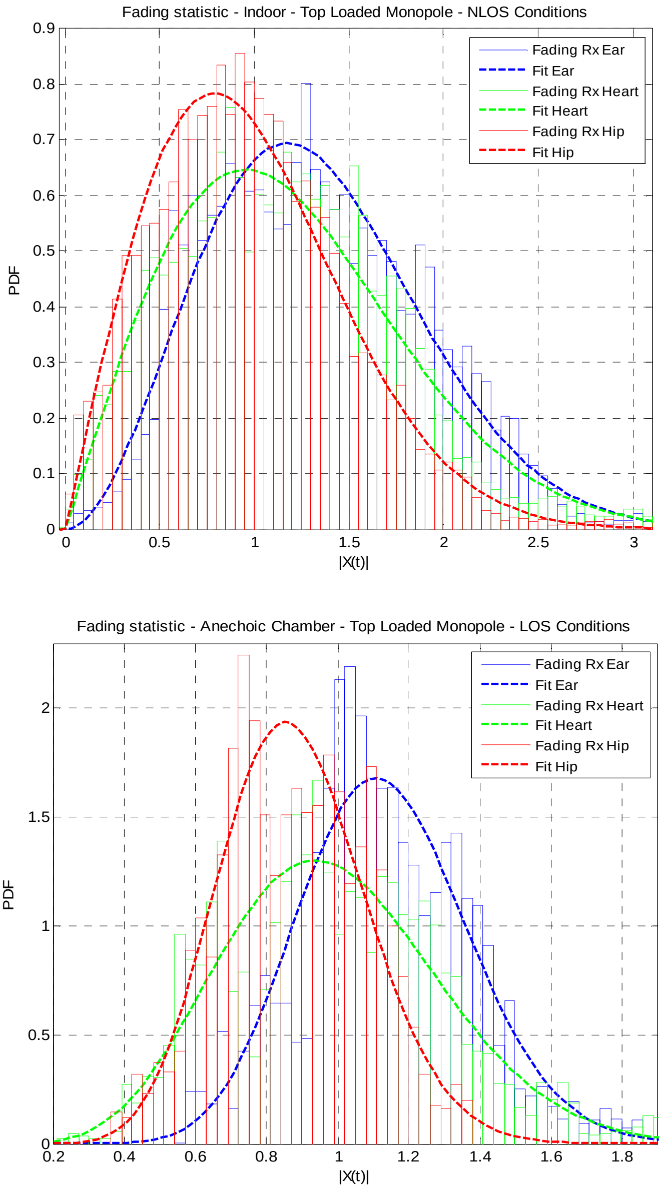

Figure 28: Cumulative distribution function of the fading data F(t): NLOS (up) and LOS (down) for TL Monopole

The study has been performed for all the possible scenarios combining the two antennas types, the different environments and the propagation conditions (LOS and NLOS). Table 31 and Table 32 present the whole sets of results obtained for the statistical characterization of the fading, as well as the mean duration of the fade in ms, its mean depth in dB and the rate of appearance in s^{-1}.

	Fading statistics - Planar Monopole										
		LOS Conditions					*NLOS Conditions*				
	Rxs	μ	*w*	*Rate* $[s^{-1}]$	*Duration [ms]*	*Depth [dB]*	μ	*w*	*Rate* $[s^{-1}]$	*Duration [ms]*	*Depth [dB]*
Anechoic Chamber	**Rx Right Ear**	1,04	0,66	2	0,41	-3,33	7,62	1,66	0,75	0,18	-1,06
	Rx Heart	12,02	1,52	0,5	0,23	-0,83	1,42	2,02	7,7	0,04	-6,11
	RxLeft Hip	11,43	1,04	1,35	0,36	-1,01	5,28	2,12	0,8	0,07	-1,6
Indoor	**Rx Right Ear**	2,11	0,98	4,3	0,14	-6,77	1,24	2,09	4,55	0,07	-7,85
	Rx Heart	5,48	0,73	1,65	0,5	-3,38	0,81	1,12	5,35	0,11	-12,24
	RxLeft Hip	2,61	2,06	2,75	0,06	-5,83	0,92	1,91	6,25	0,07	-11,55

Table 31: Fading statistics for Planar Monopole Antenna

	Fading statistics – Top Loaded Monopole										
		LOS Conditions					*NLOS Conditions*				
	Rxs	μ	*w*	*Rate* $[s^{-1}]$	*Duration [ms]*	*Depth [dB]*	μ	*w*	*Rate* $[s^{-1}]$	*Duration [ms]*	*Depth [dB]*
Anechoic Chamber	**Rx Right Ear**	5,83	1,34	1,3	0,21	-1,01	9,96	1,14	2,35	0,17	-0,8
	Rx Heart	2,74	1,08	1,05	0,5	-3,63	1,15	1,88	1,75	0,27	-5,69
	RxLeft Hip	4,68	0,81	1,5	0,47	-1,8	0,82	0,8	2,1	0,36	-7,5
Indoor	**Rx Right Ear**	2,15	0,76	3,4	0,22	-7,4	1,46	2,1	4,15	0,08	-7,16
	Rx Heart	1,28	1,45	3,2	0,14	-8,89	1,02	1,79	6,25	0,07	-10,71
	Rx Left Hip	1,46	1,49	3,3	0,13	-7,26	1,02	1,22	5,95	0,09	-11,65

Table 32: Fading statistics for Top Loaded Monopole Antenna

When moving from anechoic to indoor scenario, the values of the shape factor characterising the fading decrease. This is due to the fact that the increasing of the multipath component, related to the influence of the environment, enhances the fading, and this is directly transposed on its statistic, with a lower value of µ meaning a weaker main path propagation component.

The same consideration can be drawn for the comparison between LOS and NLOS conditions, where in the latter case the multipath is stronger than in the former due to the shadowing effect of the body and, as already explained, the propagation occurs mainly by reflected or diffracted waves.

To confirm this trend, the frequency of appearance of the fading, given by the rate values listed in tables, is sensibly higher when in indoor than in anechoic or when in NLOS than LOS case. In accordance to that, a higher fading rate is always followed by deeper fading phenomena (see depth [dB] values in tables).

As for the channel gain, the link involving the antenna on the Ear results to be peculiar. This is due to the particular shadowing condition and reciprocal antenna positions.

3.3.2 ANGLE DEPENDENT MODEL: CIRCULAR MOVEMENT

In the previous sub-section, it has been presented a model for the Off-Body channel where only the dependence on the distance d from the external gateway has been taken into account.
This section is focused on the effect of body rotation, i.e. the angle set up between the subject and the transmitter antenna, which affects the propagation channel. An evaluation of the mean shadow effect due to the human body while it performs a complete 360° rotation (starting from LOS, α=0°) is performed.
For this kind of analysis circular, both static and dynamic, measurements have been used. The circular static measurements performed allow the evaluation of the channel gain for every angular position with a step of 45°. For instance in Figure 29 we show the angular dependent path loss, when receiver is on the Ear (blue line), Heart (green line) and Hip (red line), for both antennas.

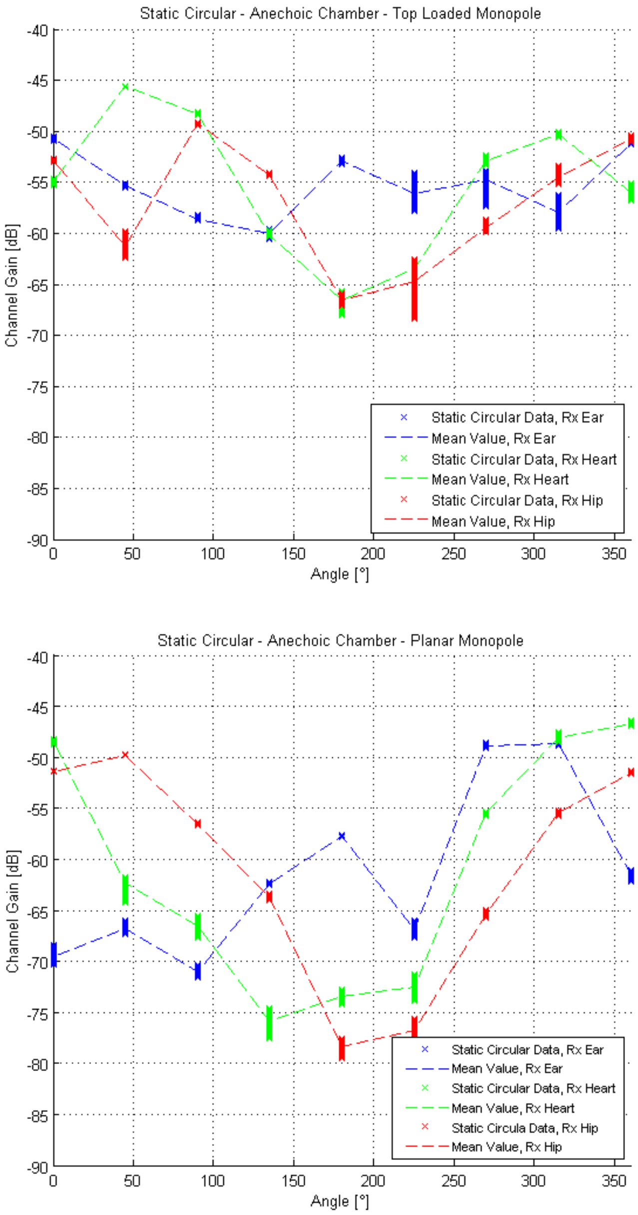

Figure 29: Static circular acquisition for Off-Body channel with PL Monopole (up) and TL Monopole (down) in quasi-anechoic chamber

The vertical sets of crosses represent the acquired data at every angular step, from 0° to 360°, while the dashed line links the mean values of each group of acquisitions, representing a sort of mean shadowing effect of the body.

As it could be expected, it appears clearly that the two sets of antennas are characterized by different shadowing trends, and this is due to the fact that their radiation pattern end polarization characteristics are significantly dissimilar.

The same considerations could be done also for the measurements performed in indoor, whose graph are not here presented only for the sake of briefness.

The analysis has been performed for every possible scenario, Table 33 and Table 34 list all the values obtained:

	Rx Right Ear						Rx Heart						Rx Left Hip					
	max		mean		std		max		mean		std		max		mean		std	
	PL	TL	PL	TL	PL	TL	PL	TL	PL	TL	PL	TL	PL	TL	PL	TL	PL	TL
0°	/	/	/	/	0,22	1,21	/	/	/	/	0,2	1,79	/	/	/	/	0,19	1,27
45°	-7,12	-0,91	-8,73	0,33	1,7	0,36	-2,4	10,15	-2,77	11,41	0,49	0,61	3,98	0,03	3,97	1,26	0,22	0,48
90°	-3,26	-6,75	-4,58	-7,28	1,22	1,53	-9,41	8,34	-9,5	9,88	0,28	0,86	-0,34	5,1	-0,16	5,99	0,11	0,6
135°	-2,97	-9,31	-2,8	-8,68	0,18	0,93	-25,68	-1,03	-27,34	0,84	1,6	0,46	-9,86	7,18	-10,2	9	0,41	0,1
180°	-2,5	-3,47	-3,65	-4,89	0,86	1,68	-23,33	-0,66	-24,99	0,41	1,39	1	-13,38	-11,58	-16,7	-13,26	2,47	2,45
225°	2,6	-9,04	1,12	-8,79	1,43	0,8	-15,84	0,77	-17,03	2,48	0,81	0,41	-12,4	-8,88	-15,2	-9,75	2,34	1,6
270°	9,63	-4,45	9,53	-3,36	0,61	0,35	-20,81	8,03	-22,77	9,8	1,3	0,55	-12,35	2,15	-15,5	3,62	1,62	0,5
315°	9,07	-10,33	9,14	-13,17	0,27	3,39	-11,57	9,21	-12,4	10,74	1,03	0,71	-3,68	6,46	-6,23	7,52	2,06	0,72
360°	3,81	-3,02	4,09	-2,17	0,12	0,64	-1,94	-0,4	-2,25	1,21	0,41	0,51	-1,71	0	-1,76	0	0,32	1,27

Table 33: Shadowing effect for TL Monopole and PL Monopole in Indoor Environment

	Rx Right Ear						Rx Heart						Rx Left Hip					
	max		mean		std		max		mean		std		max		mean		std	
	PL	TL	PL	TL	PL	TL	PL	TL	PL	TL	PL	TL	PL	TL	PL	TL	PL	TL
0°	/	/	/	/	0,43	0,1	/	/	/	/	0,14	0,18	/	/	/	/	0,03	0,09
45°	2,37	-4,6	2,83	-4,65	0,24	0,09	-13,48	9,06	-13,92	9,38	0,39	0,03	1,56	-7,13	1,61	-8,38	0,03	0,67
90°	-1,96	-7,74	-1,49	-7,95	0,24	0,12	-17,3	6,53	-18,11	6,68	0,6	0,11	-5,1	3,54	-5,17	3,59	0,08	0,1
135°	6,18	-9,02	7,19	-9,32	0,07	0,23	-26,41	-5,06	-27,49	-5,12	0,66	0,17	-12	-1,43	-12,3	-1,43	0,19	0,06
180°	10,8	-2,12	11,87	-2,28	0,05	0,2	-24,55	-10,99	-25,06	-11,56	0,38	0,61	-26,3	-13,23	-27	-13,75	0,37	0,28
225°	2,42	-3,56	2,68	-5,51	0,43	1,24	-23	-7,89	-24,09	-8,43	0,65	0,48	-24,3	-9,87	-25,4	-11,86	0,65	1,86
270°	19,84	-3,37	20,66	-4,09	0,14	0,88	-7,06	2,33	-7,06	2,1	0,11	0,25	-13,7	-5,93	-14	-6,62	0,21	0,32
315°	20,06	-5,71	20,94	-7,29	0,17	0,96	0,7	4,52	0,34	4,7	0,33	0,14	-3,89	-0,71	-4,09	-1,68	0,13	0,54
360°	7,38	-0,41	8,06	-0,53	0,24	0,09	1,86	-0,49	1,73	-1,03	0,13	0,44	-0,07	2,26	-0,15	2,16	0,06	0,12

Table 34: Shadowing effect for TL Monopole and PL Monopole in Quasi-Anechoic chamber

Every row represents an angular position, while the columns present the maximum value of the channel gain, its mean and standard deviation normalized to the results obtained for α=0° (first row). The aim is to define an additional loss contribution that could be added to the distance dependent component of the global channel gain (G0|dB); this additional term takes into account the angular shift of the body with respect to the position of the external transmitter.

As to confirm the fact that the two sets of antenna behave in a different way while the subject moves circularly, the values in the Max and Mean columns of PL and TL present completely different trends. In order to verify the reliability of the data acquired in the static circular measurements, a comparison with the dynamic circular acquisitions has been performed. Figure 30 shows the good agreement between the two sets of measurements. The dashed line links the mean value of the discrete samples, whereas the dotted curve represents the continuous acquisition while the subject moves circularly. To better compare the curves, a mean shadowing effect component has been extracted from the dynamic data averaging them on a sliding temporal window of a proper size (continuous line). The trends of the dashed and the continuous line result to be very similar, despite the loss of synchronism while performing the dynamic circular walk. This confirms the reliability of the results obtained for the characterization of the body effect in function of the angle.

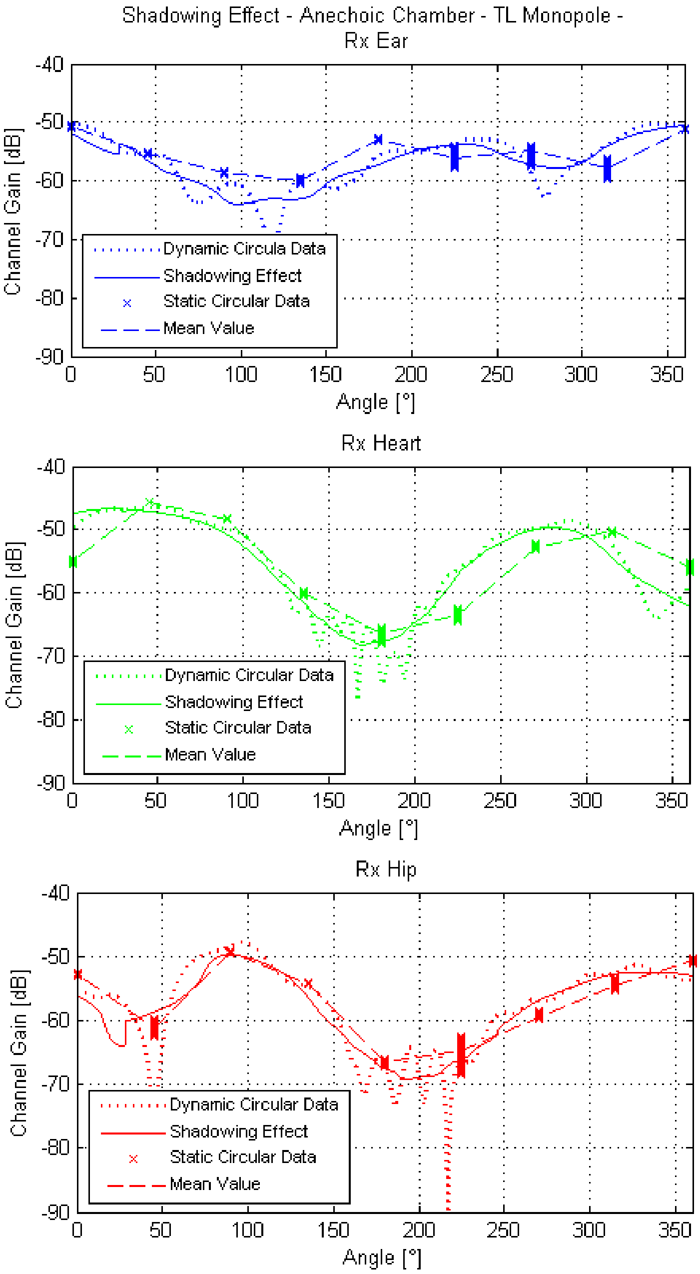

Figure 30: Comparison between body shadowing effect computed from static and dynamic measurements

Additionally, dynamic circular walks have been realized at different distances (2m, 3m and 4m far from the external transmitter).

Figure 31 shows that the trend of the body shadowing remains always the same no matter which is the distance it is referred to. The variation of the channel gain values as a function of the distance results to be in good accordance with the results previously presented and listed in Table 29 and Table 30 for α=0° and α=180°.

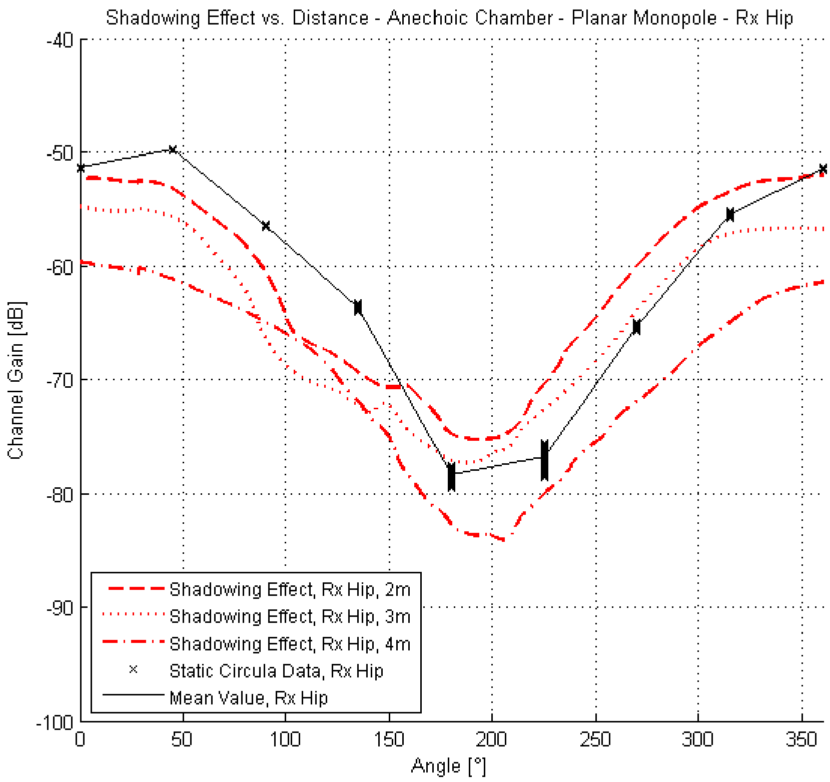

Figure 31: Comparison of the body shadowing effect at different distances for the PL Monopole case

3.4. CEA BODY-TO-BODY CHANNEL INVESTIGATIONS

Previous measurement campaigns have been carried out at CEA for the investigation of narrow band channels at 2.45GHz in body-to-body contexts [46]. Thus, we present in this section a space-time varying channel model where each end of the communication channel is "worn" by a different human subject and located in a specific on-body position.

The main idea that stands behind the analysis performed is to model the channel gain ($G_{|dB}$) extracting a main component dependent on the distance ($G_{0|dB}$) plus a random variable ($F_{|dB}$) that accounts for the movement of the subject and the environment considered, defining in that way a sort of fading contribution. The model could be represented through the following:

$$G(d)_{|dB} = G_{0|dB} + F_{|dB} = G(d_0)_{|dB} + 10n\log_{10}(d/d_0) + F_{|dB} \qquad \textbf{(36)}$$

where d_0 is the reference distance equal to 1 m.

3.4.1 CHANNEL GAIN AND FADING MODEL

In order to extract the distance dependent component of the channel gain ($G_{0|dB}$) different sets of measurement have been realized while one subject walks towards (LOS) or backwards (NLOS) the other one who stands still in the meantime, for both sets of antenna but just in indoor premises.

Figure 32 gives two examples of the acquisitions obtained: the one on the top represents LOS conditions while the other one NLOS. It is clear that the latter case suffers more from a fading effect with respect to the former one. When one subject walks backward the other one (NLOS), the entire body stands in between the transmitters and the receivers and the propagation occurs mainly by reflections and diffraction on the body and/or on the environment; this leads to a more significant multipath effect, strictly related to the fading component.

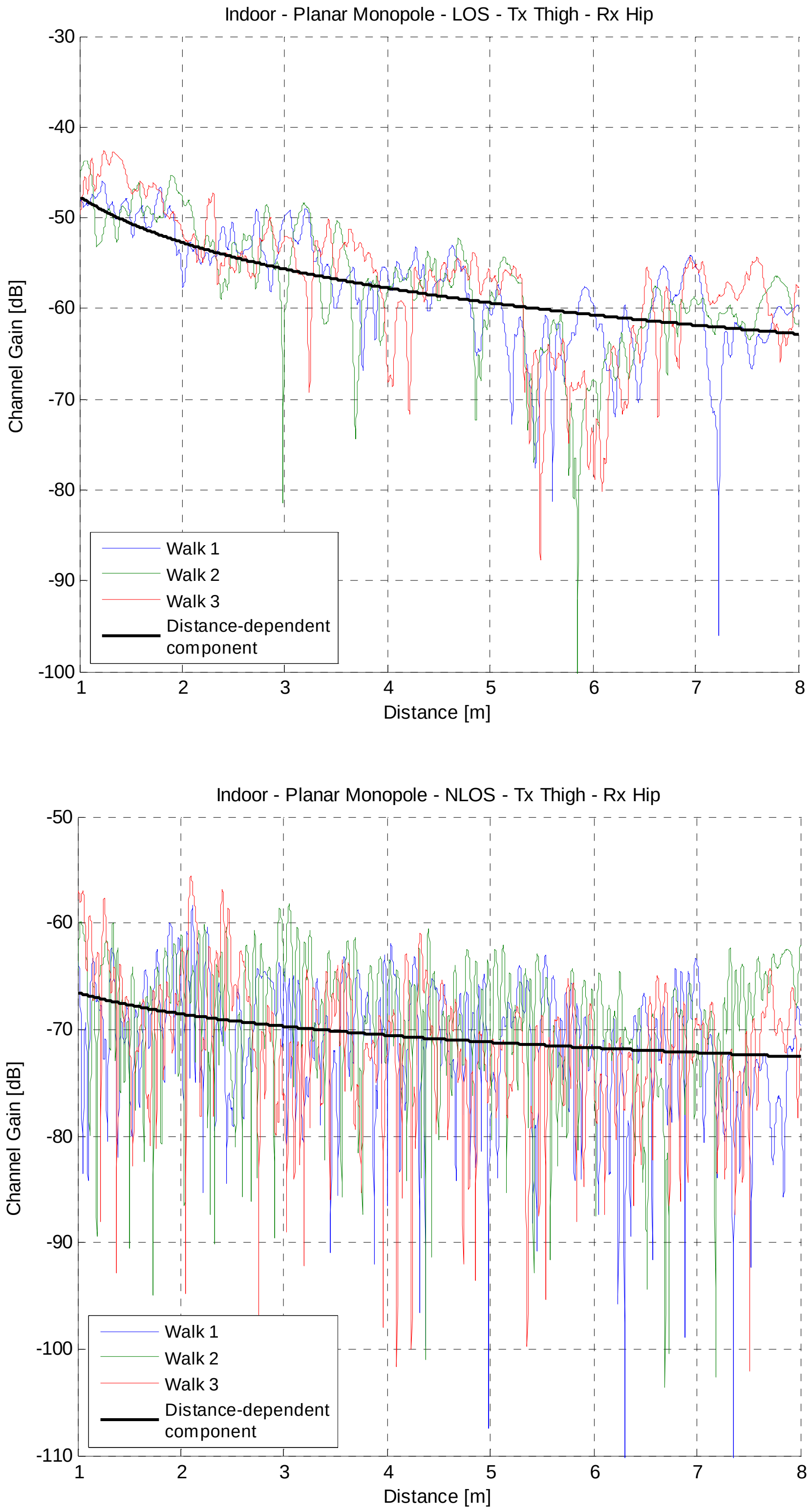

Figure 32: Examples of acquired data while one subject performs a walk towards (up) and backwards (down) the other one

In order to characterize the distance dependent component of the channel gain it is necessary to evaluate *G(d₀)* and *n*, respectively the channel gain at the reference distance *d₀* and the path loss exponent. Those values have been extracted using a polynomial fitting of the data acquired. The results are listed in Table 35 and Table 36 for all the possible body-to-body scenarios and a graphical example is given in Figure 32, where the black line represents the log-distance fit.

Planar Monopole - Indoor							
		Tx Right Hip		*Tx Left Thigh*		*Tx Right Hand*	
		n	*G(d₀)*	*n*	*G(d₀)*	*n*	*G(d₀)*
LOS	Rx Left Ear	-1,14	-56,8	-0,75	-58,33	-0,69	-57,6
	Rx Right Hip	-3,33	-37,88	-1,68	-47,64	-2,8	-36,1
	Rx Heart	-1,14	-54,02	-1	-57,67	-0,74	-51,3
NLOS	Rx Left Ear	-0,8	-70,59	-0,82	-67,53	-1,07	-64,38
	Rx Right Hip	-1,15	-66,33	-0,67	-66,5	-1,17	-58,8
	Rx Heart	-0,67	-70,77	-0,46	-70,3	-0,72	-63,46

Table 35: G_0 characterisation: $G(d_0)$ and n values for Planar Monopole antennas

Top Loaded Monopole - Indoor							
		Tx Right Hip		*Tx Left Thigh*		*Tx Right Hand*	
		n	*G(d₀)*	*n*	*G(d₀)*	*n*	*G(d₀)*
LOS	Rx Left Ear	-0,95	-52,97	-1,33	-52,9	-1,2	-48,34
	Rx Right Hip	-1,7	-46,89	-1,99	-47,1	-1,86	-45,2
	Rx Heart	-2,19	-44,85	-2,57	-41,67	-2,46	-43,7
NLOS	Rx Left Ear	-0,77	-60,3	-0,92	-59,76	-0,7	-58,06
	Rx Right Hip	-1,47	-55,47	-1,28	-56,77	-1,01	-56,53
	Rx Heart	-1,64	-56,1	-1,99	-53,86	-1,91	-52,46

Table 36: G_0 characterisation: $G(d_0)$ and n values for Top Loaded Monopole antennas

From the data presented above some general considerations could be drawn: first of all the path loss exponent significantly decreases when switching from LOS to NLOS scenario, meaning that the multipath phenomenon that greatly affects the propagation in the latter case reduces the distance dependence of the mean channel gain. This behavior is true for both the sets of antenna used, even if it is more stressed for the Planar Monopoles, and not always valid for the link which involves the ear. As already stated, this channel is kind of particular, considering that LOS and NLOS conditions are not referred to a complete masking effect of the body, but are equivalent just to an inversion of the antenna position, from right side of the head to the left side.

Another observation that could be done is that the values of *n* strongly depends on the specific position of the receiver more than that of the transmitter, this could be explained by the fact that the three Txs are placed approximately on the same horizontal line, i.e. barely at the same height from the floor, so the different position of the Rxs play a more important role in the channel performance. To confirm this assumption, if looking to a single row (both in LOS or NLOS), the *n* values are very similar for the three transmitters, with a maximum dispersion of 0.35 in the worst case. To generalize this conclusion, it is possible to say that the path loss exponent strongly depends on the specific relative position of the ends of the communication links.

As far as the $G(d_0)$ value is concerned, when the user passes from LOS to NLOS condition the path loss could increase significantly, with a difference up to 29 dB for PL monopole, and 12 dB for TL Monopoles.

In general, Top Loaded antennas present higher values for the channel gain (up to 14dB more), but this is not true for a couple of links (i.e. Hip-Hand and Hip-Hip) confirming that the specific node location and the antenna type play an important part in the definition of the channel characteristics.

In order to complete the characterization of the body-to-body channel, the fading $F(t)$ has to be extracted and then statistically described.

It has been calculated subtracting the distance dependent component $G_0|dB$, defined through the values listed in Table 35 and Table 36, from the data acquired through the dynamic measurements.

The analysis results show that fast fading follows a Nakagami distribution, which is defined through a shape parameter and a spread parameter, respectively μ and w. Figure 33 shows graphical examples of distribution fit obtained in for two different scenarios, respectively LOS and NLOS for Top Loaded Monopole.

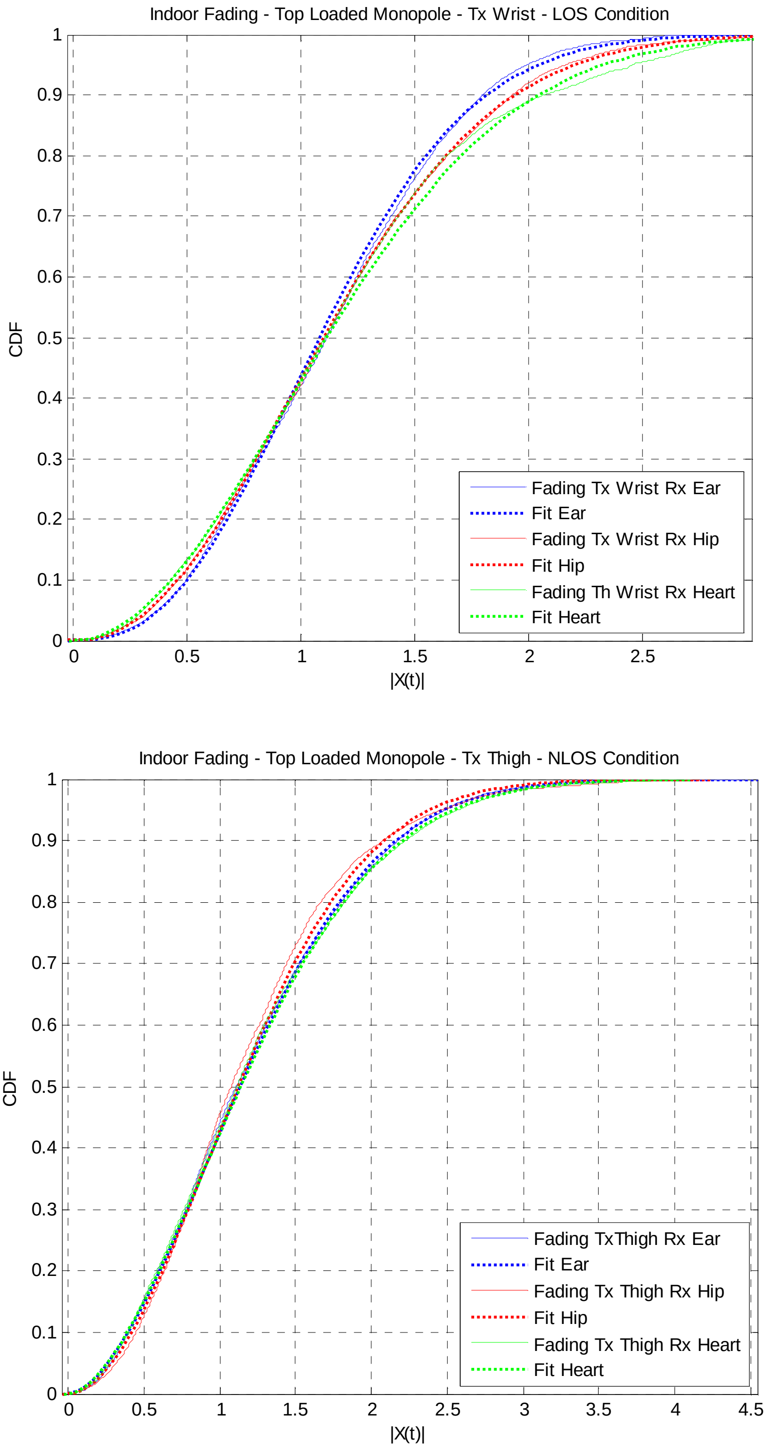

Figure 33: Cumulative distribution function of the fading data F(t): LOS (up) and NLOS (down) for TL Monopole

The study has been performed for all the possible scenarios combining the two antenna types and the propagation conditions (LOS and NLOS). Table 37 and Table 38 present the whole sets of results obtained for the statistical characterization of the fading, as well as the mean duration of the fade in ms, its mean depth in dB and the rate of appearance in s^{-1}.

	Fading statistics - Planar Monopole										
		LOS Conditions					*NLOS Conditions*				
	Rxs	*μ*	*w*	*Rate [s^{-1}]*	*Duration [ms]*	*Depth [dB]*	*μ*	*w*	*Rate [s^{-1}]*	*Duration [ms]*	*Depth [dB]*
Tx Right Hip	**Rx Right Hip**	1,05	1,73	2,06	0,22	-7,41	0,79	2,12	6,17	0,07	-10,6
	Rx Heart	0,62	2,68	1	0,52	-10,8	0,52	3,33	4,67	0,11	-10,67
	RxLeft Ear	0,59	2,87	1,77	0,27	-11,4	0,74	2,26	5,57	0,08	-10,94
Tx Right Hand	**Rx Right Hip**	1,15	1,64	2,31	0,16	-7,12	0,98	1,8	8,8	0,05	-9,95
	Rx Heart	1,05	1,73	2,31	0,17	-6,37	0,8	2,09	7,09	0,07	-10,04
	RxLeft Ear	0,76	2,2	2,37	0,2	-9	0,82	2,06	6,69	0,07	-10,52
Tx Left Thigh	**Rx Right Hip**	1,26	1,56	2,26	0,17	-6,06	0,91	1,9	7,11	0,06	-11,3
	Rx Heart	0,75	2,21	1,83	0,25	-7,47	0,69	2,4	5,34	0,09	-10,94
	RxLeft Ear	0,9	1,9	2,74	0,16	-7,93	0,81	2,07	6,43	0,07	-9,9

Table 37: Fading statistics for Planar Monopole Antenna

	Fading statistics – Top Loaded Monopole										
		LOS Conditions					*NLOS Conditions*				
	Rxs	*μ*	*w*	*Rate [s^{-1}]*	*Duration [ms]*	*Depth [dB]*	*μ*	*w*	*Rate [s^{-1}]*	*Duration [ms]*	*Depth [dB]*
Tx Right Hip	**Rx Right Hip**	0,95	1,84	3,57	0,12	-10,88	0,99	1,79	7,06	0,06	-10,02
	Rx Heart	0,93	1,87	2,94	0,15	-10,45	0,86	1,97	5,43	0,08	-11,3
	RxLeft Ear	0,92	1,88	3,29	0,13	-9,58	0,96	1,83	7,49	0,06	-11,31
Tx Right Hand	**Rx Right Hip**	1,1	1,68	4,63	0,09	-9,86	1,01	1,76	6,94	0,06	-10,47
	Rx Heart	0,98	1,8	4,31	0,1	-10,84	0,87	1,97	5,66	0,08	-10,89
	RxLeft Ear	1,31	1,53	3,66	0,12	-7,93	0,8	2,1	5,57	0,08	-10,46
Tx Left	**Rx**	0,93	1,87	4,67	0,09	-10,83	0,94	1,86	6,89	0.07	-10,76

Thigh	**Right Hip**										
	Rx Heart	0,94	1,85	3,43	0,12	-10,21	0,84	2,02	5,49	0.08	-10,24
	RxLeft Ear	0,89	1,93	4,8	0,09	-9,9	0,87	1,96	6,77	0.07	-11,44

Table 38: Fading statistics for Top Loaded Monopole Antenna

It is interesting to notice that moving from LOS to NLOS scenario, the shape parameter slightly decreases, but, differently from the Off-Body case previously considered.
Nevertheless, to confirm the more significant fading contribution when the subject is in NLOS conditions, fades result to be more frequent than in LOS (up to 7,5 times per seconds), as well as deepest, with a mean value up to -11 dB in the worst case.

A second set of measurements has been performed in order to quantify the average body shadowing effect on the channel performance. The data has been acquired while one subject stands still and the other one performs a complete rotation, starting from LOS (α=0°), passing to NLOS conditions (α=180°) and finishing in the starting position (α=360°). The moving subject wears the Tx only in the Heart position and the circular walks have been repeated at different distances from the still user (1m, 3m, 5m, 7m).
The mean body masking effect has been calculated averaging the samples recorded over a temporal sliding window of a proper size, following the slow variations of the curves. An example of the results obtained is presented in Figure 34.

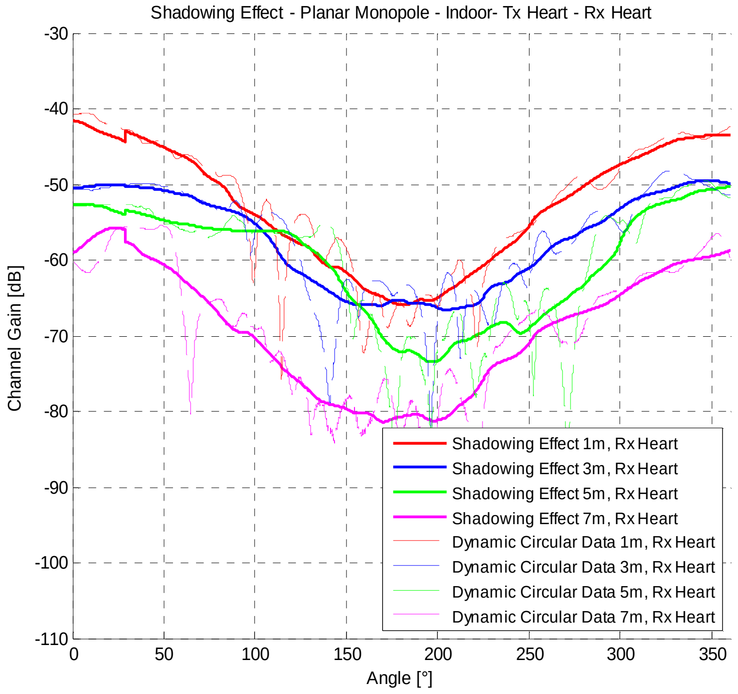

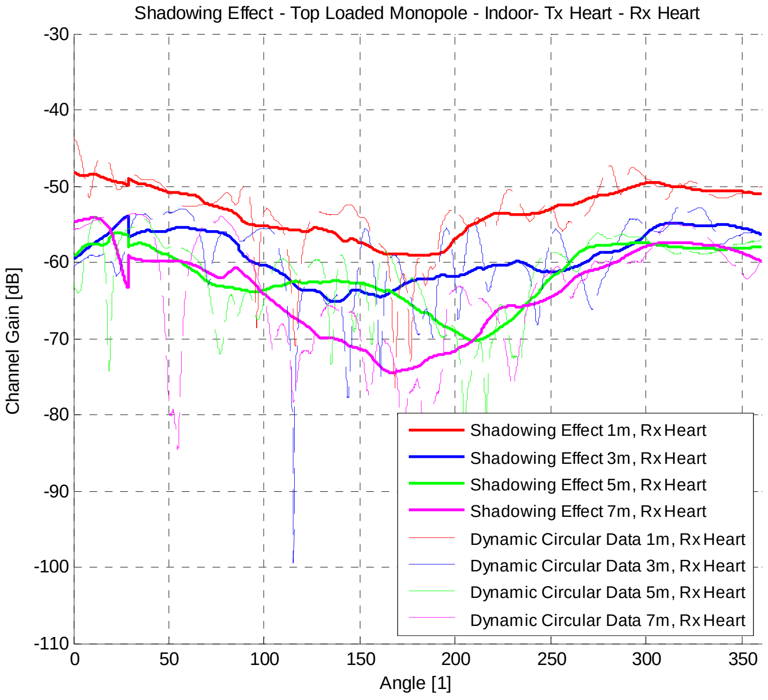

Figure 34: Mean shadowing effect of the body for PL Monopole (up) and TL Monopole (down) in function of the distance with the Rx placed on the Heart

The dashed lines represent the acquired data while the subject performs the dynamic circular movement, each one related to a particular distance, whereas the continuous curves refer to the averaged contribution, representing the shadowing effect of the body.

It is possible to notice that the two sets of curves, related to the different antenna types, present quite similar trends, even if the ones obtained for PL Monopole show a deepest dip, meaning that they suffer from a stronger shadowing when moving from LOS to NLOS conditions.

This phenomenon is also confirmed in Table 39, where the values for the mean body shadowing effect are listed. They have been computed as the mean difference between the maximum and minimum values of the slow varying curves shown in Figure 34.

Except for the case where the Rx is placed on the Ear, Planar Monopole generally present a higher value of the mean shadowing in respect to what has been found for Top Loaded antennas.

Mean Shadowing Effect [dB] - Dynamic Circular - Tx Heart - Indoor					
		1 meter	***3 meter***	***5 meter***	***7 meter***
Planar Monopole	***Rx Right Ear***	18,69	16,5	15,23	13,7
	Rx Heart	23,5	17,23	19,71	21
	Rx Left Hip	23,39	16,84	19,18	17,36
Top Loaded Monopole	***Rx Right Ear***	19,6	14,32	15,2	13,57
	Rx Heart	14,24	13,97	14,12	15,5
	Rx Left Hip	17,44	15,4	11,42	14,83

Table 39: Mean shadowing body effect for the two sets of antenna as a function of the distance

Finally, another consideration that could be drawn from Figure 34 is that the trend of the channel gain as a function of the angle is not strictly dependent on the distance at which the movement has been performed. For both the antenna sets, the curves present in fact approximately the same trends. However, the depth of the fade could vary in function of the distance considered, as shown in Table 39.

Considering that the transmitter is not located in the same position as for the previously illustrated measurements, it is not so easy to make a direct comparison between the values in Table 39 and those in Table 29 and Table 30. Anyway, considering the reference distance of 1 meter, it is possible to notice a good agreement between the data that reveals a very similar shadowing effect, with a relatively small dispersion mainly due to the different node emplacement.

4. BAN CHANNEL CHARACTERIZATION AND MODELS

4.1. RELEVANT CHANNEL MODELS FOR CORMORAN

Taking into account the application scenarios defined in the CORMORAN D1.1 deliverable, we describe in this sub-section relevant channel models which will be used for the design and the performance evaluation of PHY and MAC layers.

Let us note that these models correspond to indoor environments which are applicable to most of the operating environment defined in D1.1, especially for CGN scenarios.

4.1.1 ON-BODY CHANNEL MODELS

- *Link budget modeling [31]*

As explained in section 2.4, the radio link budget $P(t_n)$ is characterized by the channel gain G_0, the slow $S(t_n)$ and the fast fading $F(t_n)$. This parameter is necessary to determine the signal to noise ratio (SNR) of the received signal. It is defined by the following equation:

$$P(t_n) = G_0 \cdot S(t_n) \cdot F(t_n) \tag{37}$$

Channel gain

The channel gain is specific to a human subject and a radio link (Tx and Rx antenna locations). For a given movement scenario, it does not vary in time. Therefore, the first step to generate a radio channel link budget is to set the channel gain value.

It has been concluded in the paragraph 2.4.1 that the channel gain follows a log-normal distribution:

$$G_0\big|_{dB} \sim N(\mu_{0S}, \sigma_{0S}) \tag{38}$$

The mean value and the standard deviation values depending of the radio link and the movement scenario are given in Table 40 and Table 41.

Let us note that the Table 40 should be privileged for CGN applications since the prefered antenna location, mentioned in D1.1, is on the head and the ears.

TX on hip RX on		Anechoic chamber				Indoor			
		ISM 2.45 GHz		UWB [3–5] GHz		ISM 2.45 GHz		UWB [3–5] GHz	
		μ_{0_S} (dB)	σ_{0_S}(dB)	μ_{0_S} (dB)	σ_{0_S} (dB)	μ_{0_S} (dB)	σ_{0_S} (dB)	μ_{0_S} (dB)	σ_{0_S} (dB)
Still	Chest	−60.8792	4.1500	−56.0735	4.3555	−54.6518	4.8124	−52.6205	4.3557
	Thigh	−64.3146	1.5457	−67.9143	3.1032	−60.7145	2.6247	−63.3036	2.3128
	R wrist	−63.2105	2.6178	−62.6940	2.7450	−57.8699	5.1064	−59.9577	3.2800
	R foot	−67.1255	5.1838	−72.4117	1.8445	−60.4444	2.2669	−62.9308	1.6910
Walking	Chest	−53.3737	7.8693	−51.1525	2.1419	−51.7554	7.2704	−51.1099	5.1969
	Thigh	−61.9708	6.4907	−64.5859	4.8125	−59.4894	3.0444	−62.3148	1.5189
	R wrist	−62.1787	5.9615	−61.6258	5.3892	−59.5920	4.2025	−61.7206	2.6024
	R foot	−68.6067	7.4110	−70.5375	4.9560	−58.3369	2.5985	−61.6193	1.4452
Running	Chest	−52.7866	3.3482	−52.4244	4.8385	−47.9470	7.5404	−49.1412	5.2697
	Thigh	−59.1210	4.4368	−62.6505	4.8607	−57.8446	3.5210	−60.7294	2.6594
	R wrist	−65.8698	4.3149	−63.8395	2.2846	−61.7829	3.8987	−60.1702	3.3161
	R foot	−71.2233	8.4303	−72.3628	7.4711	−60.4773	1.9647	−64.4700	1.1307

Table 40: Channel gain : transmitter on hip

TX on left ear RX on		Anechoic chamber				Indoor			
		ISM 2.45 GHz		UWB [3–5] GHz		ISM 2.45 GHz		UWB [3–5] GHz	
		μ_{0_S} (dB)	σ_{0_S} (dB)	μ_{0_S} (dB)	σ_{0_S} (dB)	μ_{0_S} (dB)	σ_{0_S} (dB)	μ_{0_S} (dB)	σ_{0_S} (dB)
Still	R Ear	−63.2533	6.3566	−63.4038	1.9335	−60.2220	3.1504	−59.9519	2.3074
	Hip	−60.1378	8.9410	−66.0411	2.4280	−60.2879	6.0754	−62.6346	3.9294
	R wrist	−72.9014	2.6375	−75.4553	1.4040	−64.4708	3.2828	−67.2240	0.9855
	R foot	−75.3591	4.5385	−77.8079	2.2942	−62.7263	2.1910	−65.0598	1.1077
Walking	R ear	−61.0003	2.7018	−62.1485	1.8514	−60.0321	3.0879	−60.6388	3.6631
	Hip	−57.9352	7.1715	−63.6140	2.2443	−58.7770	4.9483	−61.8767	2.2518
	R wrist	−71.8550	2.9189	−73.3252	2.8333	−63.0413	1.9839	−65.7443	1.5340
	R foot	−72.9939	4.6507	−74.9548	2.3615	−61.0049	1.3100	−63.0086	1.0698
Running	R ear	−61.3644	3.6490	−62.7325	3.3694	−60.7473	5.3087	−59.0271	3.6600
	Hip	−63.8337	7.5450	−68.4237	2.6864	−60.7622	5.7060	−62.7400	1.6554
	R wrist	−71.9968	2.2282	−69.1763	2.9781	−63.5684	2.2375	−62.7320	2.4954
	R foot	−77.7146	3.4217	−78.3609	2.0264	−62.7026	1.1543	−66.0428	0.8888

Table 41: Channel gain : transmitter on left ear

Slow fading

The shadowing strictly depends on the movement condition. In the paragraph 2.4.2, it has been modeled by a log-normal distribution with zero mean:

$$S(t_n)\big|_{dB} \sim N\left(0,\sigma_{sS}\right) \qquad \textbf{(39)}$$

The standard deviation σ_{sS} values are given in Table 42 and Table 43. Once again, Table 43 should be privileged for CGN applications since the transmitter is located on an ear. The parameters values given for the anechoic chamber environment could be exploited for the

LSIMC and CGN in outdoor sparse environment, which corresponds respectively to 37.5% and 20% of the working environment.

		TX on Hip			
		Chest	Thigh	R Wrist	R Foot
Anechoic	Still	0.6329	0.4269	1.0185	0.4564
	Walking	2.2892	5.4279	4.4565	5.2028
	Running	2.3997	2.5117	3.6504	2.8322
Indoor	Still	0.638	0.2578	0.2706	0.2593
	Walking	1.6049	3.486	2.7915	2.734
	Running	2.0977	2.0965	2.5062	1.8854

Table 42 : Shadowing parameters - TX on hip

		TX on Left Ear			
		R ear	Hip	R Wrist	R Foot
Anechoic	Still	0.7205	1.1237	1.781	0.8133
	Walking	0.7293	2.1193	3.5141	4.4149
	Running	0.5409	2.9261	3.1742	1.7009
Indoor	Still	0.5768	1.5246	0.8373	0.7621
	Walking	0.9393	2.2444	1.8723	2.1241
	Running	0.7259	2.282	1.9811	1.3007

Table 43 : Shadowing parameters - TX on ear

	Fast Fading		Slow Fading	
	Depth [dB]	Duration [ms]	σ_{ss} [dB]	Duration (ms)
Chest	4.39	78.10	1.52	432.80
Thigh	6.93	86.20	3.27	631.00
R Wrist	6.54	81.90	2.66	532.80
R Foot	7,98	82,70	2.57	579.90

Table 44 : Fading characteristics at 2.45GHz (BW=10MHz) - TX on hip – walking scenario

Antenna polarization influences

Antenna polarization and radiation pattern can have some impacts on the link budgets. We remind in Table 45, Table 46 and Table 47 some parameters values when Top Loaded Monopole (TLM) and Planar Monopole (PM) antennas are used.

	Tx Heart Top Loaded Monopole		**Tx Heart Planar Monopole**	
	Quasi-anechoic chamber	*Indoor Office*	*Quasi-anechoic chamber*	*Indoor Office*

	Rxs	μ_{OS} [dB]	σ_{OS} [dB]	μ_{OS} [dB]	σ_{OS} [dB]	μ_{OS} [dB]	σ_{OS} [dB]	μ_{OS} [dB]	σ_{OS} [dB]
Walking	Right Thigh	-38,45	1,06	-38,65	1,15	-66,77	3,35	-62,72	2,41
	Rigth Hand	-47,07	2,16	-49,47	1,2	-63,87	6	-60,15	5,79
	Left Hand	-43,86	2,46	-42,97	3,19	-60,42	4,35	-58,35	1,5
	Left Ear	-48,62	3,62	-46,82	4,57	-61,06	5,18	-60,48	3,5
Sitting/ Standing	Right Thigh	-39,45	1,59	-41,04	1,44	-63,96	5,36	-58,02	3,61
	Rigth Hand	-46,54	2,46	-47,73	4,6	-58,41	2	-56,06	4,89
	Left Hand	-43,52	2,35	-43,02	2,76	-54,62	3,07	-56,21	3,53
	Left ear	-48,34	2,43	-43,47	1,98	-63,07	2,72	-59,13	4,47
Standing Still	Right Thigh	-38,75	0,92	/	/	-68,34	4,92	/	/
	Rigth Hand	-46,58	1,69	/	/	-66,25	6,17	/	/
	Left Hand	-42,12	1,87	/	/	-62,43	2,36	/	/
	Left Ear	-45,01	1,36	/	/	-60,96	2,27	/	/

Table 45 : Channel gain values for scenarios where Tx is placed on heart

		Tx Left Hip - Top Loaded Monopole				**Tx Left Hip - Planar Monopole**			
		Quasi-anechoic chamber		*Indoor Office*		*Quasi-anechoic chamber*		*Indoor Office*	
	Rxs	μ_{OS} [dB]	σ_{OS} [dB]	μ_{OS} [dB]	σ_{OS} [dB]	μ_{OS} [dB]	σ_{OS} [dB]	μ_{OS} [dB]	σ_{OS} [dB]
Walking	Right Thigh	-38,78	2,06	-38,4	1,17	-63,85	2,4	-60,77	4,89
	Rigth Hand	-52,09	4,58	-53,09	2,89	-67,54	7,5	-61,69	6,9
	Left Hand	-40,32	3,17	-40,74	4,32	-50,38	1,08	-49,62	2,95
	Left Ear	-47,24	2,02	-48,3	2,69	-68,45	5,4	-64,26	3,3
Standing Still	Right Thigh	-42,78	2,26	/	/	-61,17	1,06	/	/
	Rigth Hand	-48,35	4,8	/	/	-68,97	1,29	/	/
	Left Hand	-34,52	1,37	/	/	-47,59	2,4	/	/
	Left Ear	-46,77	1,46	/	/	-69,77	3,63	/	/

Table 46 : Channel gain values values for scenarios where Tx is placed on right ear

	Tx Right Ear - Top Loaded Monopole		**Tx Right Ear - Planar Monopole**	
	Quasi-anechoic chamber	*Indoor Office*	*Quasi-anechoic chamber*	*Indoor Office*

	Rxs	μ_{OS} [dB]	σ_{OS} [dB]	μ_{OS} [dB]	σ_{OS} [dB]	μ_{OS} [dB]	σ_{OS} [dB]	μ_{OS} [dB]	σ_{OS} [dB]
Walking	Right Thigh	-55,13	3,29	-57,57	1,84	-72,53	5,96	-67,01	2,77
	Rigth Hand	-53,82	3,92	-53,31	3,19	-64,61	4,49	-59,18	2,27
	Left Hand	-66,59	4,98	-57,57	0,91	-74,89	2,63	-65,67	4,63
	Left Ear	-35,81	0,82	-37,01	2	-58,54	6,05	-54,67	4,73
Sitting/ Standing	Right Thigh	-56,77	2,99	-57,78	2,56	-72,27	3,58	-65,93	4,41
	Rigth Hand	-54,2	2,97	-55,18	1,95	-61,83	5,41	-61,22	2,5
	Left Hand	-61,52	3,62	-58	1,52	-73,82	3,26	-64,79	3,63
	Left ear	-36,33	1,56	-36,43	2,08	-57,41	8,28	-55,44	6,33
Standing Still	Right Thigh	-53,82	1,99	/	/	-76,22	3,05	/	/
	Rigth Hand	-49,92	2,47	/	/	-67,77	2,47	/	/
	Left Hand	-66,87	3,43	/	/	-78,83	2,05	/	/
	Left Ear	-33,69	0,81	/	/	-68,02	4,12	/	/

Table 47 : Channel Gain values for scenarios where Tx is placed on Right Ear

Fast fading for narrow band at 2.45GHz

Fast fading and slow fading depth and duration values are given in Table 44 for walking scenario in indoor environment when the transmitting antenna is located on the hip.

It has been shown that the fast fading follows a Rice distribution:

$$pdf_{\chi} = \frac{\chi}{\sigma_{\chi}^{2}} \exp\left(\frac{-\chi^{2}+\nu_{\chi}^{2}}{2\sigma_{\chi}^{2}}\right) I_{0}\left(\frac{\chi\nu_{\chi}}{\sigma_{\chi}^{2}}\right) \tag{40}$$

where $I_0(.)$ represents the modified Bessel function of the first kind with zero order, and ν_χ and σ_χ are the parameters of the distribution. Their values are given in Table 48 for all the movement conditions and for a transmitting antenna located on the hip.

	Still			Walking			Running		
	ν_χ	σ_χ	K	ν_χ	σ_χ	K	ν_χ	σ_χ	K
Chest	0,998	0,220	10,266	0,991	0,351	3,983	0,981	0,413	2,821
Thigh	0,999	0,210	11,328	0,923	0,566	1,331	0,944	0,533	1,568
R Wrist	0,998	0,114	38,424	0,962	0,519	1,720	0,001	0,943	0,000
R Foot	1,000	0,109	42,030	0,582	0,825	0,249	0,740	0,754	0,482

Table 48 : Fading statistics at 2.45GHz (BW=10MHz) – TX on hip

- *Channel impulse response modeling [38]*

The delay spread is the most common parameter characterizing the delay dispersion. It has been observed that its value is the lowest for the LOS scenarios. Table 49 gives its values for different radio links and movement conditions.

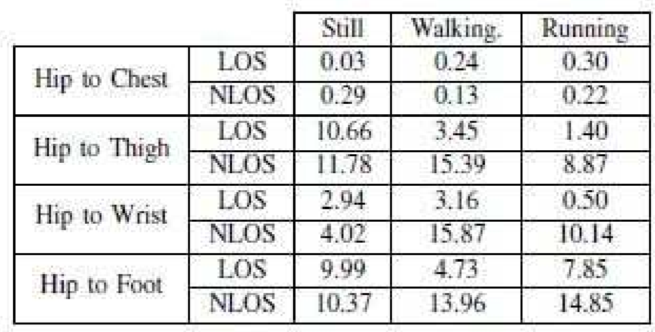

		Still	Walking	Running
Hip to Chest	LOS	0.03	0.24	0.30
	NLOS	0.29	0.13	0.22
Hip to Thigh	LOS	10.66	3.45	1.40
	NLOS	11.78	15.39	8.87
Hip to Wrist	LOS	2.94	3.16	0.50
	NLOS	4.02	15.87	10.14
Hip to Foot	LOS	9.99	4.73	7.85
	NLOS	10.37	13.96	14.85

Table 49 : Delay spread in nanoseconds

The CIR can be modeled by a conventional Saleh-Valenzuela model. The path amplitude is modeled by an exponential decay (t_n) and a Rician factor $\gamma_0(t_n)$ as:

$$\mathbb{E}[\alpha_k(t_n)|_{dB}] \propto \gamma_0(t_n) + 10\log_{10}\left\{\exp\left[-\frac{\tau_k(t_n)}{\Gamma(t_n)}\right]\right\} \tag{41}$$

The inter-ray arrival delay is modeled by a Poisson distribution:

$$p(\tau_{k,n}|\tau_{k-1,n}) = \Lambda \cdot \exp\left[-\Lambda\left(\tau_{k,n} - \tau_{k-1,n}\right)\right] \tag{42}$$

The variation around the amplitude mean value has been described by a normal distribution:

$$\alpha_k(t_n)|_{dB} \sim \mathcal{N}(\mathbb{E}[\alpha_k(t_n)|_{dB}], \sigma_\alpha) \tag{43}$$

The values of these parameters are given in Table 50. The average path number $\widetilde{K}$ is also given. It has also been observed that the stronger the shadowing is, the higher the number of significant path is. Thus, $K(t_n)$ is modeled by an exponential function of $S(t_n)|_{dB}$ whose parameters m and m_0 are given in Table 51.

$$K(t_n) = \exp(m \cdot S(t_n)|_{dB} + m_0) \tag{44}$$

		LOS	Trans.	NLOS
Hip to Chest	Γ [ns]	25.9	-	-
	$\overline{\gamma_0}$ [dB]	3.37	-	-
	K	26	-	-
	Λ^{-1} [ns]	2.13	-	-
	σ_α	4.02	-	-
Hip to Thigh	Γ [ns]	24.9	46.7	58.9
	$\overline{\gamma_0}$ [dB]	2.1	1.6	1.6
	K	7	19	30
	Λ^{-1} [ns]	3.13	2.46	2.35
	σ_α	4.62	4.58	4.32
Hip to Wrist	Γ [ns]	22.3	45.5	63
	$\overline{\gamma_0}$ [dB]	2.3	2.7	2.5
	K	5	13	27
	Λ^{-1} [ns]	3.27	2.69	2.39
	σ_α	4.55	4.28	4.31
Hip to Foot	Γ [ns]	29	40.5	55
	$\overline{\gamma_0}$ [dB]	3.3	2.2	1.4
	K	10	23	32
	Λ^{-1} [ns]	2.98	2.37	2.21
	σ_α	4.57	4.61	4.65

Table 50 : PDP decay - walking subject

Channel	$\rho_{i,j}$			m	m_0
Hip to Thigh	1,00	-0,51	0,65	-0.2431	2.601
Hip to Wrist	-0,51	1,00	-0,48	-0.2491	2.1588
Hip to Foot	0,65	-0,48	1,00 1	-0.2266	2.8305

Table 51 : Shadowing correlation and exponential decay of $K(t_n)$ vs. $S(t_n)_{|dB}$ – walking scenario – TX on the hip

- *Model of temporal evolution of shadowing [38]*

In the previous paragraph, a delay spread model has been described in function of the shadowing. In movement condition, shadowing values can evolve especially if the antennas are located on limbs.

Here, we give an Auto-regressive (AR) model which describes the temporal evolution of shadowing in walking scenarios. It is defined by the following equation:

$$\sum_{p=0}^{P} a_p \widehat{S}(n-p) = \mathcal{E}(n) \tag{4-1}$$

where $\widehat{S}(n)$ represents the estimation of shadowing in dB, which is given by a linear combination of the past P outputs plus a zero-mean white noise input $\mathcal{E}(n)$. The weights a_p values are given in Table 52.

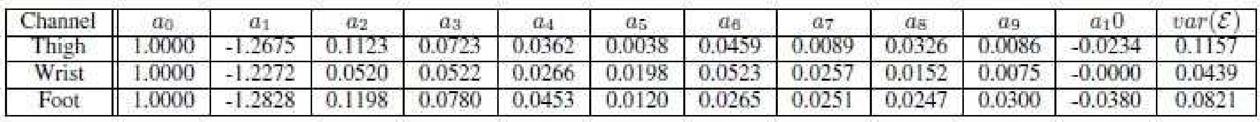

Channel	a_0	a_1	a_2	a_3	a_4	a_5	a_6	a_7	a_8	a_9	a_10	$var(\mathcal{E})$
Thigh	1.0000	-1.2675	0.1123	0.0723	0.0362	0.0038	0.0459	0.0089	0.0326	0.0086	-0.0234	0.1157
Wrist	1.0000	-1.2272	0.0520	0.0522	0.0266	0.0198	0.0523	0.0257	0.0152	0.0075	-0.0000	0.0439
Foot	1.0000	-1.2828	0.1198	0.0780	0.0453	0.0120	0.0265	0.0251	0.0247	0.0300	-0.0380	0.0821

Table 52: Coefficients of the AR model in walking scenarios – TX on hip

- *Space–time correlation modeling*

To assess the performances of cooperative communication systems, it is necessary to model the space-time correlation between different radio links (*i,j*). Some correlation values $\boldsymbol{\rho}_{i,j}$ are given Table 51.

$$\rho_{i,j} = \frac{\mathbb{E}\left[\left(S_{TX,i} - \mathbb{E}[S_{TX,i}]\right)\left(S_{TX,j} - \mathbb{E}[S_{TX,j}]\right)\right]}{\sqrt{\mathbb{E}\left[S_{TX,i}^2 - \mathbb{E}^2[S_{TX,i}]\right]\mathbb{E}\left[S_{TX,j}^2 - \mathbb{E}^2[S_{TX,j}]\right]}} \tag{45}$$

- *Doppler spectrum modeling [45]*

In the case of movement conditions, a Doppler effect appears. We model it with the following equation:

$$D_{TOT}(\nu) = D_{ON-BODY}(\nu) \cdot D_{OFF-BODY}(\nu) \tag{46}$$

where ν is the mobility speed of the body, $D_{ON\text{-}BODY}$ is the Doppler spectrum component related to the on-body scatterers and $D_{OFF\text{-}BODY}$, that related to off-body scatterers. These Doppler spectra are modeled by the following equations:

$$D_{ON-BODY}(\nu) = \frac{1}{\gamma + \nu^2} \tag{47}$$

$$D_{OFF-BODY}(\nu)\Big|_{dB} = D_0 \cdot \exp\left[\frac{(\nu - \nu_m)^2}{2\sigma_\nu{}^2}\right] \tag{48}$$

Table 53 gives the parameters values extracted from measurement campaigns in indoor environment and used in the previous equations.

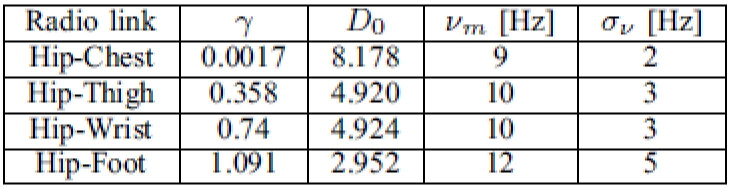

Radio link	γ	D_0	ν_m [Hz]	σ_ν [Hz]
Hip-Chest	0.0017	8.178	9	2
Hip-Thigh	0.358	4.920	10	3
Hip-Wrist	0.74	4.924	10	3
Hip-Foot	1.091	2.952	12	5

Table 53 : Doppler parameters in indoor

4.1.2 OFF-BODY CHANNEL MODELS

For off-body communication scenarios, the factors which have the most important influences on the link budget are not only the distance between the transmitter and the receiver, but also the orientation of the body. In the sequel, we remind parameters values extracted from measurement campaigns where TLM and PM antennas have been used [46].

- *Channel gain and fading model*

The radio link budget is modeled by the following equation:

$$G(d)_{|dB} = G_{0|dB} + F_{|dB} = G(d_0)_{|dB} + 10n\log_{10}(d/d_0) + F_{|dB} \qquad \textbf{(49)}$$

Table 54 and Table 55 give parameters values related to the equation above. The LOS and NLOS conditions correspond to the cases where the transmitter is in front of the body (orientation of 0°) and in the back of the body (orientation of 180°) respectively.

Planar Monopole								
	Quasi-Anechoic Chamber				Indoor			
	LOS		NLOS		LOS		NLOS	
	n	$G(d_0)$	n	$G(d_0)$	n	$G(d_0)$	n	$G(d_0)$
Rx Right Ear	-2,2	-63,48	-2,2	-51,69	-1,47	-50,24	-0,69	-53,43
Rx Heart	-1,99	-41,75	-1,8	-72,46	-2	-38,92	-0,4	-62,62
Rx Left Hip	-1,61	-50,11	-0,9	-69,09	-2	-51,94	-0,1	-68,78

Table 54: Mean channel gain characterisation: $G(d_0)$ and n values for Planar Monopole antennas

Top Loaded Monopole								
	Quasi-Anechoic Chamber				Indoor			
	LOS		NLOS		LOS		NLOS	
	n	$G(d_0)$	n	$G(d_0)$	n	$G(d_0)$	n	$G(d_0)$
Rx Right Ear	-2,18	-45,14	-2,07	-45,82	-1,62	-45,7	-2,96	-46,03
Rx Heart	-2,44	-49,11	0	-71,42	-1,37	-54,71	0	-66,33
Rx Left Hip	-1,83	-43,99	-0,24	-66,48	-1,99	-47,67	-0,59	-61,33

Table 55: Mean channel gain characterisation: $G(d_0)$ and n values for Top Loaded Monopole antennas

The fast fading component is expressed as $F(t) = |\chi(t)|^2$ where $|\chi|$ follows a Nakagami distribution. The latter is defined through a shape and a spread parameters, respectively μ and w. Their values, obtained from measurement campaigns, are reminded in the Table 56 and Table 57.

	Fading statistics - Planar Monopole										
		LOS Conditions					*NLOS Conditions*				
	Rxs	*μ*	*w*	*Rate [s-1]*	*Duration [ms]*	*Depth [dB]*	*μ*	*w*	*Rate [s-1]*	*Duration [ms]*	*Depth [dB]*
Anechoic Chamber	**Rx Right Ear**	1,04	0,66	2	0,41	-3,33	7,62	1,66	0,75	0,18	-1,06
	Rx Heart	12,02	1,52	0,5	0,23	-0,83	1,42	2,02	7,7	0,04	-6,11
	RxLeft Hip	11,43	1,04	1,35	0,36	-1,01	5,28	2,12	0,8	0,07	-1,6
Indoor	**Rx Right Ear**	2,11	0,98	4,3	0,14	-6,77	1,24	2,09	4,55	0,07	-7,85
	Rx Heart	5,48	0,73	1,65	0,5	-3,38	0,81	1,12	5,35	0,11	-12,24
	RxLeft Hip	2,61	2,06	2,75	0,06	-5,83	0,92	1,91	6,25	0,07	-11,55

Table 56: Fading statistics for Planar Monopole Antenna

	Fading statistics – Top Loaded Monopole										
		LOS Conditions					*NLOS Conditions*				
	Rxs	*μ*	*w*	*Rate [s-1]*	*Duration [ms]*	*Depth [dB]*	*μ*	*w*	*Rate [s-1]*	*Duration [ms]*	*Depth [dB]*
Anechoic Chamber	**Rx Right Ear**	5,83	1,34	1,3	0,21	-1,01	9,96	1,14	2,35	0,17	-0,8
	Rx Heart	2,74	1,08	1,05	0,5	-3,63	1,15	1,88	1,75	0,27	-5,69
	RxLeft Hip	4,68	0,81	1,5	0,47	-1,8	0,82	0,8	2,1	0,36	-7,5
Indoor	**Rx Right Ear**	2,15	0,76	3,4	0,22	-7,4	1,46	2,1	4,15	0,08	-7,16
	Rx Heart	1,28	1,45	3,2	0,14	-8,89	1,02	1,79	6,25	0,07	-10,71
	Rx Left Hip	1,46	1,49	3,3	0,13	-7,26	1,02	1,22	5,95	0,09	-11,65

Table 57: Fading statistics for Top Loaded Monopole Antenna

- *Angle dependence*

The orientation of the body or more precisely, the angle set up between the subject and the transmitting antenna, has an important impact on the radio link budget. Table 58 and Table 59 remind channel gain values for different orientations and antenna positions on the body.

	Rx Right Ear						Rx Heart						Rx Left Hip					
	max		mean		std		max		mean		std		max		mean		std	
	PL	TL	PL	TL	PL	TL	PL	TL	PL	TL	PL	TL	PL	TL	PL	TL	PL	TL
0°	/	/	/	/	0,22	1,21	/	/	/	/	0,2	1,79	/	/	/	/	0,19	1,27
45°	-7,12	-0,91	-8,73	0,33	1,7	0,36	-2,4	10,15	-2,77	11,41	0,49	0,61	3,98	0,03	3,97	1,26	0,22	0,48
90°	-3,26	-6,75	-4,58	-7,28	1,22	1,53	-9,41	8,34	-9,5	9,88	0,28	0,86	-0,34	5,1	-0,16	5,99	0,11	0,6
135°	-2,97	-9,31	-2,8	-8,68	0,18	0,93	-25,68	-1,03	-27,34	0,84	1,6	0,46	-9,86	7,18	-10,2	9	0,41	0,1
180°	-2,5	-3,47	-3,65	-4,89	0,86	1,68	-23,33	-0,66	-24,99	0,41	1,39	1	-13,38	-11,58	-16,7	-13,26	2,47	2,45
225°	2,6	-9,04	1,12	-8,79	1,43	0,8	-15,84	0,77	-17,03	2,48	0,81	0,41	-12,4	-8,88	-15,2	-9,75	2,34	1,6
270°	9,63	-4,45	9,53	-3,36	0,61	0,35	-20,81	8,03	-22,77	9,8	1,3	0,55	-12,35	2,15	-15,5	3,62	1,62	0,5
315°	9,07	-10,33	9,14	-13,17	0,27	3,39	-11,57	9,21	-12,4	10,74	1,03	0,71	-3,68	6,46	-6,23	7,52	2,06	0,72
360°	3,81	-3,02	4,09	-2,17	0,12	0,64	-1,94	-0,4	-2,25	1,21	0,41	0,51	-1,71	0	-1,76	0	0,32	1,27

Table 58: Shadowing effect for TL Monopole and PL Monopole in Indoor Environment

	Rx Right Ear						Rx Heart						Rx Left Hip					
	max		mean		std		max		mean		std		max		mean		std	
	PL	TL	PL	TL	PL	TL	PL	TL	PL	TL	PL	TL	PL	TL	PL	TL	PL	TL
0°	/	/	/	/	0,43	0,1	/	/	/	/	0,14	0,18	/	/	/	/	0,03	0,09
45°	2,37	-4,6	2,83	-4,65	0,24	0,09	-13,48	9,06	-13,92	9,38	0,39	0,03	1,56	-7,13	1,61	-8,38	0,03	0,67
90°	-1,96	-7,74	-1,49	-7,95	0,24	0,12	-17,3	6,53	-18,11	6,68	0,6	0,11	-5,1	3,54	-5,17	3,59	0,08	0,1
135°	6,18	-9,02	7,19	-9,32	0,07	0,23	-26,41	-5,06	-27,49	-5,12	0,66	0,17	-12	-1,43	-12,3	-1,43	0,19	0,06
180°	10,8	-2,12	11,87	-2,28	0,05	0,2	-24,55	-10,99	-25,06	-11,56	0,38	0,61	-26,3	-13,23	-27	-13,75	0,37	0,28
225°	2,42	-3,56	2,68	-5,51	0,43	1,24	-23	-7,89	-24,09	-8,43	0,65	0,48	-24,3	-9,87	-25,4	-11,86	0,65	1,86
270°	19,84	-3,37	20,66	-4,09	0,14	0,88	-7,06	2,33	-7,06	2,1	0,11	0,25	-13,7	-5,93	-14	-6,62	0,21	0,32
315°	20,06	-5,71	20,94	-7,29	0,17	0,96	0,7	4,52	0,34	4,7	0,33	0,14	-3,89	-0,71	-4,09	-1,68	0,13	0,54
360°	7,38	-0,41	8,06	-0,53	0,24	0,09	1,86	-0,49	1,73	-1,03	0,13	0,44	-0,07	2,26	-0,15	2,16	0,06	0,12

Table 59: Shadowing effect for TL Monopole and PL Monopole in Quasi-Anechoic Environment

4.1.3 BODY-TO-BODY CHANNEL MODELS

- *Channel gain and fading model [72]*

Similarly to off-body communication scenarios, the link budget is characterized by:

$$G(d)_{|dB} = G_{0|dB} + F_{|dB} = G(d_0)_{|dB} + 10n\log_{10}(d/d_0) + F_{|dB} \qquad \textbf{(50)}$$

Table 60 and Table 61 give parameters values related to the equation above in LOS and NLOS conditions corresponding to the cases where the bodies are face-to-face and face-to-back respectively.

Planar Monopole - Indoor							
		Tx Right Hip		***Tx Left Thigh***		***Tx Right Hand***	
		n	***G(d₀)***	***n***	***G(d₀)***	***n***	***G(d₀)***
LOS	Rx Left Ear	-1,14	-56,8	-0,75	-58,33	-0,69	-57,6
	Rx Right Hip	-3,33	-37,88	-1,68	-47,64	-2,8	-36,1
	Rx Heart	-1,14	-54,02	-1	-57,67	-0,74	-51,3
NLOS	Rx Left Ear	-0,8	-70,59	-0,82	-67,53	-1,07	-64,38
	Rx Right Hip	-1,15	-66,33	-0,67	-66,5	-1,17	-58,8
	Rx Heart	-0,67	-70,77	-0,46	-70,3	-0,72	-63,46

Table 60: G_0 characterisation: $G(d_0)$ and n values for Planar Monopole antennas

Top Loaded Monopole - Indoor							
		Tx Right Hip		***Tx Left Thigh***		***Tx Right Hand***	
		n	***G(d₀)***	***n***	***G(d₀)***	***n***	***G(d₀)***
LOS	Rx Left Ear	-0,95	-52,97	-1,33	-52,9	-1,2	-48,34
	Rx Right Hip	-1,7	-46,89	-1,99	-47,1	-1,86	-45,2
	Rx Heart	-2,19	-44,85	-2,57	-41,67	-2,46	-43,7
NLOS	Rx Left Ear	-0,77	-60,3	-0,92	-59,76	-0,7	-58,06
	Rx Right Hip	-1,47	-55,47	-1,28	-56,77	-1,01	-56,53
	Rx Heart	-1,64	-56,1	-1,99	-53,86	-1,91	-52,46

Table 61: G_0 characterisation: $G(d_0)$ and n values for Top Loaded Monopole antennas

Like off-body communications, the fast fading is modeled by a Nakagami distribution whose values are summarized in the Table 62 and Table 63.

	Fading statistics - Planar Monopole										
		LOS Conditions					*NLOS Conditions*				
	Rxs	μ	*w*	*Rate* $[s^{-1}]$	*Duration [ms]*	*Depth [dB]*	μ	*w*	*Rate* $[s^{-1}]$	*Duration [ms]*	*Depth [dB]*
Tx Right Hip	**Rx Right Hip**	1,05	1,73	2,06	0,22	-7,41	0,79	2,12	6,17	0,07	-10,6

	Rx Heart	0,62	2,68	1	0,52	-10,8	0,52	3,33	4,67	0,11	-10,67
	RxLeft Ear	0,59	2,87	1,77	0,27	-11,4	0,74	2,26	5,57	0,08	-10,94
Tx Right Hand	**Rx Right Hip**	1,15	1,64	2,31	0,16	-7,12	0,98	1,8	8,8	0,05	-9,95
	Rx Heart	1,05	1,73	2,31	0,17	-6,37	0,8	2,09	7,09	0,07	-10,04
	RxLeft Ear	0,76	2,2	2,37	0,2	-9	0,82	2,06	6,69	0,07	-10,52
Tx Left Thigh	**Rx Right Hip**	1,26	1,56	2,26	0,17	-6,06	0,91	1,9	7,11	0,06	-11,3
	Rx Heart	0,75	2,21	1,83	0,25	-7,47	0,69	2,4	5,34	0,09	-10,94
	RxLeft Ear	0,9	1,9	2,74	0,16	-7,93	0,81	2,07	6,43	0,07	-9,9

Table 62: Fading statistics for Planar Monopole Antenna

	Fading statistics – Top Loaded Monopole										
		LOS Conditions					*NLOS Conditions*				
	Rxs	*μ*	*w*	*Rate [s-1]*	*Duration [ms]*	*Depth [dB]*	*μ*	*w*	*Rate [s-1]*	*Duration [ms]*	*Depth [dB]*
Tx Right Hip	**Rx Right Hip**	0,95	1,84	3,57	0,12	-10,88	0,99	1,79	7,06	0,06	-10,02
	Rx Heart	0,93	1,87	2,94	0,15	-10,45	0,86	1,97	5,43	0,08	-11,3
	RxLeft Ear	0,92	1,88	3,29	0,13	-9,58	0,96	1,83	7,49	0,06	-11,31
Tx Right Hand	**Rx Right Hip**	1,1	1,68	4,63	0,09	-9,86	1,01	1,76	6,94	0,06	-10,47
	Rx Heart	0,98	1,8	4,31	0,1	-10,84	0,87	1,97	5,66	0,08	-10,89
	RxLeft Ear	1,31	1,53	3,66	0,12	-7,93	0,8	2,1	5,57	0,08	-10,46
Tx Left Thigh	**Rx Right Hip**	0,93	1,87	4,67	0,09	-10,83	0,94	1,86	6,89	0.07	-10,76
	Rx Heart	0,94	1,85	3,43	0,12	-10,21	0,84	2,02	5,49	0.08	-10,24
	RxLeft Ear	0,89	1,93	4,8	0,09	-9,9	0,87	1,96	6,77	0.07	-11,44

Table 63: Fading statistics for Top Loaded Monopole Antenna

4.2. PLANNED CORMORAN BAN CHANNEL MEASUREMENT

In this sub-section, we present the measurement campaigns which will be carried out for off-body and body-to-body channel modeling. Different channel characteristics will be investigated. First of all, we will focus on the influence of the body on the estimation of the angles of arrival of the paths for off-body scenarios. Then, analysis of radio link budgets (channel gain, slow and fast fading) and delay dispersion will be carried out for different movement conditions in cooperative communication scenarios combining off-body and body-to-body radio links.

4.2.1 OFF-BODY CHANNEL MEASUREMENT CAMPAIGNS

- *Frequency-domain measurement setup*

One of the objectives of the off-body measurement campaigns will be the study of the body influences on the estimation of the angles of arrival of the paths. The other objective will be the UWB radio budget link modeling for the different off-body radio links. The body will be simulated by a phantom showed in Figure 35.

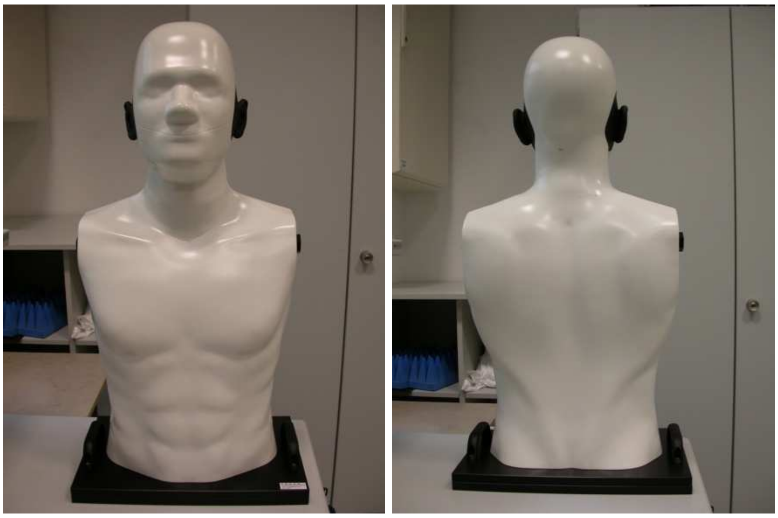

Figure 35: Phantom used for measurement campaigns

To estimate the angles of arrival of the paths, an antenna array at the receiver side is necessary. A channel estimation algorithm processes the channel transfer functions measured between the transmitter and the different receiving antennas to estimate the angles of arrival. For this purpose, we will use the SAGE algorithm [73] [74] which will be presented in sub-section 4.3.

In a realistic antenna array, the antennas have not the same radiation patterns because of the mutual coupling effect. The latter has to be taken into account in the channel estimation algorithm which increases its complexity. To avoid this inconvenient, a classical method consists in using only one antenna and changing its position to simulate the antenna array. This method allows obtaining a so-called virtual antenna array avoiding the mutual coupling effect. For this purpose, we will use the (X,Y) positioner showed in Figure 36.

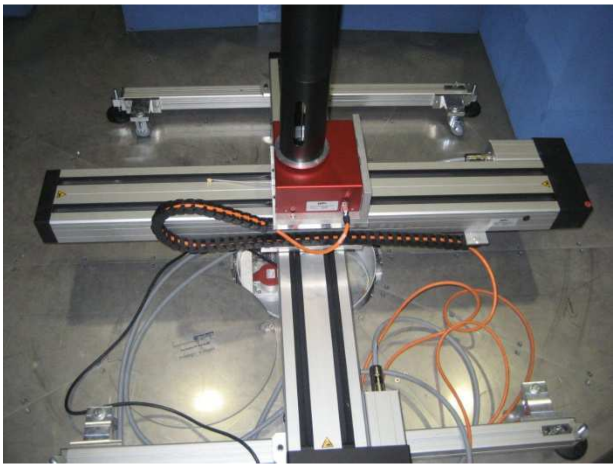

Figure 36: (X, Y) positionner

The measurements will be performed in the [3-5] GHz frequency band, covering the lower UWB band. For this purpose, a Vector Network Analyzer (VNA) showed in Figure 37 will be used.

Figure 37: Rohde & Schwarz ZVA 24 Vector Analyzer

Let us note that due to the time necessary for the positioner to reproduce a virtual antenna array and that needed by the VNA for UWB channel measurement, performing the measurements in a dynamic environment is not possible. In the next measurement campaigns, body movement conditions will be included in the scenarios.

- *Measurement campaign description*

In order to assess the influences of the presence of the body on the estimation of the angles of arrival, it is necessary to perform reference measurements, i.e. without phantom as illustrated in Figure 38. The square in the figure represents the grid on which the Rx antenna moves to reproduce the virtual antenna array.

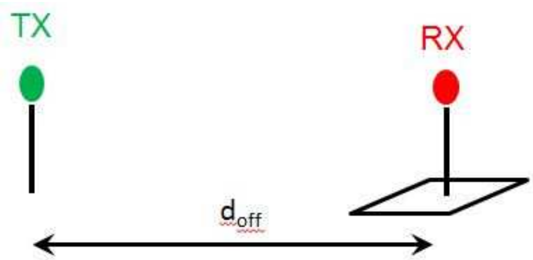

Figure 38: Reference measurement illustration

Then, measurements in the same environment and the same conditions will be carried out with the phantom. Since the VNA allows using four antennas, three antennas will be positioned on the phantom. According to the preferred antenna on-body locations identified in the CORMORAN deliverable D1.1 and due to the fact that the phantom does not have any limb, we choose to position the antennas on the torso, the back and the left shoulder as illustrated in Figure 39.

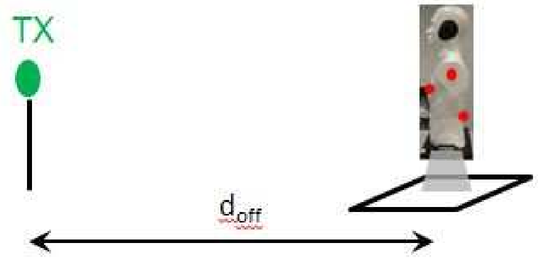

Figure 39: Off-Body measurement illustration

The measurements will be carried out for several distances d_{off} between the transmitter and the phantom. According to the anchor density specified in D1.1, d_{off} will vary from 1 meter to 8 meters with a step of 1 meter.
Furthermore, the phantom will present different orientations Φ as illustrated in Figure 40. The orientation values will be 0°, 45°, 90°, 135° and 180°.

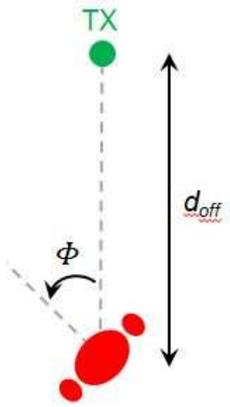

Figure 40: Phantom orientation for off-body measurements

Finally, in addition of the analysis of the degradation caused by the presence of the phantom on the estimation of the angles of arrival, an UWB path loss model will be provided in function of the distance d_{off} and the orientation Φ.

4.2.2 CHANNEL MEASUREMENT CAMPAIGNS FOR COOPERATIVE SCENARIOS

One of the main objectives of the CORMORAN project is to show the interest of using cooperative radio links. For instance, for the absolute positioning of a BAN in a *Global Coordinate System* (GCS), off-body radio links have to be exploited. To improve the absolute positioning system performance, one or several cooperative *body-to-body* radio links could also be exploited.

Off-body and *body-to-body* channel measurements have to be carried out in parallel, i.e. at the same time. For this purpose a human subject, in addition of the phantom, will be used for the measurement campaigns.

- *Measurement campaigns description*

Static UWB measurements

First of all, UWB statics measurements will be performed using the VNA, i.e. the human subject will not move and will be located at different positions (illustrated by crosses in Figure 41) during the measurements. For convenience, we number the antennas from 1 to 4.

Figure 41: Static UWB measurement campaign illustration in a cooperative scenario –view from the side

According to the maximum inter-body distances defined in D1.1, the distance d_{B2B} separating the human subject and the phantom will vary from 1m to 7m. The off-body distance d_{off} between the external gateway and the phantom will be set at 8m.

Two antennas will be located on the torso and the back of the human subject and one on the torso of the phantom. The influence of the body orientation Φ on the path loss will also be investigated. The torso orientation of the phantom will take the same values than those chosen for the off-body measurement campaign, i.e. 0°, 45°, 90°, 135° and 180°.
Thus, body-to-body and off-body channel investigations will be performed in the case of an obstruction caused by a human subject in function of the phantom orientation, the human subject antenna location and the phantom orientation.

Furthermore, investigations on the delay dispersion will be performed for off-body and body-to-body scenarios in function of the distances and the bodies' orientation.

Dynamic narrow band measurements

Measurements will also be performed in walking and running scenarios. The human subject will walk or run along the positions previously defined for the static measurement campaigns while the phantom will not move as illustrated in Figure 42.
Similarly to the previous measurement campaigns, the phantom will take different orientations Φ (0°, 45°, 90°, 135° and 180°) and will be located to different distances d_{off} (3.5 to 6.5m).

Figure 42: Dynamic narrow band measurement campaign illustration in a cooperative scenario

Since the VNA can not perform UWB measurements fast enough compared to the time coherence of the channel which depends of the human subject moving speed, the measurements will be performed in narrow band at 2.45GHz which corresponds to the central frequency of an ISM band.

Finally, a mean channel gain model and a fast fading model will be provided for off-body and body-to-body narrow band channel in function of the phantom orientation.

4.3. MODELISATION TOOLS

4.3.1 OVERVIEW

A *Space Alternating Generalized Expectation-maximization* (SAGE) algorithm has been developed at CEA Leti and will be exploited as a tool for UWB channel modeling in off-body scenarios. Based on the *Expectation Maximization* (EM) algorithm [75], SAGE algorithm has been proposed for the first time for channel parameters estimation by B. Fleury in [73]. In [76], Chong *et al.* proposed a frequency-domain version of SAGE for Single-Input Multiple-Output (SIMO) system, which has been extended by Matthaiou *et al*, to Multiple-Input Multiple-Output (MIMO) systems [77]. UWB and spherical wave features have been introduced by Haneda *et al.* in [78] and [79]. Finally, S. Van Roy *et al.* adapted the UWB SAGE algorithm for BAN scenarios.

The SAGE algorithm is an iterative process which allows the estimation of the parameters of the multipath components (MPC). In our case, we will focus on the estimation of the number of paths, their amplitudes, delays and angles of arrival (AoA). As mentioned in the last sub-section, the AoA estimation necessitates the use of an antenna array at receiver side.

Similarly to the EM method, the SAGE algorithm is characterized by an expectation step (E-step) and a maximization step (M-step). The M-step is a maximum likelihood (ML) detector. It consists in testing all the possible values of the parameters of each path and retaining the most likely. The E-step is an interference cancellation function. It consists in cancelling the contributions of the interfering MPCs from the measured channel transfer function (CTF). Thus, it is easier to estimate the parameters of a considered MPC in the M-step.

In the sequel, we present the principles of the UWB SAGE algorithm in frequency domain.

4.3.2 ALGORITHM DESCRIPTION

First of all, let us express the channel transfer function (CTF) measured on the m-th antenna at the n-th frequency point of the considered bandwidth. It is equal to the sum of all the MPCs contributions:

$$H(m,n) = \sum_{l=1}^{L} \alpha_l(n) \underbrace{\exp(-j2\pi f_n \tau_l)}_{\text{phase rotation due to delay}} \underbrace{\exp\left(-j2\pi \frac{\langle e(\phi_l,\theta_l), r_m\rangle}{\lambda_n}\right)}_{\text{phase rotation due to antenna position and AoA}} \underbrace{D(n,\phi_l,\theta_l)}_{\substack{=1 \\ \text{if isotropic} \\ \text{antenna}}} + W(m,n) \tag{4-2}$$

- l and L are the MPC index and the total number of MPCs respectively
- α_l is the amplitude
- τ_l is the delay
- ϕ_l and θ_l are the angles of arrival (AoA) in azimuth and in elevation respectively
- $e(\phi_l, \theta_l)$ is a unitary vector whose the direction is that of the l-th path
- r_m is the coordinates of the m-th antenna
- λ_n is the wavelength for the frequency f_n
- $D(n, \phi_l, \theta_l)$ is the product of Tx and Rx complex antenna gains depending of the frequency f_n and the angles of arrival
- $W(m,n)$ is an additive white Gaussian noise sample.

- *E-step*

The E-step allows estimating the signal contribution of the l-th MPC by subtracting the other MPCs contributions from the measured CTF as:

$$\widehat{\boldsymbol{X}}_l = \boldsymbol{H} - \sum_{\substack{l'=1 \\ l'\neq l}}^{L} \widehat{\boldsymbol{X}}_{l'}(\widehat{\boldsymbol{\psi}}_{l'})$$

(4-3)

where $\boldsymbol{\hat{X}}_l$ is the estimated contribution of the l-th MPC and $\boldsymbol{\hat{\psi}}_l$ represents the estimated parameters of the l-th MPC. This operation is performed by a parallel interference cancellation (PIC). However, it has been showed in [76] that in a rich multipath environment, a successive interference cancellation (SIC) has a better performance. In this scheme, the MPCs are ordered according to their received powers and the MPCs are estimated and cancelled successively from CTF. Thus, only the MPCs whose power is higher than that of the considered MPC are cancelled from the CTF.

$$\boldsymbol{\hat{X}}_l = \boldsymbol{H} - \sum_{l'=1}^{l-1} \boldsymbol{\hat{X}}_{l'}(\boldsymbol{\hat{\psi}}_{l'})$$

(4-4)

- *M-step*

It is then possible to estimate the l-th MPC parameters using a ML detector, corresponding to the M-step. For this purpose, a correlation function is defined as:

$$z_l(\tau, \phi, \theta\,;\, \boldsymbol{\hat{X}}_l) = \sum_{n=1}^{N}\sum_{m=1}^{M} \exp(+j2\pi\, f_n\, \tau)\ \exp\left(+j2\pi \frac{\langle e(\phi\,, \theta), r_m\rangle}{\lambda_n}\right) \times \hat{X}_l(m, n)$$

(4-5)

The M-step consists in testing all the possible τ, ϕ and θ values and retaining those which maximize the absolute value of the correlation function. In order to limit the complexity of this step, the parameters of each MPC are not estimated in parallel but successively. Classically, the first parameter to be estimated is the delay. For this purpose, the angles of arrival values estimated during the previous iteration are used in the correlation function as showed in equation (4-6). Then, the angles of arrival are estimated taking into account the updated estimated delay.

$$\hat{\tau}_l^{(i)} = \arg\max_{\tau}\ \left|z_l\left(\tau, \hat{\phi}_l^{(i-1)}, \hat{\theta}_l^{(i-1)}; \boldsymbol{\hat{X}}_l\right)\right|^2$$

$$\hat{\phi}_l^{(i)} = \arg\max_{\phi}\ \left|z_l\left(\hat{\tau}_l^{(i)}, \phi, \hat{\theta}_l^{(i-1)}; \boldsymbol{\hat{X}}_l\right)\right|^2$$

$$\hat{\theta}_l^{(i)} = \arg\max_{\theta}\ \left|z_l\left(\hat{\tau}_l^{(i)}, \hat{\phi}_l^{(i)}, \theta\,; \boldsymbol{\hat{X}}_l\right)\right|^2$$

(4-6)

Once the delay and angles of arrival of a MPC is estimated, the amplitude is simply computed by the following equation:

$$\hat{\alpha}_l = \frac{1}{M} z_l\left(\hat{\tau}_l^{(i)}, \hat{\phi}_l^{(i)}, \hat{\theta}_l^{(i)}\,; \boldsymbol{\hat{X}}_l\right)$$

(4-7)

Let us note that here, one average amplitude is estimated by MPC for all the bandwidth. In the case of an UWB channel, the amplitude can vary significantly. Haneda and Takada proposed in [78] to divide the considered frequency band in sub-bands. Hence, the M-step is carried in all the sub-bands in parallel. Thus, one estimated average amplitude is computed by sub-band by MPC. This method allows a better estimation of the MPC amplitude. However, it reduces the time resolution of the algorithm since it is function of the inverse of the considered bandwidth. In other words, the delay estimator performance decreases.

- *Initialization cycle*

At the start of the algorithm, no estimation of the MPCs parameters is available. Therefore, no interference cancellation can be carried out for the estimation parameters of the first MPC and no estimated value of the angles of arrival is available for delay estimation of the MPCs.

In [74], B. Fleury proposed an initialization cycle (i=0) in which a SIC is exploited for E-step and the correlation function is modified for M-step. More precisely, delay estimation is performed without taking into account the effects of the angles of arrival in the initialization cycle. The initialization allows providing not only initial estimations of the MPC parameters but also, an estimation of the total number of MPCs. For this purpose, SIC and M-step are performed successively until the estimated power of a MPC is not significant.

Different criterion can be used to determine if an estimated MPC is significant or not. It can be the comparison with the power of the strongest path or the noise power. A classical criterion used is the comparison of the regenerating CTF power (corresponding to the estimated interference in E-step) with that of the measured CTF. For instance, if regenerating CTF power is higher to 90% of the measured CTF power, it is considered that the estimation of other MPCs parameters is not necessary. Figure 43 summarizes in a flow chart the initialization cycle principle of SAGE algorithm.

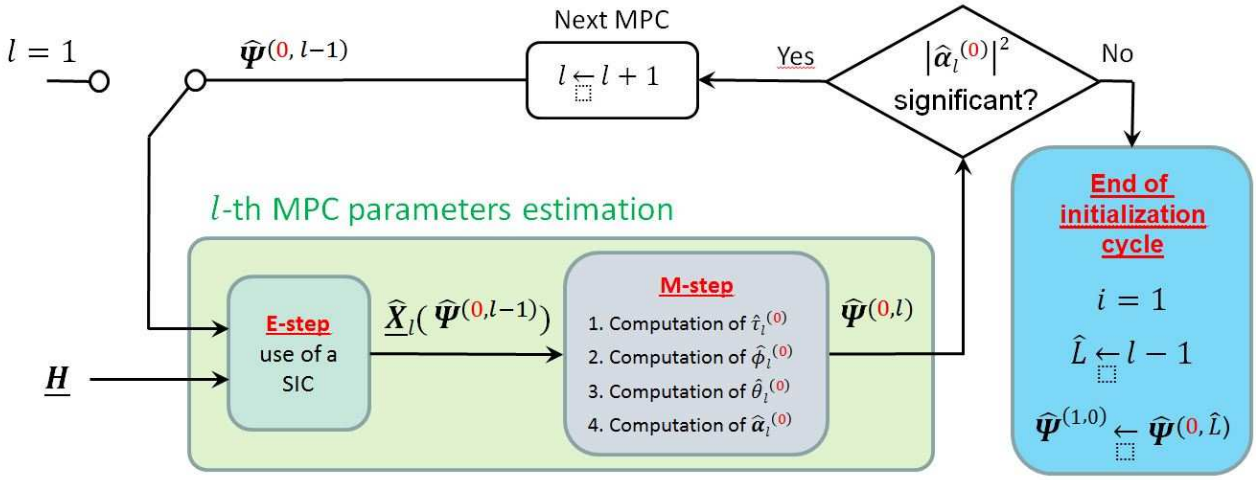

Figure 43: Flow chart of SAGE algorithm during the initialization cycle

5. DETERMINISTIC CHANNEL MODEL TOOLS

5.1. INTRODUCTION

Ray tracing (RT) tools have been developed for accurate radio propagation predictions [81], [82], [83], [84], [85]. Those RT tools are based on geometrical optics (GO) and geometric/uniform theory of diffraction (GTD/UTD) which allow to define the optical paths between two points using an electromagnetic formulation of propagation phenomena such as reflection, transmission, and diffraction. In order to perform simulation with RT tools, a detailed 3D site geometry, material properties, transmitter/receiver locations, and antenna properties are required. Once this complete information is given, a RT task is executed. Then, after the identification of rays that are captured by the receiver antenna, the channel transfer function is calculated.

Conventional RT tools take usually much time to simulate a radio link. This delay makes those tools not suitable for real time communication and localization techniques. In this paper, a new technique of RT is presented. This technique is based on graph theory i.e the modeling of environment layouts using graphs. A faster technique to compute rays is proposed based on those graphs [86]. The proposed technique is applied to estimate location dependent parameters (RSSI and TOA). The comparison between measurements and simulations reveals a good match even without taking into account the pieces of furniture present in the environment during measurements. These results would allow using RT tools in localization systems to complement/replace the measurement campaigns.

5.2. PYLAYERS: GRAPH-BASED RAY TRACING SIMULATOR

PyLayers simulator [87] describes the data structure of the indoor layout through the definition of the following graphs:

- The structure graph G_s
- The visibility graph G_v
- The topological graph G_t
- The graph of rooms G_r
- The graph of interactions G_i

Definitions and examples of these graphs are given from Figure 44 to Figure 48. The adopted multi-graph description contains meta information from the layout which can be exploited for both incremental identification of rays and simulation of indoor pedestrian mobility.

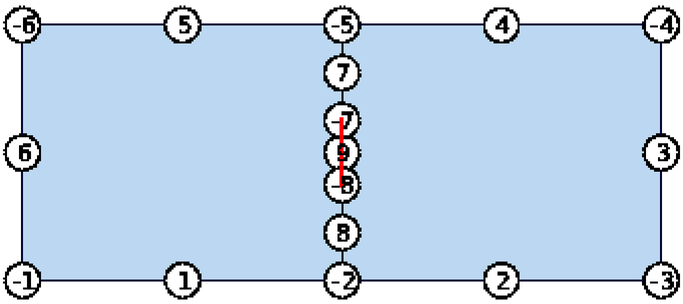

Figure 44: G_s representation of 2 rooms separated by a door (in red), positive nodes are walls and negative nodes are vertices.

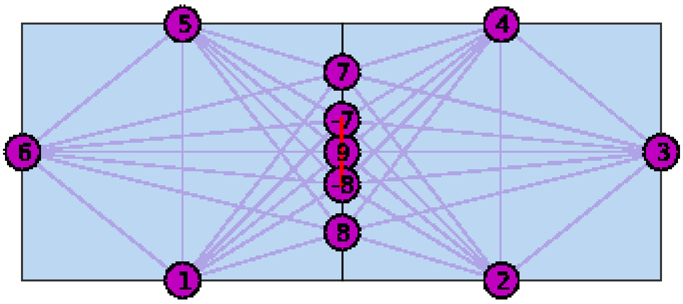

Figure 45: Visibility graph G_v has the same nodes of G_s but edges are defined differently. Two nodes are connected if they share an optical visibility relationship.

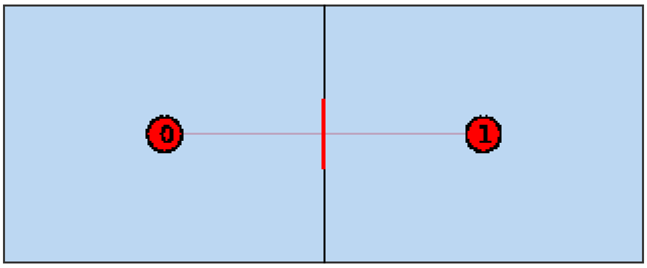

Figure 46: Topological graph G_t. It results from the determination of all cycles of the graph G_s. G_t contains a valuable topological information. Each cycle contains various attributes as for example the set of nodes and edges of the cycle.

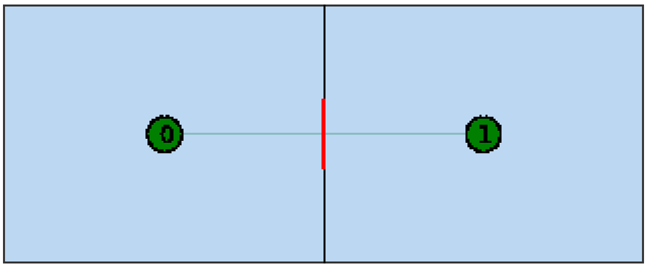

Figure 47: Graph of rooms G_r. It is the subgraph of G_t retaining only cycles which possess at least one door (i.e. doors).

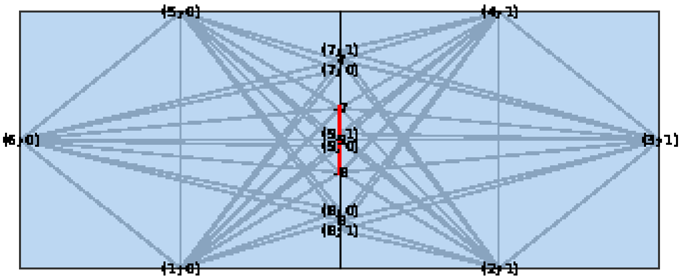

Figure 48: Graph of interactions G_i. It results from the determination of all possible interactions between the nodes of G_s. The nodes of G_i are either a tuple (id of G_s node, id of room) in case of reflection or a simple number (negative for diffraction and positive for transmission).

Let first define a ray with N_i interactions as an ordered list of $N_i + 2$ points starting at transmitter position $\mathbf{t}_x$ and ending at receiver position $\mathbf{r}_x$.

$$\mathcal{R} = \{\mathbf{t}_\mathbf{x}, \mathbf{p}_0, \cdots, \mathbf{p}_{N_i-1}, \mathbf{r}_x\} = \{\mathbf{t}_x, \mathcal{P}, \mathbf{r}_x\} \tag{5- 1}$$

where $\mathcal{P}$ is the ordered list of N_i interaction points $\{\mathbf{p}_0, \cdots, \mathbf{p}_{N_i-1}\}$. The ray tracing (RT) consists then in determining the list $\mathcal{P}$. Based on the graphs described previously, we first construct rays signatures and then we apply a two-steps technique to obtain 2D rays from signatures. Those 2D rays are then transformed into 3D rays using geometric transformations.

The signature of $\mathcal{R}$ is defined as the sequence of structure ids of $\mathcal{P}$. The structure id of a point is simply the identification number either of the diffraction point (id<0) or the segment number (id>0), this is directly a node number from graph G_s or G_v defined previously. Id(p) is a function which returns the layout index number of p.

$$\mathcal{S}(\mathcal{R}) = \mathcal{S}(\mathcal{P}) = \{\mathrm{Id}(\mathbf{p}_0), \cdots, \mathrm{Id}(\mathbf{p}_{N_i-1})\} \tag{5- 2}$$

Conventionally, the signature of the LOS path is the empty set: $\mathcal{S}(\{\mathbf{t}_x, \mathbf{r}_x\}) = \emptyset$

Notice that when at least one ending point of the radio link is moving, all the points of $\mathcal{P}$ are moving correspondingly. This is not the case of the signature $\mathcal{P}$ which can remain stationary in the vicinity region of the moving point.

In a first step the algorithm seeks for the nodes $\mathcal{V}_{tx}$ of G_s which are visible from $\mathbf{t}_x$, and the set of nodes $\mathcal{V}_{rx}$ of G_s which are visible from $\mathbf{r}_x$. The second step consists in exploiting the 2 subsets $\mathcal{V}_{tx}$ and $\mathcal{V}_{rx}$ for determining $N_t \times N_r$ first order signatures where $\text{card}(\mathcal{V}_{tx}) = N_t$ and $\text{card}(\mathcal{V}_{rx}) = N_r$. The algorithm determines then all the simple paths (paths with no repeated nodes) between any pair of nodes in the graph G_i.

```
Require: $\mathbf{t}_x$,$\mathbf{r}_x$
Require: $\mathcal{G}_s$,$\mathcal{G}_v$,$\mathcal{G}_r$
  $\mathcal{L} = \emptyset$ Initialize a list of signatures
  $\mathcal{V}_{tx} \leftarrow$ get visible nodes($\mathcal{G}_r, \mathbf{t}_x$)
  $\mathcal{V}_{rx} \leftarrow$ get visible nodes($\mathcal{G}_r, \mathbf{r}_x$)
  for $nt \in \mathcal{V}_{tx}$ do
    for $nr \in \mathcal{V}_{rx}$ do
      $\mathcal{S}_{it,ir}$ = all-simple-paths($\mathcal{G}_i, n_t, n_r$)
      $\mathcal{L} \leftarrow \mathcal{L}$.append($\mathcal{S}_{it,ir}$)
    end for
  end for
```

The determination of a ray from its signature is a two steps process. The first step consists in calculating a set of intermediate points starting from the transmitter $\mathbf{t}_x = [x_t, y_t]^T$. Once calculated, those intermediate points can be used for any receiver position with the same signature. The signature can be either valid or not valid for a given receiver depending on its coordinates. We consider a signature of length N which can contain three types of interaction: diffraction (D), reflection (R), transmission (T). From this signature, two ordered lists of points are retrieved.

$$\mathbf{p}_a = [\mathbf{a}_0, \ldots, \mathbf{a}_{N-1}] \quad (5\text{-}3)$$

$$\mathbf{p}_b = [\mathbf{b}_0, \ldots, \mathbf{b}_{N-1}] \quad (5\text{-}4)$$

$$\mathbf{a}_k = [x_{Ak}, y_{Ak}]^T, \ \mathbf{b}_k = [x_{Bk}, y_{Bk}]^T \quad (5\text{-}5)$$

In the case of a diffraction the point appears identical in each list otherwise $\mathbf{p}_a$ and $\mathbf{p}_b$ contains respectively tail points and head points of the signature segments. The sequence of intermediate points can be determined from the knowledge of the transmitter point, the sequence of segments and also importantly the type of interaction (R|T|D). This sequence of intermediate points is: $\mathbf{m} = [\mathbf{m}_0, \ldots, \mathbf{m}_{N-1}]$

with $\mathbf{m}_k = [x_k, y_k]^T$. Depending on the very nature of the interaction the intermediate point is either:

- (R) : the image of the current point w.r.t the segment,
- (T) : the current point itself
- (D) : the diffraction (interaction) point itself

$\mathbf{m}_0$ depends on the type of the first interaction as:

$$\begin{array}{l}(\mathrm{R}) : \mathbf{m}_0 = \mathbf{S}_0\mathbf{t}_x + \mathbf{v}_0 \\ (\mathrm{T}) : \mathbf{m}_0 = \mathbf{t}_x \\ (\mathrm{D}) : \mathbf{m}_0 = \mathbf{a}_0\end{array} \tag{5- 6}$$

and similarly, $\mathbf{m}_k$ depends on the type of the k^th^ interaction:

$$\begin{array}{l}(\mathrm{R}) : \mathbf{m}_k = \mathbf{S}_k\mathbf{m}_{k-1} + \mathbf{v}_k \\ (\mathrm{T}) : \mathbf{m}_k = \mathbf{m}_{k-1} \\ (\mathrm{D}) : \mathbf{m}_k = \mathbf{a}_k\end{array} \tag{5- 7}$$

where $\mathbf{S}_k$ (reflection matrix) and $\mathbf{v}_k$ are defined as:

$$\mathbf{S}_k = \left[\begin{array}{cc} a_k & -b_k \\ -b_k & -a_k \end{array}\right] \tag{5- 8}$$

The translation vector is defined as:

$$\mathbf{v}_k = [c_k, d_k]^T \tag{5- 9}$$

with

$$\begin{array}{ll} a_k = & \frac{(x_{Ak}-x_{Bk})^2-(y_{Ak}-y_{Bk})^2}{(x_{Ak}-x_{Bk})^2+(y_{Ak}-y_{Bk})^2} \\ b_k = & \frac{2(x_{Bk}-x_{Ak})(y_{Ak}-y_{Bk})}{(x_{Ak}-x_{Bk})^2+(y_{Ak}-y_{Bk})^2} \\ c_k = & 2\frac{x_{Ak}(y_{Ak}-y_{Bk})^2+y_{Ak}(x_{Bk}-x_{Ak})(y_{Ak}-y_{Bk})}{(x_{Ak}-x_{Bk})^2+(y_{Ak}-y_{Bk})^2} \\ d_k = & 2\frac{x_{Ak}(y_{Ak}-y_{Bk})(x_{Bk}-x_{Ak})+y_{Ak}(x_{Bk}-x_{Ak})^2}{(x_{Ak}-x_{Bk})^2+(y_{Ak}-y_{Bk})^2} \end{array} \tag{5- 10}$$

The coordinates of intermediates points are obtained by solving the following linear system:

$$\mathbf{A}\mathbf{m} = \mathbf{y}$$

(5- 11)

$$\mathbf{A} = \begin{bmatrix} \mathbf{I}_2 & & & \\ \{-\mathbf{S}_1| - \mathbf{I}_2|\mathbf{O}_2\} & \mathbf{I}_2 & & \\ & \ddots & \ddots & \\ & & \{-\mathbf{S}_{N-1}| - \mathbf{I}_2|\mathbf{O}_2\} & \mathbf{I}_2 \end{bmatrix}$$

(5- 12)

$$\mathbf{y} = \begin{bmatrix} \{\mathbf{S}_0\mathbf{t}_x + \mathbf{v}_0|\mathbf{t}_x|\mathbf{a}_0\} \\ \{\mathbf{v_1}|\mathbf{z}_2|\mathbf{d}_1\} \\ \vdots \\ \{\mathbf{v_{N-1}}|\mathbf{z}_2|\mathbf{d}_{N-1}\} \end{bmatrix}$$

(5- 13)

where $\mathbf{I}_2$ and $\mathbf{O}_2$ are respectively identity matrix and zero matrix of dimension 2, $\mathbf{z}_2$ is 2-by-1 zero column vector. The notation {R|T|D} stands for the possible matrix entries depending on the interaction type.

Let the receiver be noted by $\mathbf{r}_x = [x_r, y_r]^T$. Interaction points are points which belong to the layout segments. They are obtained from the intersection between the segments indicated by the signature and the segments joining successively the previously obtained intermediate points **m**. The unknown interaction points are $\mathbf{p}_k = [x'_k, y'_k]^T$. By introducing a parametrization on both the unknown 4-by-1 column vector is $\mathbf{x}'_k = [\mathbf{p}_k^T, \mathbf{\Gamma}_k^T]^T$ with $\mathbf{\Gamma}_k = [\alpha_k, \beta_k]^T$ Starting from the receiver and joining the last intermediate point $\mathbf{m}_{N-1}$, we obtain:

$$\mathbf{p}_0 + \alpha_0(\mathbf{r_x} - \mathbf{m}_{N-1}) = \mathbf{r_x}$$
$$\mathbf{p}_0 + \beta_0(\mathbf{a}_{N-1} - \mathbf{b}_{N-1}) = \mathbf{a}_{N-1}$$

(5- 14)

We solve successively the following linear systems

$$\mathbf{T}_0\mathbf{x}'_0 = \mathbf{y}'_0$$

(5- 15)

$$\mathbf{T}_0 = \begin{bmatrix} \mathbf{I}_2 & \mathbf{r_x} - \mathbf{m}_{N-1} & \mathbf{0}_{2\times 1} \\ \mathbf{I}_2 & \mathbf{0}_{2\times 1} & \mathbf{a}_{N-1} - \mathbf{b}_{N-1} \end{bmatrix}$$

(5- 16)

$$\mathbf{y}'_0 = [\mathbf{r_x}^T, \mathbf{a}_{N-1}^T]^T$$

(5- 17)

The interaction point $\mathbf{p}_k$ is determined identically taking advantage of the knowledge of point $\mathbf{p}_{k-1}$:

$$\begin{aligned} \mathbf{p}_k + \alpha_k(\mathbf{p}_{k-1} - \mathbf{m}_{N-(k+1)}) &= \mathbf{p}_{k-1} \\ \mathbf{p}_k + \beta_k(\mathbf{a}_{N-(k+1)} - \mathbf{b}_{N-(k+1)}) &= \mathbf{a}_{N-(k+1)} \end{aligned} \quad (5\text{-}18)$$

$$\mathbf{T}_k \mathbf{x}'_k = \mathbf{y}'_k \quad (5\text{-}19)$$

$$\mathbf{T}_k = \begin{bmatrix} \mathbf{I}_2 & \mathbf{p}_{k-1} - \mathbf{m}_{N-(k+1)} & \mathbf{0}_{2\times1} \\ \mathbf{I}_2 & \mathbf{0}_{2\times1} & \mathbf{a}_{N-(k+1)} - \mathbf{b}_{N-(k+1)} \end{bmatrix} \quad (5\text{-}20)$$

$$\mathbf{y}'_k = \left[\mathbf{p}_{k-1}^T, \mathbf{a}_{N-(k+1)}^T\right]^T \quad (5\text{-}21)$$

The parameterization of the signature segment plays a very important role, if $0<\beta_k,\alpha_k<1$ the interaction point $\mathbf{p}_k$ is valid and the calculation can proceed otherwise the interaction point is out of the segment and the signature is rejected for the current receiver coordinates. An example of obtained 2D rays is plotted in Figure 49.

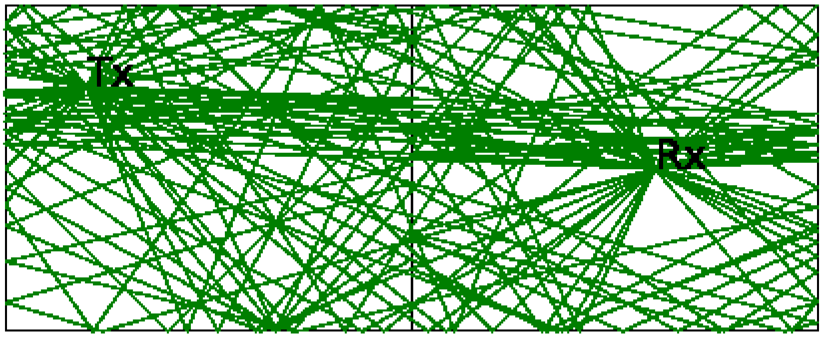

Figure 49: Example of obtained 2D rays.

6. TOWARDS PHYSICAL SIMULATOR

6.1. MOBILITY MODEL

Based on discrete event simulations, the mobility model we propose here is a model which takes into account the layout of the environment (i.e. walls, doors, corridors, rooms, etc.) in order to propose as far as possible a realistic movement of users within that environment. This is guaranteed by considering both node-node and node-layout dependencies to avoid undesired collisions between nodes and layout. The simulator is also able to define different RATs for each node-node link. The proposed implementation of this mobility model is based on the SimPy library [88].

SimPy is a discrete event simulator which allows the simulation of active components. In particular, the mechanical layer uses the Personal Rapid Transit Simulation [89], a SimPy-based library which defines the movement of persons.

In PyLayers, persons are called agents. Agents are independent instances moving into the layout. The movement of the agents is implemented by taking into account the 2 of the 3 major properties of the human mobility [90]:

- Temporal: which defines time dependent action of the movement, (frequency of visits,...)

- Spatial: which defines the physical nature of the movement. (jump size,...)

The temporal property describes where agents are moving into the layout, e.g. having a target and knowing the path to reach that target. In PyLayers, the target is defined as a room and the path as a succession of rooms. The path from a room i to a targeted room t is obtained with the help of graph G_r. Rooms i and t corresponds respectively to nodes v_r^i and v_r^t of G_r . Then, the path is obtained with $\mathcal{D}$, a Djikstra [91] shortest path algorithm:

$$\mathcal{V}_p = \mathcal{D}(v_r^i, v_r^t) \tag{5- 22}$$

The ordered set of nodes $\mathcal{V}_p$ describes the shortest path between v_r^i and v_r^t. To achieve the complete trajectory from i to t, the agent go iteratively through all the room corresponding to the nodes of $\mathcal{V}_p$. Hence, each time a node of $\mathcal{V}_p$ is reached, the next one becomes an intermediate target it, until the node v_r^t is reached.

Once the path has been computed, the agents are moving by taking into account the layout environment, such as walls and doors. This is the spatial property of the movement. That spatial property of the human mobility has been modeled using magnetic forces [92]. The magnetic force model aims to obtain a resulting acceleration vector **a** to drive the agents through the layout. The magnetic force model supposes that the agents and the layout environment can be assimilated to positive poles unlike the intermediates target which can be assimilated to negative poles.

Each agent k is potentially under the influence of several magnetic forces: an attractive magnetic force $\mathbf{F}_{it}$ which attracts the agent to its intermediate target node v_{it}; several repulsive magnetic forces $\mathbf{F}_r$, which avoid the collision of the agent with the walls or with another agent. According to [92], it is possible to approximate the attractive magnetic force $\mathbf{F}_{it}^k$ on agent k, with the Coulomb's law:

$$\mathbf{F}_{it}^k \approx \frac{q_k q_{it}}{||R_{k,ig}||^2}\hat{R}_{k,it} \tag{5- 23}$$

with q_k and q_{it} the intensities of the magnetic load of the agent and the intermediate target respectively, $R_{k,it}$ the vector from the agent k to the intermediate targeted node v_{ig}. In order to be close to a human being mobility, we suppose that agents are not grazing the walls. Then the repulsive force must be maximal along the walls. Thus, we propose to model the repulsive magnetic forces $\mathbf{F}_r$ with:

$$\mathbf{F}_r(d_{k,w}) = \frac{\alpha}{||\mathbf{d}_{k,w}||^2}\hat{\mathbf{d}}_{k,w} \quad (5\text{- }24)$$

with $\mathbf{d}_{k,w}$ the distance vector from the agent k to a wall w and α a parameter to adjust the repulsion.

Similarly, the inter-agent avoidance can be modeled by replacing $\mathbf{d}_{k,w}$ by $\mathbf{d}_{k,l}$ where k and l are two different agents. Then, the acceleration vector $\mathbf{a}_k$ of the agent k with regard to the environment can be written as the sum of three previously described interactions:

$$\mathbf{a}_k = \mathbf{F}^k_{ig} + \sum_{w}^{W} \mathbf{F}_r(d_{k,w}) + \sum_{l \neq k}^{K} \mathbf{F}_r(d_{k,l}) \quad (5\text{- }25)$$

where W is the number of walls in the vicinity of the agent k. The vicinity of the agent is determined with a simple distance threshold. The use of that threshold avoids the computation of the forces from all the walls of the entire layout. An example of operation of the mechanical layer can be seen in [93].

6.2. CHANNEL MODEL POSSIBLE IMPLEMENTATION

The combination of the human mobility model with the on-body, off-body and body-to-body channel models allows the implementation of a realistic BAN channel model. The Figure 50 describes the principle of the proposed channel model implementation.

First of all, the time invariant parameters have to be set. These parameters correspond to the antenna locations on the body, their characteristics such as their polarization and their radiation pattern, the kind of environment, the number of external gate and the number of BAN users. Once these parameters are set, their values are injected in the human mobility model. The latter gives time variant parameter values useful for the different BAN channel models. According the sub-section 4.1, these parameters are the movement conditions of the body, the orientation and the distance of the body compared with the external gateway (off-body scenario) or another body (body-to-body scenario), and the direct visibility condition. Finally, the channel characteristics such as the channel gain, the fading, the PDP characteristics and the Doppler spectra are given by the different BAN channel models.

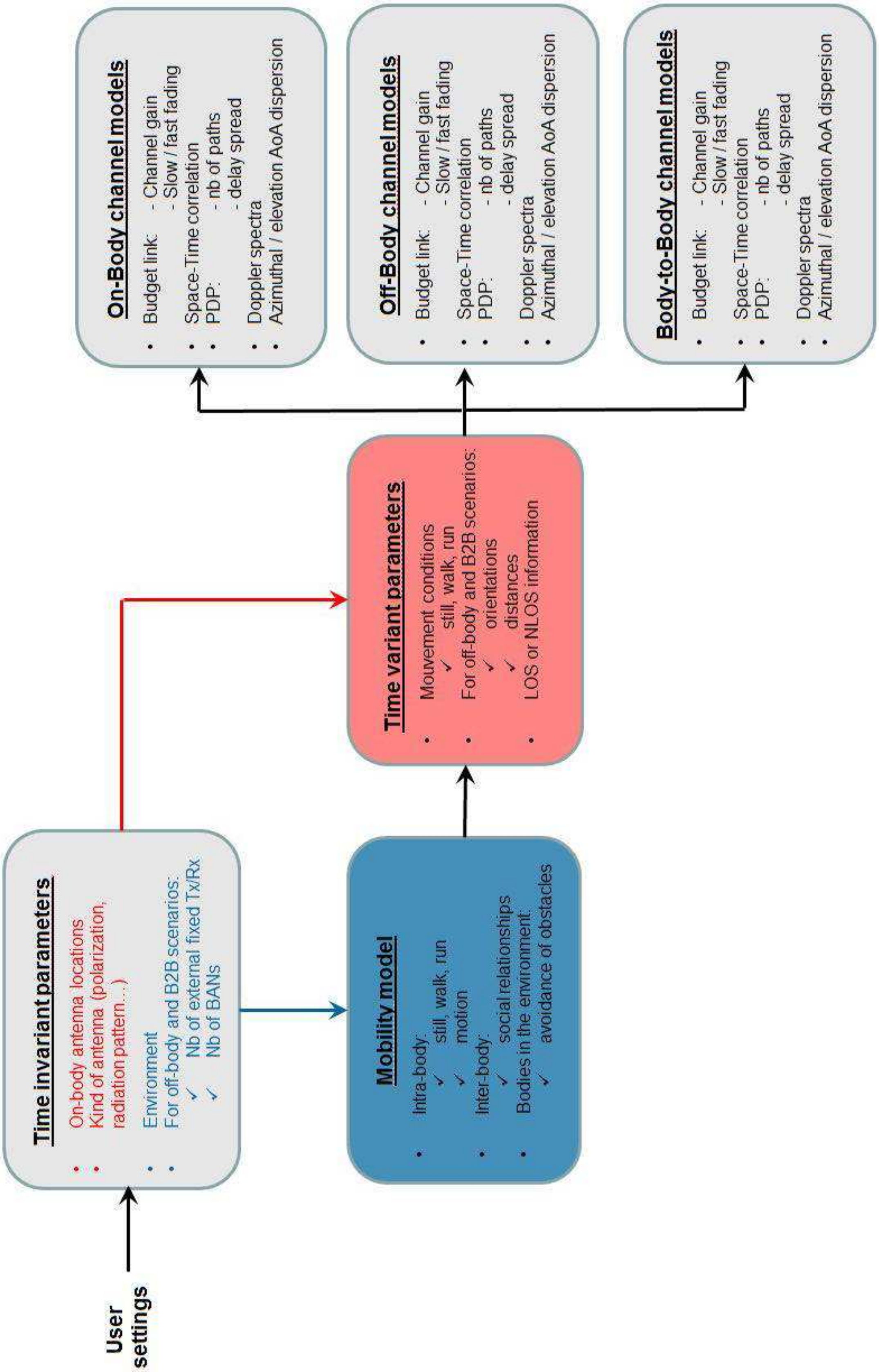

Figure 50: Physical simulator principle

7. CONCLUSIONS

This D2.2 deliverable presents channel models for different communication and mobility scenarios which are exploitable for the design of WBAN systems and the evaluation of their performances. These models mainly describe the mean channel gain, the shadowing effects and the fast fading characteristics in function of the nodes positions on the body, the body orientation and location, and the antenna characteristics for narrow band signals around 2.45GHz. Space-time correlation properties between different radio links for *on-body* communication scenarios are also described. Values of the means channel gains and their variances obtained from previous measurements campaigns performed at CEA-Leti are summarized for different mobility scenarios. A channel model describing the channel impulse response characteristics such as the delay dispersion is also presented for *on-body* communication scenarios.

A channel modeling tool namely SAGE (*Space Alternating Generalized Expectation-maximization*) has been presented and validated with indoor measurements. This tool will be used in future channel measurement campaigns for the evaluation of the degradation of the estimation of the angles of arrival of the paths caused by the presence of the body. WBAN cooperative communication aspects will also be analyzed by performing other measurement campaigns combining *off-body* and *body-to-body* radio links. All these measurement campaigns and the material which will be used such as the phantom are described in this deliverable. The analysis of these measurements and their process will be presented in the D2.3 deliverable. Other models for WBAN channel modeling are also presented such as a deterministic channel model based on a ray tracing method.

In order to evaluate the performance of WBAN systems, methods to synthesize a general physical simulator are presented. The so-obtained general WBAN channel model will combine body mobility models with the identified relevant WBAN channel models. The structure of this physical simulator will be continuously fed by novel WBAN channel models resulting from the analysis of measurement campaigns.

8. REFERENCES

[1] T. Zasowski, F. Althaus, A. Wittneben and G. Troster: UWB for noninvasive wireless body area networks: Channel measurements and results, UWBST 2003.

[2] P. S. Hall, M. Ricci and T. M. Hee: Measurement of On-Body Propagation Channels, IEEE Internal Symposium on Antennas and Propagation Digest, June 2002, pp. 310-313

[3] T. Zasowski, G. Meyer, F. Althaus, A. Wittneben : Propagation Effects in UWB Body Area Networks, 2005 IEEE International Conference on Ultra-Wideband, Zurich, 5-8 Sept. 2005.

[4] Fort, C. Desset, P. De Doncker, P. Wambacq and L. Van Biessen: An Ultra-Wideband Body Area Propagation Channel Model–From Statistics to Implementation, IEEE transactions on MTT, vol. 54, n° 4, April 2006.

[5] Fort, C. Desset, J. Ryckaert, P. De Doncker, L. Van Biessen, S. Donnay: Characterization of the Ultra Wideband Body Area Propagation Channel, 2005 International Conference on Ultra-Wideband, Zurich, 5-8 Sept. 2005.

[6] Fort, J. Ryckaert, C. Desset, P. De Doncker, P. Wambacq and L. Van Biessen: Ultra-Wideband Channel Model for Communication Around the Human Body, IEEE JSAC, vol. 24, n° 4, April 2006.

[7] S. V. Roy, C. Oestges, F. Horlin and Ph. De Doncker: On-body propagation velocity estimation using ultra-wideband frequency-domain spatial correlation analysis, El. Letters, vol. 43, n° 25, Dec. 2007

[8] P. S. Hall, Y. Hao, Y. I. Nechayev, C. Constantinou, C. Parini, M. R. Kamarudin, T. Z. Salim, D. T. M. Hee, R. Dubrovka, A. S. Owadally, W. Song, A. Serra, P. Nepa, M. Gallo, and M. Bozzetti: Antennas and Propagation for On-Body Communication Systems, IEEE AP Mag., vol. 49, n° 3, June 2007.

[9] S. L. Cotton and W. G. Scanlon: A Statistical Analysis of Indoor Multipath Fading for a Narrowband Wireless Body Area Network, Personal Indoor and Mobile Radio Communications, 2006 IEEE.

[10] S. L. Cotton and W. G. Scanlon: A Higher Order Statistics for Lognormal Small-Scale Fading in Mobile Radio Channels, IEEE Antennas and Wireless Propagation Letter, vol. 6, 2007.

[11] X. Chen, X. Lu, J. Su, and L. Zeng, "Channel Modeling of UWB-Based Wireless Body Area Networks", ICC 2011

[12] X. Lu, X. Chen, G. Sun, D. Jin, N. Ge, and L. Zeng, "UWB-based Wireless Body Area Networks Channel Modeling and Performance Evaluation", IWCMC 2011

[13] M. Hirose, H. Yamamoto, and T. Kobayashi, "Statistical Modeling of On-Body Ultra-Wideband Channels considering surrounding environments", ISWCS 2012

[14] C. Roblin, "Analysis of the separability of the on-body cluster and the off-body clusters in the modeling of the UWB WBAN channels for various indoor scenarios", EWCT 2010

[15] C. Roblin, "Analysis of the channel power delay profile of WBAN scenarios in various indoor environments", ICUWB 2011

[16] C. Roblin, "Analysis of the channel power delay profile of WBAN scenarios in various indoor environments", ICUWB 2011

[17] Nechayev, Y.I. and Hall, P.S. and Constantinou, C.C. and Hao, Y. and Alomainy, A. and Dubrovka, R. and Parini, C.G: On-body path gain variations with changing body posture and antenna position, IEEE AP-S Int. Symp./USNC/URSI Nat. Radio Sci. Meeting, pp. 731-734, 2005,

[18] Hao, Y. and Alomainy, A. and Zhao, Y. and Parini, C.G. and Nechayev, Y. and Hall, P. and Constantinou, C.C, Statistical and deterministic modeling of radio propagation channels in WBAN at 2.45 GHz, Antennas and Propagation Society International Symposium 2006, IEEE}, pp. 2169-2172, 2006,

[19] H. Ghannoum, R. D'Errico, Ch. Roblin and X. Begaud: Characterization of the UWB on-body propagation channel, Proceedings of the EuCAP, Nice, Nov. 2006.

[20] A. Taparugssanagorn, C. Pomalaza-Raez, R. Tesi, M. Hamalainen, and J. Iinatti, Effect of body motion and the type of antenna on the measured uwb channel characteristics in medical applications of wireless body area networks. In Proceedings of IEEE International Conference on Ultra-Wideband, 2009 (ICUWB 2009), Vancouver, Canada, Sept. 2009, pp. 332–336, 2009.

[21] S. L. Cotton and W. G. Scanlon, “A Statistical Analysis of Indoor Multipath Fading for a Narrowband Wireless Body Area Network”, in Proc. IEEE PIMRC’06, 2006

[22] W. Scanlon and S. Cotton, “Understanding on-body fading channels at 2.45 GHz using measurements based on user state and environment”. In Proceedings of Loughborough Antennas and Propagation Conference, 2008 (LAPC 2008), Loughborough, U.K, pp. 10–13, 2008.

[23] S. Cotton, G. Conway, and W. Scanlon, “A time-domain approach to the analysis and modeling of on-body propagation characteristics using synchronized measurements at 2.45 GHz”. IEEE Transactions on Antennas and Propagation, vol. 57, no. 4, Part 1, pp. 943–955, 2009.

[24] S.L.Cotton, W.G.Scanlon, "Characterization of the on-body channel in an outdoor environment at 2.45 GHz", Antennas and Propagation, 2009. EuCAP 2009. 3rd European Conference on , March 2009.

[25] IEEE P802.15-08-0489-01-0006 (M. Kim, J. Takada, L. Materum, T. Kan, Y. Terao, Y. Konishi, K. Nakai and T. Aoyagi): Statistical Property of Dynamic BAN Channel Gain at 4.5GHz, IEEE 802.15 Task Group 6 Document, September 2008,

[26] J.Zhang, D.B.Smith, L.W.Hanlen, D.Minutti, D.Rodda, B.Gilbert, "Stability of Narrowband Dynamic Body Area Channel", Antennas and Wireless Propagation Letters, IEEE , April 2009

[27] “Cooperative Mechanisms in On-Body Area Networks” D’Errico R., Rosini R., Maman M COST 2100 TD(10)11083 Aalborg, Denmark 2010/June/2-4

[28] E. Ben Hamida, R. D’Errico, B. Denis, “Topology Dynamics and Network Architecture Performance in Wireless Body Sensor Networks”, in Proc. IFIP NTMS’11, Paris, Feb. 2011

[29] L. Liu, P. De Doncker, C. Oestges, Fading correlation analysis for front abdomen propagation in body area networks, COST 2100 TD(08) 522, Trondheim, Norway, June 4-6, 2008,

[30] L. Liu, P. De Doncker, C. Oestge, Fading Correlation Measurement and Modeling on the Front and Back side of a Human Body, COST 2100 TD(08) 642, Lille, France, Oct. 6-8, 2008

[31] R. D'Errico, L. Ouvry, "Time-variant BAN Channel Characterization", in Proc. IEEE PIMRC'09, Tokyo, Sept. 2009

[32] IEEE P802.15-08-0418-01-0006 (G. Dolmans & A. Fort): Channel Model WBAN – Holst Centre / IMEC-NL, IEEE 802.15 Task Group 6 Document, Jul. 2008

[33] A. F. Molisch, D. Cassioli, C. Chong, S. Emami, A. Fort, B. Kannan, J. Karedal, J. Kunish and H. G. Schantz: A Comprehensive Standardized Model for Ultrawideband Propagation Channels, IEEE Transactions on Antennas and Propagation, vol. 54, n° 11, Nov. 2006.

[34] IEEE 802.15-08-0416-04-0006 (Takahiro Aoyagi, Jun-ichi Takada, Kenichi Takizawa, Hirokazu Sawada, Norihiko Katayama, Kamya Yekeh Yazdandoost, Takehiko Kobayashi, Huan-Bang Li, and Ryuji Kohno): Channel Models for wearable and implantable WBANs – NICT, IEEE 802.15 Task Group 6 Document, Nov. 2008,

[35] Guido Dolmans and Andrew Fort, "Channel models WBAN-Holst centre/IMEC-NL," IEEE 802.15-08-0418-01-0006, July 2008.

[36] IEEE P802.15-08-0421-00-0006 (D. Miniutti, L. Hanlen, D. Smith, A. Zhang, D. Lewis, D. Rodda, B. Gilbert): Narrowband Channel Characterization for BANs, IEEE 802.15 Task Group 6 Document, Jul. 2008,

[37] IEEE P802.15-08-0781-00-0006 (N.-G. Kang, C. Cho, S.-H. Park, E. T. Won): Channel Models for WBANs – Samsung Electronics, IEEE 802.15 Task Group 6 Document, Nov. 2008,

[38] R. d'Errico and L. Ouvry, "Delay Dispersion of the On-Body Dynamic Channel", European Conference on Antenna and Propagation (EuCAP 2010), 12-16 April 2010, Barcelona, Spain

[39] H. Sawada, T. Aoyagi, J. Takada, K. Y. Yazdandoost, R. Kohno, "Channel model between body surface and wireless access point for UWB band", IEEE 802.15-08-0576-00-0006, August 2008

[40] W. Jakes, Microwave mobile communications. Wiley-IEEE Press, 1994.

[41] H. Hashemi, M. McGuire, T. Vlasschaert, and D. Tholl, "Measurements

[42] and modeling of temporal variations of the indoorradio propagation channel," IEEE Transactions on Vehicular Technology, vol. 43, no. 3 Part 1, pp. 733–737,1994.

[43] P. Pagani and P. Pajusco, "Characterization and modeling of temporal variations on an ultrawideband radio link," Antennas and Propagation, IEEE Transactions on, vol. 54, no. 11, pp. 3198–3206, 2006.

[44] J. Andersen, J. Nielsen, G. Pedersen, G. Bauch, and G. Dietl, "Doppler spectrum from moving scatterers in a random environment," Wireless Communications, IEEE Transactions on, vol. 8, no. 6, pp. 3270–3277, 2009.

[45] R.D'Errico and L. Ouvry "Doppler Characteristics and Correlation Proprieties of On-Body Channelst", European Conference on Antenna and Propagation (EuCAP 2011), 11-16 April 2011, Rome, Italy.

[46] R. Rosini and R. d'Errico, "Off-Body Channel Modelling at 2.45 GHz for Two Different Antennas", 6th European Conference on Antennas and Propagation (EUCAP 2011), 11-15 April 2011, Roma, Italy

[47] S.L. Cotton, W.G. Scanlon, "The k-μ Distribution Applied to the Analysis of Fading in Body to Body Communication Channels for Fire and Rescue Personnel", Antennas and Wireless Propagation Letter, IEEE, vol.7, pp.66-69, 2008.

[48] S.L. Cotton, W.G. Scanlon, "Channel Characterization for Single- and Multiple-Antenna Wearable Systems Used for Indoor Body-to-Body Communications," Antennas and Propagation, IEEE Transactions on, vol.57, no.4, pp.980-990, April 2009.

[49] Y.Wang, I.Bonev, J.Nielsen, I.Kovacs, G.F.Pedersen, "Characterisation of the Indoor Multiantenna Body-to-Body Radio Channel", Antennas and Propagation, IEEE Transactions on , April 2010.

[50] G.F.Pedersen, J.Nielsen, O.Franek, J.B.Andersen, M.Pelosi, Y.Wang, "Measurement Based Investigations for Future Communication System Performance Evaluation", Antennas & Propagation Conference, 2009. LAPC 2009. Loughborough, November 2010.

[51] Z.H.Hu, Y.Nechyev, P.Hall, "Measurement and Statistical Analysis of the Transmission Channel between Two Wireless Body Area Networks at 2,45GHz and 5,8GHz", ICECom, 2010 Conference Proceedings, September 2010.

[52] Z.H.Hu, Y.Nechyev, P.Hall, "Fading of the Transmission Channel Between Two Wireless Body Area Networks in an Office at 2,45GHz and 5,8GHz", Antennas and Propagation Conference (LAPC), 2010 Loughborough, Novembre 2010.

[53] T.S.P.See, J.Y.Hee, C.T.Ong, L.C.Ong, Z.N.Chen, "Inter-Body Channel Model for UWB Communications", Antennas and Propagation, 2009. EuCAP 2009. 3rd European Conference on , March 2009.

[54] L.W.Hanlen, D.Minutti, D.Rodda, B.Gilbert, "Interference in Body Area Networks: Distance does not dominate", Personal, Indoor and Mobile Radio Communications, 2009 IEEE 20th International Symposium on, September 2009.

[55] A.J.Zhang, L.W.Hanlen, D.Minutti, D.Rodda, B.Gilbert, "Interference in Body Area Networks: Are signl-links and interferece-links independent?" Interference in body area networks: Are signal-links and interference-links independent?, September 2009

[56] G. Koutitas, "Multiple Human Effects in Body Area Networks", IEEE Antennas and Wireless Propagation Letters, vol.9, no., pp.938-941, 2010

[57] S.L. Cotton, W.G. Scanlon, B.K. Madahar, "Millimeter-wave soldier-to-soldier communications for covert battlefield operations", IEEE Communications Magazine, vol.47, no.10, pp.72-81, October 2009

[58] S.L. Cotton, G.W. Scanlon, K.B. Madahar, "Simulation of millimetre-wave channels for short-range body to body communications," Antennas and Propagation (EuCAP), 2010 Proceedings of the Fourth European Conference on , vol., no., pp.1-5, 12-16 April 2010

[59] S.L. Cotton, W.G. Scanlon, P.S. Hall, "A simulated study of co-channel inter-BAN interference at 2.45 GHz and 60 GHz", Wireless Technology Conference (EuWIT), 2010 European , vol., no., pp.61-64, 27-28 Sept. 2010

[60] K.I.Ziri-Castro, W.G.Scanlon, N.E.Evans, "Indoor Radio Channel Characterization and Modeling for a 5,2GHz Bodyworn Receiver", Antennas and Wireless Propagation Letters, IEEE, December 2004

[61] S.L.Cotton, W.G.Scanlon, "Indoor Channel Characterisation for Wearable Antenna Array at 868 MHz", Wireless Communications and Networking Conference, 2006. WCNC 2006. IEEE , September 2006

[62] S.L.Cotton, W.G.Scanlon, "Statistical Characterisation for a mobile Bodyworn personal area network in an indoor multipath environment at 868MHz", Antennas and Propagation, 2006. EuCAP 2006. First European Conference on, November 2006

[63] S.L.Cotton, W.G.Scanlon, "Characterisation and Modeling of the Indoor Radio Channel at 868MHz for Mobile Bodyworn Wireless Personal Area Network", Antennas and Wireless Propagation Letters, IEEE, March 2007

[64] S.L.Cotton, W.G.Scanlon, "Spatial Diversity and Correlation for Off-Body Communications in Indoor Environments at 868MHz", Vehicular Technology Conference, 2007. VTC2007-Spring. IEEE 65th, April 2007

[65] D.Smith, L.Hanlen, J.A.Zhang, D.Minutti, D.Rodda, B.Gilbert, "Characterization of the Dynamic Narrowband On-Body to Off-Body Area Channel", Communications, 2009. ICC '09. IEEE International Conference on, March 2009

[66] A.A.Goulianos, T.W.C.Brown, S.Stavrou, "Ultra-Wideband Measurement and results for Sparse Off-Body Communication Channels", Antennas and Propagation Conference, 2008. LAPC 2008. Loughborough, March 2008

[67] A.A.Goulianos, T.W.C.Brown, S.Stavrou, "A Novel Path-Loss Model for UWB Off-Body Propagation", Vehicular Technology Conference, 2008. VTC Spring 2008. IEEE, May 2008

[68] A.A.Goulianos, T.W.C.Brown, S.Stavrou, "Power delay profile modeling of the ultra wideband off-body propagation channel", Microwaves, Antennas & Propagation, IET, January 2010.

[69] P.A.Catherwood, W.G.Scanlon, "Link Characteristics for an Off-Body UWB Transmitter in a Hospital Environment", Antennas & Propagation Conference, 2009. LAPC 2009. Loughborough, November 2009.

[70] Dino Miniutti, Leif Hanlen, David Smith, Andrew Zhang, Daniel Lewis, David Rodda, Ben Gilbert, “Narrowband on body to off body channel characterization for ban,” IEEE 802.15-08-0559-00-0006, August 2008

[71] H. Sawada, T. Aoyagi, J. Takada, K. Y. Yazdandoost, R. Kohno, “Channel model between body surface and wireless access point for UWB band”, IEEE 802.15-08-0576-00-0006, August 2008

[72] R. Rosini and R. d’Errico, “Body-to-Body Communications: a Measurement-based Channel Model at 2.45 GHz”, Personal Indoor and Mobile Radio Communications (PIMRC 2012), 9-12 September, Sydney, Australia

[73] B. H. Fleury, D. Dahlaus, R. Heddergott, and M. Tschudin, “Wideband Angle of Arrival Estimation using the SAGE Algorithm”, International Symposium on Spread Spectrum Techniques and Applications, ISSSTA 1996

[74] B. H. Fleury, M. Tschudin, R. Heddergott, D. Dahlaus, K. I. Pedersen, “Channel Parameter Estimation in Mobile Radio Environments Using the SAGE Algorithm”, Journal on Selected Areas in Communications, vol. 17, no. 3, March 1999

[75] A. P. Dempster, N. M. Laird, and D. B. Rubin, “Maximum likelihood from incomplete data via the EM algorithm,” J. Royal Statist. SOc., Ser. B, vol. 39, no. 1, PP. 1-38, 1977

[76] C. Chong, D. I. Laurenson, C. Tan, S. McLaughlin, M. A. Beach, and A. Nix, “Joint detection-estimation of directional channel parameters using the SAGE algorithm”, IEEE International Conference on Communications, vol. 2, New York, USA, April 2002, pp. 906-910

[77] M. Matthaiou and N. Nrazavi-Ghods, “Characterization of an indoor MIMO channel in frequency domain using the 3D-SAGE algorithm”, in IEEE International Conference on Communications, vol. 24-28, June 2007, pp. 5868 – 5872

[78] K. Haneda and J.-I. Takada, "An application of SAGE algorithm for UWB propagation channel estimation", in IEEE Conference on Ultra Wideband Systems and Technologies, Nov. 2003, pp. 483 – 487

[79] K. Haneda, J.-I. Takada, and T. Kobayashi, "Experimental evaluation of a SAGE algorithm for ultra wideband channel sounding in an anechoic chamber," in International Workshop on Joint UWBST & IWUWBS, May 2004, pp.66-70

[80] S. Van Roy, L. Liu, C. Oestges, P. de Doncker, "An Ultra-Wideband SAGE Algorithm for Body Area Networks", in International Conference on Electromagnetics in Advanced Applications, 2009

[81] J. McKown and J. Hamilton, R.L., "Ray tracing as a design tool for radio networks," Network, IEEE, vol. 5, pp. 27 –30, nov. 1991.

[82] S. Seidel and T. Rappaport, "Site-specific propagation prediction for wireless in-building personal communication system design," Vehicular Technology, IEEE Transactions on, vol. 43, pp. 879 –891, nov 1994.

[83] P. Meissner, D. Arnitz, T. Gigl, and K. Witrisal, "Analysis of an indoor UWB channel for multipath-aided localization," in Ultra-Wideband (ICUWB), 2011 IEEE International Conference on, pp. 565 –569, sept. 2011.

[84] M. Raspopoulos, C. Laoudias, L. Kanaris, A. Kokkinis, C. G. Panayiotou, and S. Stavrou, "3D Ray Tracing for Device-Independent Fingerprintbased Positioning in WLANs," in 2012 Workshop on Positioning, Navigation, and Communication (WPNC), March 2012.

[85] M. Laaraiedh, B. Uguen, J. Stephan, Y. Corre, Y. Lostanlen, M. Raspopoulos, and S. Stavrou, "Ray tracing-based radio propagation modeling for indoor localization purposes," in Computer Aided Modeling and Design of Communication Links and Networks (CAMAD), 2012 IEEE 17th International Workshop on, pp. 276 – 280, sept. 2012.

[86] B. Uguen, N. Amiot, and M. Laaraiedh, "Exploiting the Graph Description of Indoor Layout for Ray Persistency Modeling in Moving Channel," in Proceedings of the 6th European Conference on Antennas and Propagation (EuCAP 2012), (Prague, Czech Republic), March 2012.

[87] PyLayers simulator, http://www.pylayers.org/.

[88] SimPy available at http://simpy.sourceforge.net/.

[89] K. MacLeod, Personal Rapid Transit Simulation, available at: http://sourceforge.net/projects/prt/.

[90] D. Karamshuk, C. Boldrini, M. Conti, and A. Passarella, "Human mobility models for opportunistic networks," Communications Magazine, IEEE, vol. 49, pp. 157–165, december 2011.

[91] E. Dijkstra, A Short Introduction to the Art of Programming. Holland, 1971.

[92] K. Teknomo, Microscopic Pedestrian Flow Characteristics: Development of an Image Processing Data Collection and Simulation Model. PhD thesis, Tohoku University, Japan, Sendai, 2002.

[93] PyLayer mechanical layer example : http://goo.gl/hCFtR.